UNIVERSITY OF TWENTE.
Faculty of Engineering Technology

HSLU Hochschule Luzern
Competence Centre Thermal Energy Storage

Driving Sustainability in Swiss Multi-Family Housing:

A Comprehensive Carbon Footprint and Optimisation Analysis of a Sustainable Heating System

Master thesis

Sustainable Energy Technology

Student:
Ruben Hijwegen
s26420505

Supervisors:
Dr. Mina Shahi
Prof. Dr. Jörg Worlitschek
William Orlando Delgado Diaz

Date:
24 August 2023

[This page has been intentionally left blank.]

Driving Sustainability in Swiss Multi-Family Housing:

A Comprehensive Carbon Footprint and Optimisation Analysis of a Sustainable Heating System

Faculty of Engineering Technology

Master Thesis

In fulfilment of the requirements for the degree of Master of Science in Sustainable Energy Technology.

Graduation Committee

Chair:	
Prof. dr. ir. G. Brem	University of Twente
Supervisor:	
Dr. M. Shahi	University of Twente
External members:	
Prof. dr. J. Worlitschek	Hochschule Luzern
Dr. D. Jafari	University of Twente

University of Twente
Department of Thermal and Fluid Engineering
7500 AE Enschede
the Netherlands

Hochschule Luzern – Technik und Architektur
Competence Center Thermal Energy Storage
Technikumstrasse 21, 6048 Horw
Switzerland

Horw Switzerland, August 2023

Abstract

The HyTES project focuses on developing a novel heating system for Multi-Family houses in Switzerland, employing a heat pump powered by solar panels. The generated heat is utilised for Domestic Hot Water and Spacial heating or stored in a Seasonal Thermal Energy Storage (STES) system, incorporating both latent and sensible heat storage. To identify the optimal system configuration, an optimisation process is conducted using a pre-existing system model.

This thesis describes an extension of the existing model to encompass an assessment of the system's carbon footprint. The global warming potential of the main components is calculated based on their size/capacity using derived equations from relevant literature.

In addition to the carbon footprint evaluation, the thesis concentrates on developing an optimisation strategy. A multi-objective optimisation function is formulated to account for three key performance indicators: minimal system costs, self-sufficiency, and carbon footprint. The function incorporates specific weighting and normalisation factors.

The optimisation analysis explores multiple variables, including tank types and dimensions, domestic hot water tank size, number of solar panels, and solar panel orientation. The results of a sensitivity analysis highlight the substantial influence of the dimensions of the HyTES tank and solar system variables, while variables related to the Domestic Hot Water tank have a negligible effect.

The preliminary optimisation results illustrate potential outcomes and their interpretations. Three optimisation scenarios with different levels of self-sufficiency (78%, 84%, 97%) are presented. The most optimal system of the initial optimisation runs achieved an SS of 78%, falling within the desired Self-sufficiency range. It boasts the lowest LCOH among the optimised systems and, with incentives, is almost cost-competitive with oil boilers. Moreover, its GWP is three times lower than the base case.

A prominent trend shows a significant increase in the HyTES tank volume as self-sufficiency increases. Furthermore, the results underscore the considerable impact of subsidies and feed-in tariffs on system costs. An analysis of the main contributors to system costs and carbon footprint across different scenarios identifies Operation and Maintenance costs and the solar system as the most significant cost drivers. In contrast, the solar system and grid electricity significantly influence the carbon footprint. Interestingly, the seasonal thermal energy storage's contribution to both system costs and carbon footprint escalates notably at higher levels of self-sufficiency. These findings demonstrate the utility of the carbon footprint implementation and optimisation strategy for optimising the HyTES system.

Preface

This thesis, "Driving Sustainability in Swiss Multi-Family Housing: A Comprehensive Carbon Footprint and Optimisation Analysis of a Sustainable Heating System," was completed in fulfilment of my Master's degree in Sustainable Energy Technology at the University of Twente. The research was conducted at Hochschule Luzern in collaboration with the University of Twente's Department of Thermal and Fluid Engineering.

Firstly, I extend my gratitude to William Delgado, my daily supervisor at Hochschule Luzern. His unwavering guidance, detailed feedback, and enthusiastic support significantly influenced the quality of this research. His mentorship played an instrumental role in shaping the thesis and constantly inspired me.

Additional appreciation goes to Mina Shahi, my supervisor from the University of Twente, for her invaluable assistance throughout this project. Her feedback was constructive and aided in keeping the research on course.

Moreover, I would like to extend special appreciation to Jörg Worlitschek. His extensive knowledge and insightful perspectives greatly enriched the depth and direction of this research.

Last but not least, my acknowledgements would only be complete by mentioning Gerrit Brem, whose feedback and insights supported the creation of this thesis.

This study, focusing on sustainable heating systems for Swiss Multi-Family Housing, aims to contribute to the field. The potential impact of this work on sustainable housing technology is a prospect that I find exciting and highly rewarding.

Nomenclature

Acronyms

HyTES	-	Hybrid Thermal Energy Storage
TES	-	Thermal Energy Storage
STES	-	Seasonal Thermal Energy Storage
PCM	-	Phase Change Materials
LCOH	-	Levelised Cost of Heat
KPI	-	Key Performance Indicator
PV	-	Photo Voltaics
MADS	-	Mesh Adaptive Direct Search Algorithm
DHW	-	Domestic Hot Water
DHW TES	-	Domestic Hot Water Thermal Energy Storage
SH	-	Spacial Heating
VIT	-	Vacuum Insulated Tank
GFRP	-	Glass Fibre Reinforced Plastic
GEAS	-	Advanced Waterproof Thermal Insulation Material
MADS	-	Mesh Adaptive Direct Search algorithm
SHS	-	Sensible heat storage
LHS	-	Latent heat storage
HTF	-	Heat transfer fluid
SAT	-	Sodium acetate trihydrate
GHG	-	Green House Gas
NO_x	-	Nitrogen Oxides
CH_4	-	Methane
GWP	-	Global Warming Potential
kWp	-	kW peak
CdTe	-	Cadmium-Telluride
CIS/CIGS	-	Copper-Indium-Gallium-Selenide
Multi-Si	-	Multi crystalline Silicon
Mono-Si	-	Monocrystalline Silicon
FOEN	-	Federal Office for the Environment
HDPE	-	High-Density Polyethene
V	-	Volume
PD	-	Packing Density
SSST	-	Spherical-Shaped Storage Tank
PUR	-	Polyurethane Foam
EPD	-	Environmental Product Declaration
RBS	-	Repurposed Basement Storage
SCC	-	Storage Capacity Cost
ESE	-	Energy Storage Efficiency
CU	-	Capacity Utilisation
CHF	-	Swiss Franc
EOL	-	End of Life
LCIA	-	Life Cycle Impact Assessment
WEEE	-	Waste from Electrical and Electronic Equipment
LCA	-	Life Cycle Assessment
HPC	-	Heat pump Capacity

Contents

1 Introduction

In this chapter, the overall introduction to the topic is provided. The background is explained, together with the problem description. Furthermore, the objectives of this master thesis are explained, followed by the thesis outline.

1.1 Background and problem description

Households in Switzerland are responsible for about a third of the country's total energy consumption, with heating accounting for 82% of that energy usage [1]. Over 50% of families in Switzerland live in multi-family buildings predominantly heated using fossil fuels (70%) [2]. By 2050, to eliminate heating emissions, renewable energy sources must fully meet heat demand [3].

Incorporating sustainable energy sources into the heating sector would significantly contribute to Switzerland's energy goals [4]. Seasonal heat storage technologies must be developed to increase the share of renewable energy, maximise self-sufficiency, and implement the energy strategy 2050 [5]. Furthermore, the European Technology Platform on Renewable, Heating and Cooling identified that Thermal Energy Storage (TES) is one of the critical energy technologies for the exploitation of renewable energy sources in the residential building sector [6].

Seasonal heat storage is crucial in the residential building sector in Switzerland. Examples of these systems include the multi-family sun houses in Oberburg and Huttwil by Jenni Energietechnik AG. Jenni Energietecknik places thermally insulated steel tanks in the middle of the buildings, which solar thermal collectors charge [7]. A study conducted by the Hochschule Luzern, Project OPTSAIS, assessed the optimisation of this type of hot-water seasonal thermal energy storage (STES) combined with solar collectors [8] (see Figure 1 for a system representation).

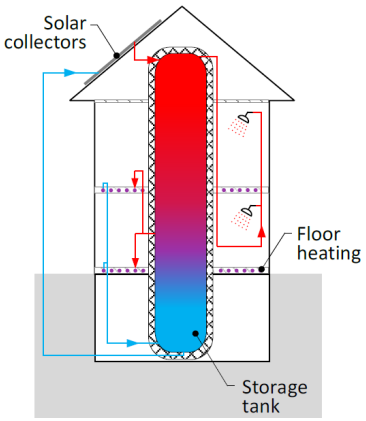

Figure 1: System representation of the OPTSAIS system [8].

This study identified that this type of TES has several disadvantages, including the loss of living space, unwanted additional heating of the building in summer due to heat losses from the storage tank, and inflexibility due to the absolute dependence on solar energy. The Project OPTSAIS also revealed that the 'Levelised Cost of Heat' (LCOH) for such sensitive seasonal heat storage is high [8]. One of the main cost drivers for the LCOH is the expensive living space occupied by the tank, as this is very expensive in Switzerland.

As a direct follow-up on the findings of the OPTAIS project, the HSLU started a new project, HyTES,

to explore a different heating system combined with STES to heat Multi-Family Houses (MFH). This heating system overcomes these disadvantages previously identified in the OPTSAIS project [9]. The new system generates heat using a Heat Pump (HP), mainly powered by photovoltaics (PV), but when needed by the electricity grid. This gives more flexibility in case of a bad year for solar power as it can always use grid electricity, reducing the need for an oversized system to compensate for the worst-case scenarios.

Furthermore, it uses a hybrid STES (HyTES), combining sensible and latent heat storage. Sensible heat is stored in water, and latent heat in encapsulated Phase Change Material (PCM). This reduces the storage volume since PCM has a much higher energy density. Instead of placing the STES in the building, the hybrid STES is placed underground, eliminating the loss of living space and the unwanted heating in the summer. The system is completely explained in subsection 2.1.

Goal of HyTES project
The main goal of the HyTES project is to find the optimal configuration for the HyTES system with lowest LCOH. The main boundary conditions for this goal are that the self-sufficiency of space heating and domestic hot water delivery must be in the range of 70 - 100%, and the system must be applicable for a representative Swiss Multi-Family House in Bern. This house is specified as an eight-apartment building with 20 residents.

To explore the hybrid sensible-latent design and its different scenarios, a comprehensive model is built in C++. An optimiser is implemented on top of that model to find the optimal configuration for the HyTES system. subsection 2.2 further explains the simulation and optimisation part of the HyTES project.

1.2 Thesis objective and research questions

Even though the comprehensive HyTES model can already completely simulate the system, including associated costs and self-sufficiency, the model must still include a calculation method to determine the system's carbon footprint to estimate its alignment with the 2050 energy strategy [3]. Furthermore, an analysis is still needed to execute the optimisation. This analysis determines the specific Key Performance Indicators (KPIs) used in the multi-objective optimisation function, the optimisation variables, and their realistic ranges (optimisation constraints).

Therefore, this thesis aims to present a complete strategy to optimise the HyTES system without executing the final, time-consuming optimisation itself, but it will provide initial results focusing on one type of tank. Several sub-goals can be derived based on this objective:

- Formulate the complete optimisation objective function.
- Determine the relevant optimisation variables of the system (e.g., storage size, amount of PV, heat pump power) and their optimisation ranges.
- Expand the existing model to consider the system's carbon footprint in the optimisation.
- Provide preliminary optimisation results on one tank type.

1.3 Report outline

The HyTES project is further described in chapter two. Chapter three presents a literature review, including the state-of-the-art on the used technologies and optimisation strategies. Chapter four describes the methodology with the multi-objective optimisation workout, and chapter five presents

the workout to include the system's carbon footprint in the optimisation process. The results are shown in chapter six, which consists of a sensitivity study into the optimisation variables, determination of normalisation factors, and initial optimisation of the HyTES system with a Vacuum Insulated Tank. The work presented is then discussed in chapter seven, looking at the added value and accuracy, reflecting, and thinking about future steps and recommendations for the HyTES project. Finally, chapter eight concludes the report.

2 The HyTES project

In this chapter, the workings of the HyTES project are explained further. This gives a better insight into the HyTES system and how it is simulated and optimised.

2.1 System description

As mentioned before, the system combines a Hybrid STES, PV, and a heat pump to provide space heating and domestic hot water services to a multi-family house (see Figure 2). The building's consumption is mapped using typical consumption profiles (heating and domestic hot water and electricity requirements). Heat losses via the storage wall are also taken into account.

The building's PV system serves as the entire system's primary energy source, powering the residents' electricity needs and the heat pump. The electricity grid supplements the PV system if there is insufficient power.

A 3/2-way valve controls the heat sink of the heat pump, which directs a heat flow of 65°C to the DHW TES or a 50°C heat flow into the underground thermal storage tank (the HyTES tank). The HyTES tank and the Domestic Hot Water Tank (DHW TES) are separate tanks due to the requirements from DHW to prevent legionella in drinking water systems. The minimum DHW temperature in the storage tank can vary from 55-58°C [10], and by separating the tanks, the HyTES tank can stay at a lower temperature than the DHW temperature standard. This approach minimises the losses in the HyTES tank over long periods and gives more flexibility for the independent operation of both services. By keeping the DHW TES as sensible heat storage, it is able to deliver the high power desired for DHW, compared to a system with latent heat storage. The DHW tank can be placed somewhere in the building, while the HyTES tank is underground.

The heat pump's heat sink is used first for DHW, then for Space Heating (SH), and finally for loading the HyTES tank. To minimise energy and exergy losses, the heat pump and PV directly supply the necessary energy for DHW and space heating whenever possible. The heat source is the outside air, which makes the heat pump an air/water heat pump.

The heat flow goes through the HyTES and directly to the space heating for space heating delivery. The space heating needs a minimum temperature of 40°C, also considered the minimum temperature of the HyTES. The maximum temperature of the HyTES tank is 50°C, enough for the PCM to melt (Sodium-Acetate Trihydrate based PCM, melt temperature 48°C) but as low as possible to minimise heat losses.

The DHW system begins by using cold tap water that is pre-heated with the HyTES tank through a heat exchanger (HEX 1, in Figure 2). A coupling of STES and DHW TES saves the heat pump from heating cold tap water to a high-temperature level. It also allows for the DHW TES to be charged by the HyTES tank, which in turn is charged with solar power, as opposed to the possibility that the heat pump has to charge the DHW TES on grid electricity fully.

After pre-heating, it flows to the DHW TES or is mixed with the existing DHW to maintain the maximum temperature of 60°C of the DHW (in case the DHW TES is fully charged to 65°C). The DHW TES is further heated to a minimum of 55°C (and a maximum of 65°C) by the heat pump via another heat exchanger (HEX 2).

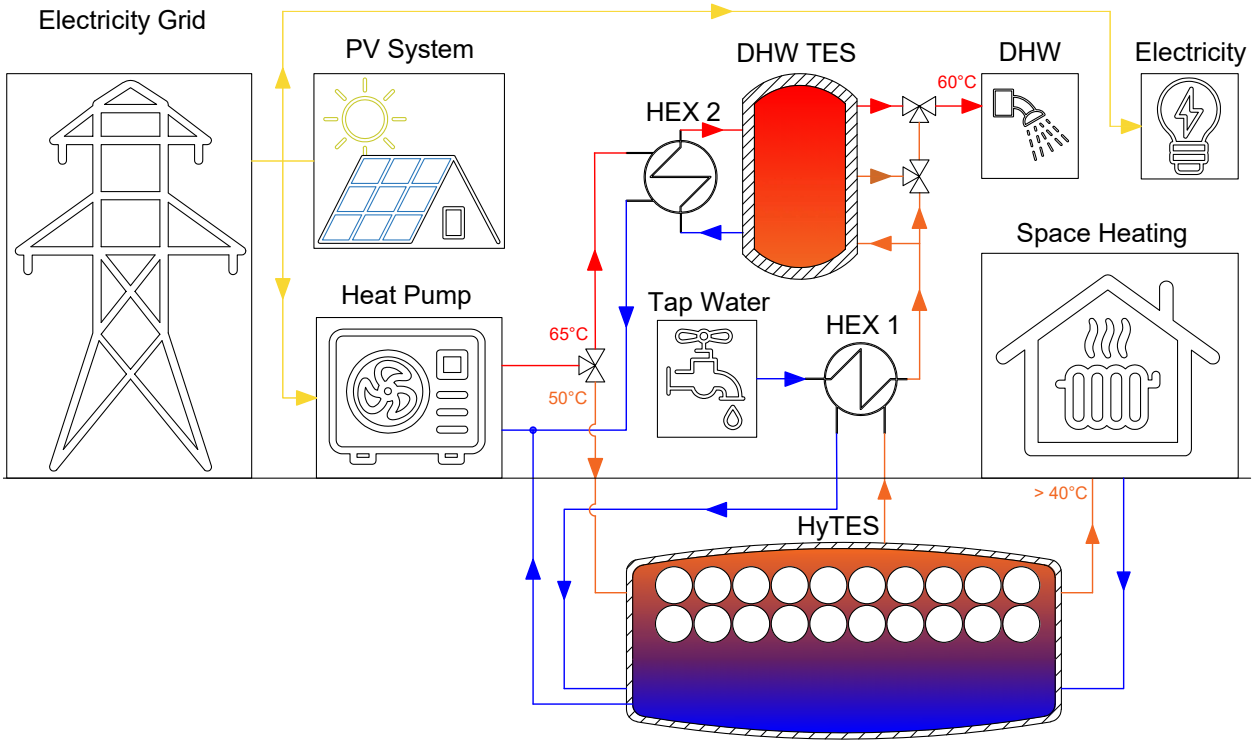

Figure 2: Complete system representation of the HyTES project.

In the event of insufficient energy in the storage (increased heat demand or low solar yield), the shortfall can be compensated for by drawing from the main power grid through the existing heat pump, eliminating the need for an oversized heating system or alternative backup solutions. Moreover, an underground storage tank removes the cost of occupying living space. Excavation costs, however, increase with increasing tank height, particularly in buried storage tanks, emphasising the need to reduce the storage volume [8].

Encapsulated PCMs are incorporated in a sensible heat storage system to reduce storage volume and heat losses (creating the HyTES tank). PCM changes phase at a constant temperature, releasing or absorbing latent thermal energy. This phase change allows storing energy in a slight temperature difference and a low maximum temperature, making using a heat pump very interesting. Depending on the system configuration, introducing PCM capsules in a sensible storage system can achieve volume reductions of up to a factor of two to five with the same storage capacity [11].

Since seasonal storage systems do not require high thermal power, these storage systems can use large capsules. Using large capsules positively affects the encapsulation or PCM cost/encapsulation cost ratio. Salt-hydrate-based PCMs are available in bulk quantities at low prices, making cost-effective and competitive seasonal storage systems potentially feasible if the PCM is chosen correctly [12].

The proposed design aims to improve traditional solar thermal systems by providing greater flexibility and reliability in energy supply throughout the year.

Different underground storages
This project considers three different scenarios of underground storage placement. These scenarios involve a long Cylinder-like double-walled vacuum-insulated tank (VIT), a spherical storage tank made of glass-fibre-reinforced plastic (GFRP), and a basement space repurposed for TES using advanced waterproof thermal insulation material (swissporXPS), as depicted in Figure 3.

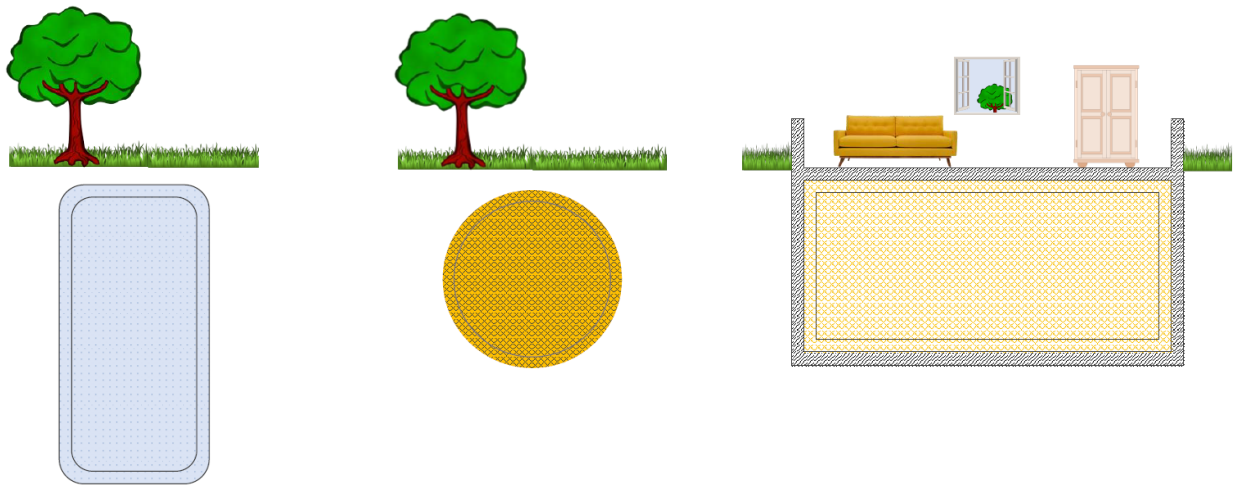

(a) Scenario 1: Vacuum insulated storage

(b) Scenario 2: Spherical-shaped storage

(c) Scenario 3: Repurposed basement storage

Figure 3: Underground storage scenarios that are considered within HyTES [12].

2.2 Simulation and optimisation

The comprehensive model built in C++ consists of a system model itself (as described in subsection 2.1), an optimiser software and a pre-and post-processing module (see Figure 4).

System modeling
A system of differential equations is utilised to describe the complex dynamics of each physical component and their intimate interaction [8]. Ordinary differential equations with time-dependent component variables are employed to model the PV module and the heat pump. Coupled energy conservation equations are used to model the thermal hybrid energy storage. The partial models are interconnected to enable data transmission. Included in this modelling is the calculation of the LCOH, which considers the investments and operational costs for the system, considering a lifetime of 20 years. Besides costs, available subsidies and the Swiss feed-in tariff for supplying back electricity from PV are included. The system model has undergone comprehensive validation employing various methods by the original authors [12].

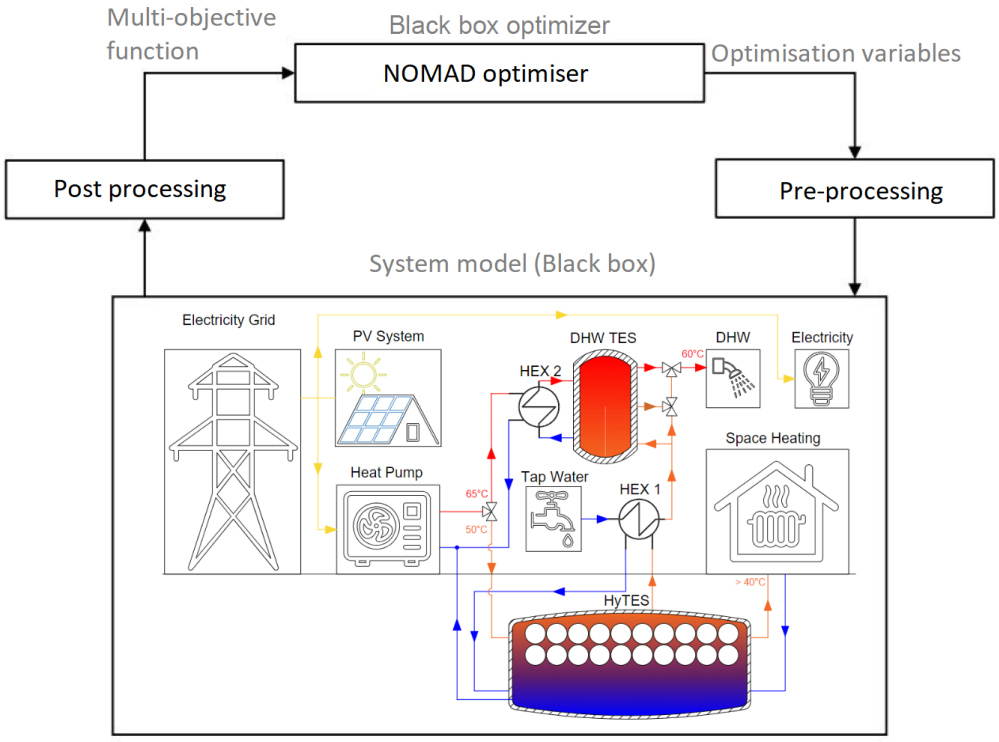

Figure 4: Operation of black box optimiser

Optimiser

To find the optimal configuration for the HyTES system, NOMAD (Nonlinear Optimisation by Mesh Adaptive Direct search), a black box optimiser, is implemented. The NOMAD software utilises simulation-based optimisation techniques for tackling various optimisation problems [13]. It is very suited for black-box optimisation, where the function's inner structure is unknown to the optimiser. This feature makes NOMAD particularly suitable for resource-intensive computer simulations, which often involve complex, non-smooth, or discontinuous functions lacking easily exploitable properties such as derivatives.

NOMAD's optimisation objective is defined by a function of relevant KPIs, which are combined as a weighted sum. The KPI functions can be represented as $f_i(x)$, and each of the functions is the specific calculation of that KPI (e.g. LCOH or carbon footprint). The specific KPIs used in the multi-objective optimisation function are determined in subsection 4.1.

The goal is to minimise the multi-objective function's value while observing given constraints. Mathematically, this optimisation problem is presented in Equation 1, where the optimiser aims to find the minimum value over a defined solution space ('Ω'). This space contains solutions x satisfying specific conditions detailed in Equation 2, defined by constraint functions $c_j(x)$ (see Equation 3), each of which should be less than or equal to zero ($c_j(x) \leq 0$). During the HyTES optimisation, the constraints are formed by the ranges of the optimisation variables. The functions $f(x)$ and $c_j(x)$ are evaluated through computer simulations to solve the optimisation problem.

$$\min_{x \in \Omega} F(x) = (f_1(x), f_2(x), \ldots, f_i(x)) \tag{1}$$

Where the solution space Ω is defined as:

$$\Omega = \{x \in X : c_j(x) \leq 0, j \in J\} \subset \mathbb{R}^n, F, c_j : X \to \mathbb{R} \cup \{\infty\} \tag{2}$$

Furthermore, j is any number in the set:

$$j \in J = \{1, 2, \ldots, m\} \tag{3}$$

NOMADs algorithm optimises by iteratively generating and refining meshes of varying dimensions, discretising the design space for efficient exploration. The algorithm evaluates each mesh point representing potential variable values to identify the optimal solution. the algorithm operates in two main stages: "Search" and "Poll". The Search stage enhances the current optimal solution by identifying beneficial mesh locations. The Poll stage generates trial mesh points near the current best solution, underpinning convergence analysis. This robust method allows NOMAD to effectively navigate complex optimisation scenarios involving non-smooth, non-convex, or discontinuous functions and uncover optimal solutions.

Pre- and post-processing

The optimisation process incorporates a multi-optimisation function to determine the sizes of optimisation parameters, which are then passed to the pre-processing stage. Pre-processing generates the required input .txt-files for the system model. Subsequently, the system model simulation is initiated. The termination criterion for the optimisation process can be defined as achieving a "steady state" or reaching a maximum predefined annual repetition limit. In this context, steady state refers to the condition where the difference in energy content of the storage system at the end of a year, compared to the energy content at the beginning of the same year, does not surpass a specific threshold. If the threshold is exceeded, another year is simulated, with the temperature distribution in the storage tank at the beginning of the year set to match the distribution at the end of the previous year. Once the simulation of the system model is completed, post-processing commences. Post-processing utilises the available data to compute the optimisation objective, which is then returned to NOMAD. Subsequently, a new optimisation pass is initiated. The optimisation process terminates when either an optimal solution is found, or a predetermined number of passes has been completed.

3 Literature review

The literature review provides insights into the hybrid latent-sensible heat storage and multi-objective optimisation in energy systems.

3.1 Hybrid Latent-Sensible Heat Storage Technologies

Hybrid Thermal Energy Storage combines Sensible Heat Storage (SHS) and Latent Heat Storage (LHS), offering potential solutions to the constraints of these individual methods. The following sections delve into the development of hybrid latent-sensible heat storage. A summary of the examined papers can be found in Table 11 within Appendix A.

Encapsulated PCMs in Water Tanks
Nallusamy et al. (2007) demonstrated that an integrated system incorporating spherical capsules of PCMs and water in an insulated tank surpassed conventional SHS performance [14]. Further research confirmed the effectiveness of this approach for solar-powered domestic hot water systems [15]. Frazzica et al. (2016) experimented with this system on a smaller scale, finding an up to 13% increase in heat storage capacity compared to standard SHS [16].

Double-Packed Bed Storage
This approach employs solid materials for sensible heat storage and encapsulated PCMs for latent heat storage within a packed bed. The heat transfer fluid (HTF) during charging or discharging is air. Adding a small amount of encapsulated PCM on top of the sensible packed bed already stabilises the outlet temperature of the HTF during discharging. It increases energy accumulation compared to SHS systems [17]. Geissbuhler et al. (2016) studied industrial-scale high-temperature (e.g. concentrated solar power storage). They found that combining steel-encapsulated Aluminium silicon alloy (AlSi12) with a packed bed of rocks reduced material costs for a maximum outflow temperature drop during discharging, achieving high exergy efficiencies and low material costs [18]. Suresh et al. (2021) designed a novel system using concrete spheres as sensible storage media and paraffin-encapsulated capsules as latent heat storage media to reduce thermocline degradation in one-tank storage systems, see Figure 5a [19].

Tank-in-Tank Storage
This method combines water and sodium-acetate trihydrate as PCM within a tank-in-tank system. The strategic placement of the PCM has shown a stabilising effect on tank temperatures [20, 21]. Lafri et al. (2019) investigated two different positions (either in the inner core or at the outer walls) for placing the PCM in the storage tank. They found that the PCM at the lateral position of the tank configuration had more molten PCM than the PCM at the centre of the tank configuration [21]. A variant of this system featuring an internal spiral heat exchanger within the PCM tank was proposed by Englmair et al. (2020) [22]. The research suggested intermittent discharge through the mantle to overcome heat transfer limitations, yielding a more consistent outlet temperature.

A. Frazzica et al. (2023) did the most recent study on hybrid TES [23]. They developed and experimentally characterised an innovative tank-in-tank hybrid sensible-latent thermal energy storage system for DHW provision in residential buildings. The system design is a tank-in-tank architecture, integrating macro-encapsulated commercial PCM inside vertical rods in the external tank for DHW provision. The results showed that the developed configuration could increase the energy storage capacity and corresponding DHW provision by up to 16%. The study provides evidence of the

potential benefits of combined latent-sensible heat storage as a tank-in-tank hybrid system for DHW provision in residential buildings.

Inverted Shell-and-Tube Configuration

Zauner et al. (2017) proposed a novel design that uses a commercial shell-and-tube heat exchanger with PCM encapsulated within the tubes and thermal oil as the sensible heat storage and heat transfer medium [24]. The prototype demonstrated a satisfactory correlation between experimental findings and computational models.

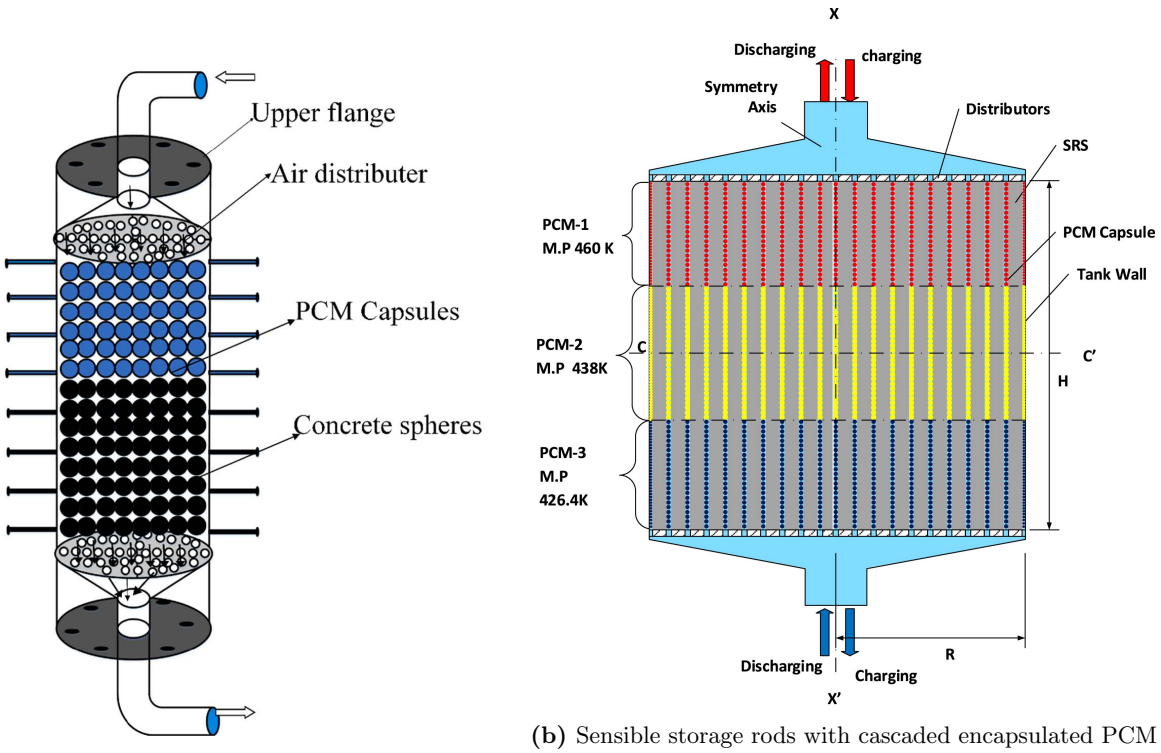

(a) Double packed bed storage [19].

(b) Sensible storage rods with cascaded encapsulated PCM storage [25].

Figure 5: Schematic representation of different researched system designs.

Solid Rods and Encapsulated PCM

Ahmed et al. (2019) and (2020) introduced a hybrid system combining sensible heat storage in solid rod structures and PCM capsules interspersed between the rods [26, 25]. A further innovation was using cascaded PCM with different melting temperatures along the tank height, offering an efficient and cost-effective solution [25].

Latent Rods in Sensible Storage Tank

Pop et al. (2021) assessed the thermal performance of large latent rods in a sensible storage tank, observing a 25% reduction in nominal tank volume while maintaining the required temperature [27]. Subsequent studies by Frazzica et al. (2022, 2023) on a hybrid system integrating PCM macro-capsules in vertical rods achieved increased energy storage capacity [28, 23]. Using PCMs in combination with sensible heat storage systems can be a promising solution to enhance the thermal performance of DHW systems, leading to significant reductions in storage volumes and increasing energy storage density.

Overall, these hybrid latent-sensible heat storage technologies enhance thermal performance, thus significantly reducing storage volumes and boosting energy storage density. However, this literature review reveals a research gap in the seasonal application of hybrid TES systems, underscoring the novelty and potential of the HyTES design. To the best of the author's knowledge, this confirms that the HyTES design is working in a gap in the literature.

3.2 Multi-objective optimisation in energy systems

This review targets recent multi-objective optimisation applications in energy system design with STES, highlighting the relevant optimisation variables and key performance indicators (KPIs).

S.K. Shah et al. (2020) employed multi-objective optimisation for STES, focusing on minimising life cycle costs (LCC) and Green House Gas Emissions (GHGE) [29]. They incorporated carbon trading and considered future carbon pricing. They used the optimisation variables of solar collector area (SCA) and borehole length (BHL). Through multi-objective optimisation, they simultaneously minimised life cycle cost and GHGE, illustrating a trade-off between them through a Pareto front. A Pareto front represents the collection of all Pareto-efficient solutions, which implies that an optimal solution is achieved for a particular weighting of individual objectives, where no action or allocation can improve one individual's situation without harming another. The study reveals that a decrease in GHGE costs leads to an increase in LCC, with the opposite trend also true.

Siraganyan et al. (2019) optimised a decentralised Energy System in Geneva using three KPIs: Levelised Cost Of Energy (LCOE), self-sufficiency, and carbon footprint [30]. The optimisation was carried out by varying scenarios with different types of technology, resulting in four scenarios with varying capacities. The study found that the grid price, the battery, and the solar PV investment cost reduction had the most significant impact on the LCOE out of all input variables.

V. Tulus et al. (2016) used a multi-objective approach to design a central solar heating plant with seasonal storage (CSHPSS), integrating TRNSYS software and GenOpt optimisation algorithm [31]. The decision variables included the solar collector's aperture area ratio to the total heating demand and the storage tank volume ratio. The goal was to optimise economic (net present cost) and environmental (aggregated impact factor) objectives. The authors used LCA principles to assess the environmental objective on all fronts, which measures the impact caused at every stage in the energy system's life cycle.

A set of Pareto points answered the multi-objective problem, representing the optimal trade-off between economic and environmental objectives. The extreme points of this Pareto frontier are the so-called anchor points, which correspond to the individual minimum of each objective. The authors calculated the Pareto solutions via the weighted-sum method, which relies on formulating an auxiliary single-objective model that optimises a linear weighted sum of the original objectives [32].

The weighting method assigns weights to the environmental impact (k) and cost (1-k) objectives, enabling control over the trade-off between the two. The Pareto frontier in Figure 6 was generated using a range of k values from 0 to 1, in increments of 0.1.

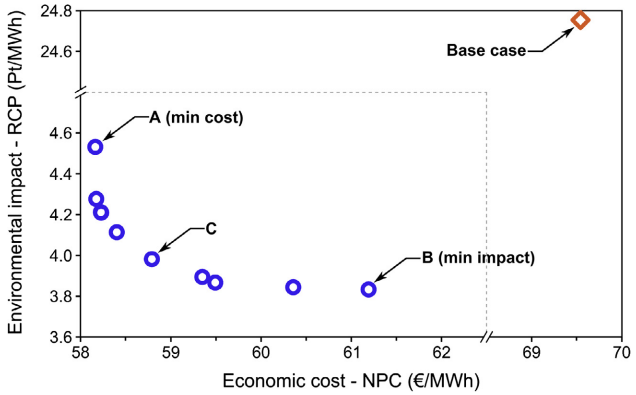

Figure 6: Pareto set of optimal configurations of a CSHPSS plant [31]. Anchor points A and B are the minimum cost and minimum impact solutions, respectively; solution C is an intermediate CSHPSS design obtained with k = 0.5; the base case represents a conventional heating system.

F. Pelella et al. (2023) optimised a residential heat pump system that uses various sources (air/sun/ground) and thermal storage (either water or PCM), using a genetic algorithm to maximise the seasonal coefficient of performance (SCOP) and minimise investment costs [33]. Variables such as the volume of the storage tank, surface area of solar thermal and photovoltaic collectors, surface area of heat exchangers, electric battery capacity, presence of a geothermal heat exchanger, type of storage tank (water or PCM), and PCM melting temperature. The objective was to achieve the highest SCOP and the lowest investment costs. The optimisation results show the investment costs versus the seasonal coefficient of performance and Pareto fronts for each climate condition studied; see Figure 7 for one example graph.

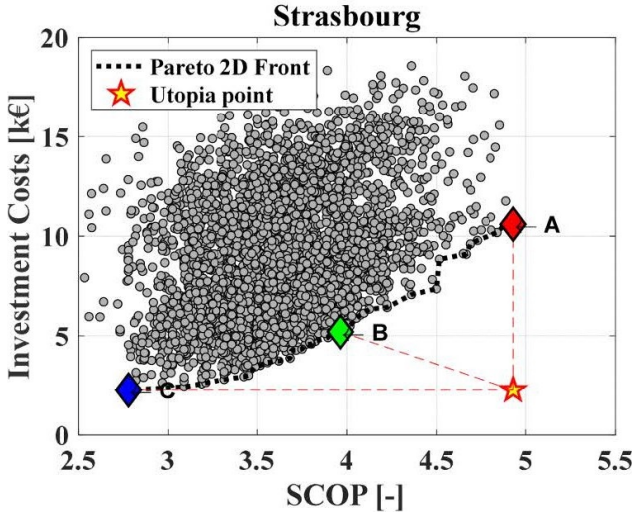

Figure 7: Results from Pelella et. al. [33], The comparison between the costs of investing and the SCOP for Strasbourg plotted with the Pareto front. Point A signifies the solution with the least investment cost, point C represents the solution with the highest SCOP, and point B represents the solution closest to the Utopia point, which is depicted as a star.

In conclusion, these studies highlight the efficiency of multi-objective optimisation in enhancing energy systems design, considering several optimisation variables and KPIs simultaneously. Various

indicators such as LCC, GHGE costs, LCOE, self-sufficiency, and SCOP were utilised. The Pareto front was a standard tool to display trade-offs between economic and environmental objectives. One study also used carbon pricing to optimise Green House Gas emissions [29].

4 Methodology Multi-objective Optimisation

This chapter presents the desired multi-objective optimisation strategy for the NOMAD optimisation in the context of the HyTES project. It discusses the relevant KPIs, and the weighting method for the objectives, presents the complete optimisation objective, and selects the optimisation variables. Lastly, it describes a base case to compare the results.

4.1 Key performance indicators for optimisation

To define the optimisation objective, it is crucial to identify the appropriate KPIs that align with the goals of the HyTES project. The primary goal is to optimise seasonal storage for minimal system costs while maintaining a self-sufficiency range of 70-100% for DHW and SP. Additionally, reducing carbon emissions in Switzerland is crucial to achieving the 2050 goals to eliminate heating emissions [3].

System costs
The LCOH is a standard KPI used to measure the average cost of generating a unit of energy over the system's lifetime. It considers all costs associated with the system, including construction, operation, maintenance, and grid electricity. In the context of the HyTES project, the LCOH is expressed in Swiss Francs per unit of heat (CHF kWh^{-1}).

Self-sufficiency
The client has set self-sufficiency as a boundary condition for optimisation, ranging between 70% and 100%. Self-sufficiency refers to thermal Self-sufficiency, defined as the percentage of energy supplied by the system's generation without relying on the external grid. In the case of HyTES, it includes all PV-generated electricity used for heat generation by the heat pump. Excess PV electricity fed back to the grid is excluded. Self-sufficiency can be calculated by dividing the heat generated with PV electricity by the total heat demand.

Increasing self-sufficiency requires increasing the capacity variables, such as PV panels and storage capacity, possibly resulting in higher system cost and carbon footprint. However, it decreases grid electricity usage, associated costs, and the carbon footprint of grid electricity. This gives no apparent desired direction for self-sufficiency (either towards 70% or to 100%), as it has counteracting consequences.

Since the client also only specified the range and not whether higher or lower is desirable, it is proposed to aim for a variable self-sufficiency to address the entire range of self-sufficiency in the optimisation. Multiple optimisations will run; each optimisation is aimed at a different self-sufficiency level (between 70% and 100%). This will generate multiple separate optimised systems, each optimised for minimising the other KPIs and a preferred self-sufficiency level. How this is archived is elaborated further in Equation 4.2. The client can then evaluate the results of the various run based on the archived value of the KPIs and corresponding SS to determine which combination is most preferred.

Carbon Footprint
To align with the project's goal of reducing Switzerland's carbon footprint, it is essential to include the system's GHGE in the optimisation and aim for the system with the minimum GHGE. This approach directly incorporates environmental considerations into the system optimisation.

GHGs encompass various gases, including CO_2, nitrogen oxides (NO_x), methane (CH_4), and fluorinated gases (refrigerants), among others. To provide a unified measurement, the Global Warming Potential (GWP) is used, which quantifies the greenhouse effect of a specific gas compared to CO_2 in a 100-year time frame [34]. Therefore, the GWP is expressed in kg CO_2-equivalent ($CO_{2\text{-eq}}$). GWP serves as an indicator to compare and evaluate the environmental impact of different technologies, contributing to the assessment of sustainability and "green" qualities. In section 5, a model implementation for estimating the systems GWP is explained.

To facilitate a comparative assessment with the LCOH, the carbon footprint can also be expressed in monetary units. This can be achieved through carbon pricing, as demonstrated in the study by V. Tulus et al. [31]. Carbon pricing attaches a cost to greenhouse gas emissions, incentivising emission reduction efforts. In Switzerland, the government has implemented a Carbon pricing system, with a fixed price of 120 Swiss Francs (CHF) per tonne of CO_2 as determined by the Federal Office of Environment. This price can be utilised to express the GWP of the system in monetary terms. To fully align with LCOH, the GWP in CHF should also be divided by the total generated heat, enabling measurement in the same unit (CHF kWh^{-1}).

4.2 Weighting factors of Key Performance Indicators

Weighting plays a crucial role in multi-objective optimisation functions as it allows the expression of preferences and priorities among competing objectives. Assigning weights depends heavily on the client's preferences [35].

To accommodate the NOMAD optimisers' requirement of a single-function problem, the weighted sum method is used, which represents multiple objectives as a single function. The single objective function is constructed by summing objective functions f_i multiplied by weighting coefficients w_i, as shown in Equation 4. These coefficients are mathematically defined in Equation 5.

$$\min_{x \in \Omega} F(x) = \sum_{i=1}^{j} w_i \cdot f_i(x) \tag{4}$$

$$w_i \geq 0, \forall i = 1, \ldots, j \text{ and } \sum_{i=1}^{j} w_i = 1 \tag{5}$$

Weights are assigned based on the decision-maker's knowledge of the problem. However, a weighting factor should also contain normalisation to ensure fair consideration. The combined weighting factor is described as Equation 6, where p_i represents the assigned weights and θ_i denotes the normalisation factors [36].

$$w_i = p_i \cdot \theta_i \tag{6}$$

Weighting factors

The weighting factors (p_i) steer the optimisation towards a particular desired outcome. As mentioned earlier, the desired outcomes mainly revolve around a variable SS (between 70% and 100%). In order to set up the optimisation function for various levels of SS, a total weighting factor of 1 (100%) can be divided over weighting factors for the KPIs. By putting a more significant emphasis on the SS, by increasing the SS weighting factor 'p_{SS}', the optimisation results in higher levels of SS.

Determining the appropriate weighting factors in advance is unrealistic, so a parameter sweep of p_{SS} is necessary to find the suitable values corresponding to certain SS levels.

Regarding the optimisation goals for LCOH and GWP, the weighting factors are denoted as p_{LCOH} and p_{GWP}, respectively. The remaining weighting value is evenly split between these two objectives, as shown in Equation 7. This distribution is considered fair since both objectives are expressed in the same unit, and the normalisation factors, θ_i, equalise their magnitudes (explained in the following subsection).

$$\begin{aligned} p_{LCOH} &= \frac{(1 - p_{SS})}{2} \\ p_{GWP} &= \frac{(1 - p_{SS})}{2} \end{aligned} \tag{7}$$

Normalisation factor

The normalisation method described by O. Grodzevich et al. (2006) determines the normalisation factor, adjusted for this specific optimisation [36]. The method exploits variances in optimal function values to define optimisation boundaries by identifying two key points within the solution set: the Utopia and Nadir points.

The Utopia point (U) represents the theoretical best value for each objective. Its components (z_i^U) are calculated using Equation 8, which determines the optimal solution for each objective function (f_i). While the Utopia point is often unattainable due to conflicting objectives, it provides the lower bounds of the Pareto optimal set.

$$z_i^U = \min_x f_i(x) : x \in \Omega \tag{8}$$

Conversely, the Nadir point (N) represents the least favourable outcome for each objective. Its components (z_i^N) are calculated using Equation 9, which finds the maximum values of the objective functions.

$$z_i^N = \max_x f_i(x) : x \in \Omega \tag{9}$$

To find this project's Utopia and Nadir points, the NOMAD optimiser is executed three times, using Equation 10. With $p_{LCOH} = 1$, the optimisation finds the lowest LCOH and its corresponding GWP and SS. Similarly, with $p_{GWP} = 1$, the optimisation identifies the minimum GWP and its corresponding LCOH and SS. Finally, it is run for $p_{SS} = 1$, which finds the highest SS and the corresponding other values. The pinpointing of the Nadir and Utopia points is shown in subsection 6.2.

$$\begin{gathered} \min_{x \in \Omega} F(x) = p_{LCOH} \cdot f_{LCOH} + p_{GWP} \cdot f_{GWP} + (1 - p_S) \cdot f_{SS} \\ \text{for:} \\ p_{LCOH} = 1, p_{GWP} = 0, p_{SS} = 0 \\ p_{LCOH} = 0, p_{GWP} = 1, p_{SS} = 0 \\ p_{LCOH} = 0, p_{GWP} = 0, p_{SS} = 1 \end{gathered} \tag{10}$$

The normalising method leverages the differences in optimal function values between the Nadir and Utopia points to calculate the normalisation factor θ_i using Equation 11. This normalisation scheme ensures optimal normalisation results, bounding objective function values between 0 and 1 (see Equation 12).

$$\theta_i = \frac{1}{z_i^N - z_i^U} \tag{11}$$

$$0 \leq \frac{f_i(x) - z_i^N}{z_i^N - z_i^U} \leq 1 \tag{12}$$

Computing normalisation weights is a process that involves solving optimisation problems to secure specific values. This task, though, can be computationally demanding, especially when dealing with more intricate problem types. Nevertheless, finding exact solutions for each optimisation problem is only sometimes a necessity [36]. Knowing the estimates of Utopia and Nadir points makes it possible to derive suitable normalisation factors. Modifications and relaxations can be utilised to counter the computational burdens. For instance, the parameters of the optimisation solver can be adjusted, like enlarging tolerances or duality gap criteria, to decrease the time taken for solutions. Another method, called 'relaxing constraints', can also be used to ease the computational load. This involves loosening or eliminating 'hard' constraints.

4.3 Complete optimisation objective

The complete optimisation function integrates the KPIs, weighting factors, and normalisation into a single objective function. This function, denoted as $F(x)$, represents the objective to be minimised during the optimisation process. The function is expressed as Equation 13.

$$\min_{x \in \Omega} F(x) = \frac{(1 - p_{SS})}{2} \cdot \theta_{LCOH} \cdot f_{LCOH} + \frac{(1 - p_{SS})}{2} \cdot \theta_{GWP} \cdot f_{GWP} + p_{SS} \cdot (1 - f_{SS}) \tag{13}$$

The optimisation Equation 13 encapsulates the multi-objective nature of the problem, providing a comprehensive representation of the objectives and their relative importance. The NOMAD optimiser uses this function to iteratively search for the optimal solution that minimises the overall objective, considering the trade-offs between LCOH, carbon footprint, and self-sufficiency.

4.4 Optimisation variables

The optimisation process involves a variety of variables, each influencing the system's overall performance. These variables are adjusted through an iterative process until the optimiser determines the system configuration that optimally satisfies the multi-objective function. As described in section 2, the model used for simulation is an extensive model with numerous parameters. Despite the sheer number of these parameters, most cannot be manipulated as they are present in the model (examples include PCM-related parameters, component specifications, lifetime, financial parameters, and building-related parameters) or are internally computed (such as PCM packing density, thermal losses, and the heat pump's Coefficient of Performance).

It is essential to keep the number of variables as small as possible, given that optimisation run time tends to increase with the number of variables exponentially. The following possible optimisation variables are identified:

- HyTES tank type
- HyTES size (Height, Diameter)
- PCM capsules Packed bed size (Starting position, Thickness)
- Minimum HyTES energy level
- DHW tank size (Height, Diameter)
- Amount of PV panels
- PV orientation (Azimuth and Tilt)
- HP power (Electrical)

HyTES tank
Variables associated with the HyTES tank itself consist of the specific type (as discussed in subsection 2.1) and its dimensions (height and diameter).

First, the different tank types, varying in material, shape, and implementation, can yield different operational results. This is because energy losses, PCM capsule packing density, tank costs and GWP depend on the storage tank type. Further, the tank's dimensions significantly impact the thermal energy storage for space heating and preheating domestic hot water while also influencing the degree of heat losses.

The burial depth mainly limits the optimisation range for the dimensions of the HyTES. The burial depth and thus the height of the reservoir is limited to 4 m because, from this depth, the burial costs rise disproportionately [8]. The width of the HyTES is also a limiting factor, as the types of tanks each have their height and width ratios. As it is impossible to simulate the system with multiple tanks to consider their individual dimensions limits, it is chosen not to limit the HyTES tank width based on the height and width ratio commonly found with these tanks. This way, the optimisation can give the optimised storage volume it needs. Therefore the maximum range for the height of the HyTES is 4 m, and the width is assumed at a diameter of 10 m. This width is used for the initial runs; based on the results of the initial runs (see section 6), the maximum could be increased, or the range can be decreased.

PCM capsules packed bed
The PCM capsules packed bed in the HyTES tank can also be variated. This is done by variating at which vertical level of the HyTES tank the packed bed starts and which thickness the packed bed has (see Figure 8). This, for example, could mean that the bottom 50 % of the HyTES tank is filled with PCM capsules; the rest would be only sensible storage. It could also occur that the middle is filled and that the filling starts at, for example, 10% of the total height from the bottom and ends 20% from the top.

The starting point of the PCM is defined as the centre of the packed bed ($start_{PB}$) relative to the total height of the HyTES tank, and the thickness of the best is indicated as $Thickness_{PB}$ also relative to the total height of the HyTES tank.

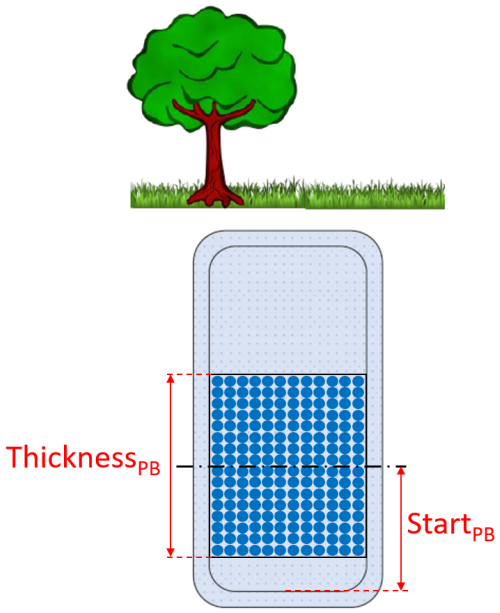

Figure 8: Definition of packed bed variables

Both $start_{PB}$ and $Thickness_{PB}$ can be variated for the complete height of the HyTES tank (0 til 100%). However, the $Thickness_{PB}$ is restricted as described in Equation 14 so that the packed bed will not exceed the tank at the bottom or the top.

$$\begin{aligned} For: 0\% \leq start_{PB} \leq 50\% \Rightarrow \\ Thickness_{PB} \leq 2 \cdot start_{PB} \end{aligned}$$
$$\begin{aligned} For: 50\% \leq start_{PB} \leq 100\% \Rightarrow \\ Thickness_{PB} \leq 2 - 2 \cdot start_{PB} \end{aligned} \tag{14}$$

Minimum HyTES energy level

The HyTES system has a control system, a safety measure to ensure enough heat is always available. When the tank reaches the minimum allowed energy storage level ($\leq$ 10% of maximum storage capacity) in the HyTES tank, the system is forced to recharge to a certain energy level again, using grid electricity. This makes sure the system has enough energy again to supply its demand. To which energy level the system recharges again depends on the system and, therefore, a suited variable to optimise. The variable is a relative value to the total amount of storage capacity.

It was found during multiple previous optimisation runs that the range of the variable is best to be kept between 10% and 40% as any recharge level above 40% prohibits the model from reaching a steady state. This is due to how the model checks for a steady state, which compares the total energy content of the HyTES with the previous year. As long as this is not equal, the model simulates another year. When a recharge level above 40% is chosen for the simulation, the energy content of the HyTES keeps oscillating while never reaching a steady state.

DHW TES

The optimal DHW TES size can significantly influence the total needed HP power, as the peak DHW demand can be fully supplied from the DHW TES if sized correctly. Besides the peak demand, a smaller DHW TES might lead to a more significant reliance on the heat pump (preheated by the HyTES tank) during low solar power periods, necessitating grid electricity.

For the range of the DHW TES, the average DHW consumption and the product catalogue of a DHW TES supplier are used. In Switzerland the average DHW consumption per resident is about 50 l of hot water at 60 °C per day [10]. The reference building has 20 residents, so they consume 1 m^3 pf DHW of 60°C (same temperature as the DHW TES) combined. According to the product overview of the DHW TES builder 'Sirch', this translates to a tank with a height of 2 m and a diameter of 0.8 m [37]. However, it is more likely that the tank needs to be more significant because the consumption and charge profiles might not be in optimal relation. Besides that, as the DHW is discharged, the temperature can decrease, requiring more water than the exact amount. As the DHW TES in the HyTES system is coupled with the HyTES tank, it is also possible that the optimal size might be slightly less. Therefore, the ranges of the DHW TES are assumed to be the same as the ranges of the standard DHW TES tanks of Sirch [37]. The minimal tank is 0.5 m^3 or (h x d) 1.7 x 0.5 m, and the maximum size tank is 5 m^3 or 2.2 x 1.8 m.

PV system

As the primary energy supplier, the PV system has several potential optimisation variables. However, the model's authors already fixed the specifics of the PV panel itself beforehand (Suntech Ultra S mini [38]). In Table 1, the main properties of the panel are shown.

Table 1: Overview of properties of Suntech Ultra S mini [38].

Properties	**Value**
Maximum Power [kW_{peak}]	380
Efficiency [%]	20.8
Solar cell [-]	Monocrystalline silicon
Height [mm]	1756
Width [mm]	1039
Thickness [mm]	35
Weight [kg]	20.3

Thus, the possible optimisation variables are the number of panels used and the panel orientation, both the Azimuth (horizontal angle, ϕ) and the tilt (vertical angle, α). The number of PV panels directly indicates the system's power capability. An increase in panels converts more solar energy into electricity, enhancing the system's energy self-sufficiency. Nevertheless, it also adds to the system's cost and GWP, necessitating a balance.

PV panel orientation plays a pivotal role in maximising solar energy capture. The location dictates the optimal orientations depending on local climate conditions, solar path, and the sun's angle throughout the year. Therefore, finding the ideal orientation ensures optimal utilisation of the PV system across all seasons. The Azimuth and the tilt can be adjusted since the MFH used for the HyTES project is considered to have a flat roof. This was determined in the OPTSAIS project, where this reference building was already specified. The study's building features analysis relies on information from the 'Swiss Federal Statistical Office' and the building guidelines from the Bern

and Zürich cantons [8]. The authors specified that the average MFH has a flat roof with a total available roof area of 264 m^2. This total available roof area also determines the maximum number of panels (Max_{PV}) that can be used in the system.

However, the maximum amount of panels and the panel orientation also depend on each other. This is due to their shade when placed at a tilt angle. With an increasing tilt angle, the distance between the rows of panels has to increase to prevent shade for the row in front. This reduces the maximum amount of panels that can be used. This gives it a trade-off; on the one hand, the maximum amount of panels has the most considerable potential to generate electricity. However, the low tilt angle may give a low efficiency during winter when the sun has a low elevation.

On the other hand, an optimal tilt angle for wintertime significantly reduces the maximum amount of panels. In order to properly take this into account, the upper range limit for the number of panels is determined on the Azimuth and Tilt angle, as well as the available roof area (A_{roof}) of 264 m^2. The actual amount of used panels will be a relative value of this maximum, varying from 0 to 100%.

To calculate the upper range limit for the number of panels while considering shade, the maximum allowable PV panels on the roof must be calculated for the December Solstice in Bern, when the solar elevation is at its lowest. In Figure 9, a visual representation is given of the calculation. To determine the maximum allowable PV panels on the roof, each panel's actual needed surface area, including its shade, is needed. The panels are assumed to be placed in a landscape position. The length of the panel (L_{PV}), therefore, is the indicated height in Table 1. The total width of a row of panels (W_{row}) is variable and calculated by Equation 15 [39].

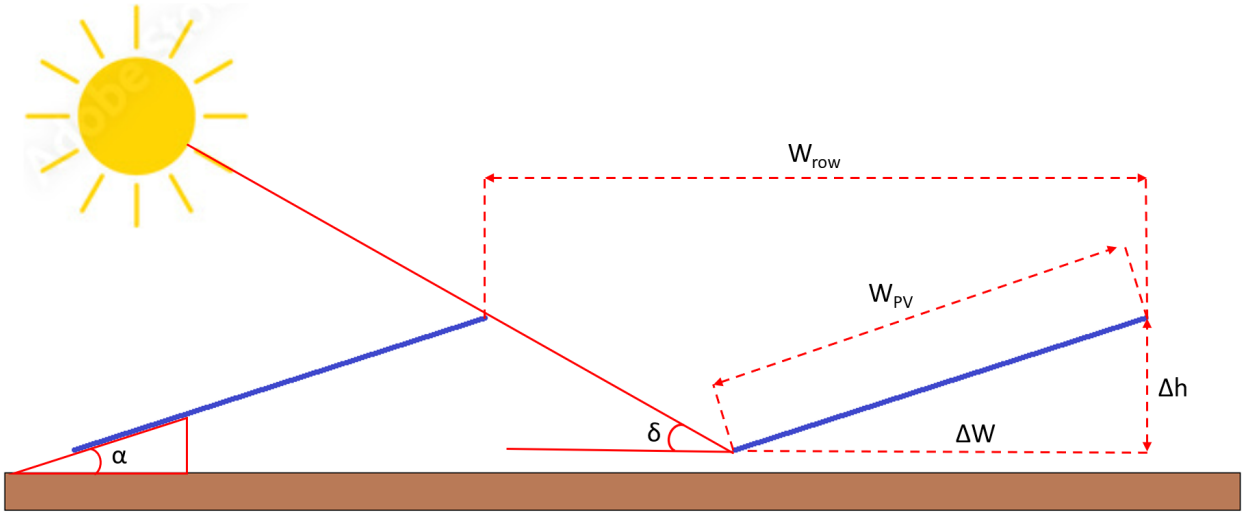

Figure 9: Visual representation of calculating the total row width based on the PV orientation.

In Equation 15, the first half of the first term ($\frac{\Delta h}{\tan \delta}$) calculates the width of the shade thrown by the effective height of the panel (Δh), at the chosen solar elevation (δ). The second half ($\cos(\phi_{PV} - \phi_{solstice})$) takes into account the difference in ϕ between the sun at the minimum elevation (δ) taken into account. As the sun reaches the same height twice daily (dawn and dusk), the minimum elevation (δ) is reached twice at two different azimuths. Therefore, the smallest difference is always taken into account. For example, when the solar panels have an $\phi_{PV} = 210°$, the Azimuth of sun dusk is considered to calculate the difference in azimuth angle.

The second term calculates the PV panel's effective width (ΔW). Combined, they form the total width of a row of panels (W_{row}).

The W_{PV} is the indicated width in Table 1. During the December Solstice, it is assumed that the PV systems need to be out of the shadow between 9 AM and 3 PM, corresponding to a solar elevation (δ) of 10° at the azimuth ($\phi_{solstice}$) of 140° for sun dawn and 220° for sun dusk [40]. The Tilt angle (α) and PV Azimuth (ϕ_{PV}) are two variables the optimiser determines. This is all summarised in Equation 16.

$$\begin{aligned} W_{Row} &= \frac{\Delta h}{\tan(\delta)} \cdot \cos(\phi_{PV} - \phi_{solstice}) + \Delta W \\ &With: \\ \Delta h &= W_{PV} \cdot sin(\alpha) \\ \Delta W &= W_{PV} \cdot cos(\alpha) \end{aligned} \tag{15}$$

$$\begin{aligned} W_{Row} &= \frac{W_{PV} \cdot sin(\alpha)}{\tan(\delta)} \cdot \cos(\phi_{PV} - \phi_{solstice}) + W_{PV} \cdot cos(\alpha) \Rightarrow \\ W_{Row} &= \frac{1.039 \cdot sin(\alpha)}{\tan(10)} \cdot \cos(\phi_{PV} - \phi_{solstice}) + 1.039 \cdot cos(\alpha) \end{aligned} \tag{16}$$

The total width of a row of panels can then be used to calculate the maximum amount of PV panels using Equation 17. In this equation, the roof area (A_{roof}) is divided by the total surface area of a PV panel, including shadow, giving the amount of PV panels based on the Tilt angle and Azimuth.

$$\begin{aligned} Max_{PV} &= \frac{A_{roof}}{W_{Row} * L_{PV}} \Rightarrow \\ Max_{PV} &= \frac{264}{W_{Row} * 1.756} \end{aligned} \tag{17}$$

The range of the Azimuth is derived from the path of the sun. The sun comes up in the East ($\phi = 90°$) and sets in the West ($\phi = 270°$). Therefore, those are also considered the minimum and maximum values for optimising the Azimuth variable. As for the Tilt angle of the panels, this can range from $\alpha = 0°$ to $\alpha = 45°$; otherwise, the shading would become too large during wintertime.

Heat pump

The possible optimisation variables of the air source heat pump are reduced to the max electrical power in the model, indirectly dictating the maximum heat output (together with the internally calculated COP). By varying the electrical power, the model sizes the heat pump on all fronts, influencing factors like cost, GWP, and ability to charge the HyTES tank. Thus, the selected electrical power level affects the system's overall operation.

The initial range of the electric power of the HP is assumed to be from 2 kW to 20 kW. These values are used for the initial runs, and based on the results of the initial runs (see section 6), the maximum could be increased, or the range can be decreased. This range is well within the maximum range of available air source heat pumps [41].

Overview of optimisation variables
In Table 2, all the variables and the corresponding ranges are summarised.

Table 2: Overview of the ranges for the optimisation variables

Properties	**Lower bound**	**Upper bound**
HyTES tank height [m]	1	4
HyTES tank width[m]	1	10
PCM packed bed starting position [-]	0	1
PCM packed bed thickness [-]	0	1
Minimum HyTES energy level [-]	0	0.4
DHW tank height [m]	1.7	2.2
DHW tank width [m]	0.5	1.8
Relative amount of PV panels [-]	0	1
PV Azimuth angle [°]	90	270
PV Tilt angle [°]	0	45
Electrical power HP [kW_{elec}]	2	20

4.5 Base case

To provide better insights into the meaning of the values of LCOH and GWP, it is essential to establish a reference point by comparing these values to a base case. Considering that fossil fuels, mainly fuel oil, are predominantly utilised for heating in multi-family houses, the base case involves comparing the HyTES system against using fuel oil boilers [2].

Levelised Cost of Heat of an oil boiler
An extensive study was performed by M.J.S. Zuberi et al. (2021) about the potential cost of various heating systems in Switzerland's residential areas [42]. Their study showed that the LCOH of different heating technologies for MFH hardly differed throughout the cantons. In Figure 10, they presented an overview of the different investigated heating technologies in MFH in Switzerland for three different residential areas: urban, suburban, and rural. Figure 10 shows the LCOH of an oil boiler to be 0.14 CHF kWh^{-1} for an MFH in an urban area. This study assumed an operational lifetime for the boiler of 20 years. It also has to be noted that this study did not consider the projected increase in oil prices. Therefore, the LCOH of 0.14 CHF kWh^{-1} could be considered a best-case scenario.

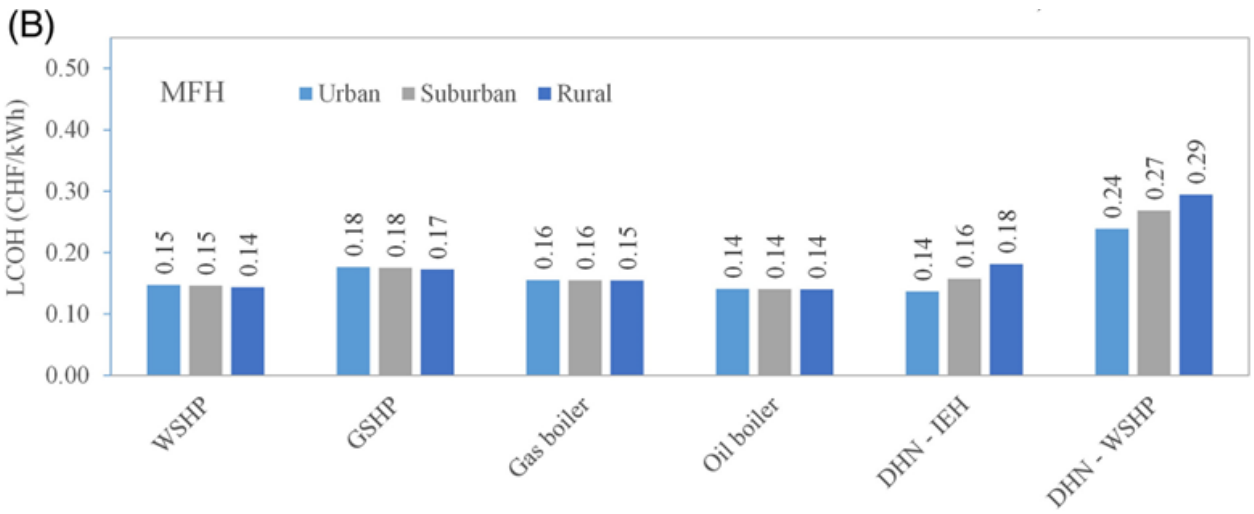

Figure 10: Levelised Costs Of Heat for different heating technologies in multi-family houses in Switzerland (WSHP = Water Source HP, GSHP = Ground Source HP, DHN = District Heating Network and IEH = Industrial Excess Heat) [42].

Global Warming Potential of an oil boiler

To calculate the GWP of an oil boiler, it is assumed that the GWP induced by the boiler itself is negligible compared to the GWP from the fuel. According to the Bundes Ampt für Umwelt, the emission factor of Light fuel oil used in oil boilers is 0.265 kg $CO_{2-eq} kWh^{-1}$ [43]). This value has to be adjusted for the efficiency of an oil boiler. M.J.S. Zuberi et al. (2021) specified the average efficiency of an oil boiler to be 83% [42]. Finally, as the preferred unit in this optimisation is CHF kWh^{-1}, to align with LCOH, the emission factor need to be multiplied by the carbon price of CHF 120 per tonne of CO_2. Equation 18 shows that the final GWP of an oil boiler (GWP_{OB}) is 0.03831 CHF kWh^{-1}.

$$GWP_{OB} = \frac{0.265}{0.83} * 0.120 = 0.03831 \ \ CHF \ \text{kWh}^{-1} \tag{18}$$

5 Global Warming Potential Model Implementation

This chapter describes the methodology for integrating an GWP estimation into the existing simulation model. It evaluates the GWP throughout the life cycle of main components, including the PV system, heat pump, various Hybrid Thermal Energy Storage units, and the DHW TES. It excludes aspects like heat distribution systems, heat exchangers, valves, and piping since their contribution is assumed to be negligible compared to the main components.

The system's GWP is split into production and disposal, and operational phases. The production and disposal GWP is fixed, determined by component size, and unaffected by system operation, and the operational GWP is influenced by grid electricity use.

This chapter first examines and parametrises each component's fixed GWP of production and disposal. It then accounts for the operational phase's GWP concerning grid electricity use before finally integrating all data and functions into the model.

5.1 PV panels

The GWP of PV panels over their lifetime is independent of their use phase; whether a panel produces much electricity or not, the GWP remains precisely the same [44]. Therefore, the GWP per installed kW peak (kWp) is used to consider the GWP of PV panels. Using GWP kWp^{-1} allows for a scalable value, depending on system size instead of electricity production. A report from the 'International Energy Agency: Photovoltaic Power Systems Program' by R. Frischknecht et al. did a complete Life Cycle Assessment (LCA) on photovoltaic systems in Europe in 2020 [45]. The model uses their results as the source to determine the GWP of the PV system.

The assessment covers an average residential PV system of 3 kWp roof-mounted PV system in Europe. The scope of the assessment includes the PV panel, cabling, mounting structure, inverter, and system installation. The life cycle stages of the PV system evaluated in the assessment include manufacturing, transport, installation, use, and end of life, including dismantling, recycling, and waste management. The assessment analysed the following four PV module technologies with their corresponding efficiencies: Cadmium-Telluride (CdTe, 18%), Copper-Indium-Gallium-Selenide (CIS/CIGS, 16%), Multi crystalline Silicon (multi-Si BSF, 18%), and Monocrystalline Silicon (mono-Si BSF, 19.5%).

The lifetime of the PV system is 30 years for panels and 15 years for the inverter, with linear degradation of the electricity output of 0.7% per year. The assessment considers the initial annual production of the PV system, which is 975 kWh/kWp. It was also their conclusion that almost all emissions of a PV system are related to the manufacturing of the system.

Additional research showed that the amount of g CO_{2-eq} kWh^{-1} that was found for the Silicon-based panels is in line with other reviews [44], [46], [47]. In addition, the Swiss Federal Office for the Environment determined a comparable GWP for solar energy in Switzerland. In 2018, they calculated the average GWP for solar energy to be 0.0417 kg CO_{2-eq} kWh^{-1} [48], which is also in line with the other findings.

As earlier said, the desired functional unit of the GWP is per kWp instead of their used GWP per kWh. However, this is easily calculated based on their results and boundary conditions. To calculate the GWP per kWp, the found g CO_{2-eq} kWh^{-1} for each technology is multiplied by the assumed total produced electricity over the 30-year lifetime, see Equation 19.

$$\text{Total Electr.} = \sum_{i=1}^{30} PR \times (1 - ADR)^i \tag{19}$$

Where PR represents the initial energy production rate in kWh per kWp at peak performance (975 kWh kWp^{-1}), and ADR represents the annual degradation rate as a percentage (0.7%). The expression $(1 - \text{ADR})^i$ represents the fraction of energy produced relative to the previous year, considering the annual degradation rate. When multiplying this with the $\text{CO}_{2-\text{eq}}$ kWh^{-1} for each technology, the following total GWP per kWp over their lifetime is:

- CdTe: 696.4 kg $\text{CO}_{2-\text{eq}}$ kWp^{-1}
- CIS/CIGS: 954.0 kg $\text{CO}_{2-\text{eq}}$ kWp^{-1}
- Multi-Si: 1111.7 kg $\text{CO}_{2-\text{eq}}$ kWp^{-1}
- Mono-Si: 1116.9 kg $\text{CO}_{2-\text{eq}}$ kWp^{-1}

To calculate the amount of GWP attributed to the PV system, the above values can be multiplied by the total installed max power of the system.

In conclusion, various PV technologies have different GWPs, with mono-Si exhibiting the highest due to its energy-intensive production process. Consequently, when implementing large amounts of PV panels and much free space, it could be worth using less efficient PV panels with a lower GWP to reduce the system's GWP.

5.2 Heat pump

Research on various heat pump types and their GWP shows that their GWP is mainly influenced by the electricity consumed during their operational lifetime rather than the construction of the pump itself [49], [50], [51], [52]. The GWP can differ significantly across regions due to regional variations in electricity GWP. Heat pump construction and end-of-life (EOL) contribute only 2-4% to the total GWP [50], [51], [52]. However, their importance increases with lower electricity GWP.

The GWP of heat pumps was evaluated using data from Switzerland's Federal Office for the Environment (FOEN), which provides inventories for 7, 15, and 50 kW air-water heat pumps [53]. The components are primarily made of steel and copper, and the material amounts are determined by scaling based on average weights from various pumps.

Energy data for production was obtained from heat pump producer Viessmann Werke GmbH [54]. Standard transport distances were assumed following the Ecoinvent methodology [55]. Recyclable materials include steel, copper, and coolant R410a, while non-recyclable materials are incinerated. Refrigerant emissions result from 3% filling loss during manufacturing and 19% disposal, totalling 22%. Other emissions are electrical input converted to waste heat.

Heat pumps are disposed of according to EU standards as industrial devices to Waste from Electrical and Electronic Equipment (WEEE) and hazardous waste incineration. 85% of the initial refrigerant input is disposed of, assuming a 15% loss. The remaining metal fragments are recycled.

The LCA results from FOEN for each heat pump capacity are shown in Table 3. These values can predict the GWP of other capacities, assuming the same trend applies.

Table 3: Overview of the total GWP of the three investigated heat pump capacities (HPC) excluding the use phase [53].

No.	HPC (kW)	GWP (kg CO_{2-eq})
1	7	3,060
2	15	3,670
3	50	13,700

A quadratic equation calculates the trend line; see Equation 20. Refer to subsection C.1 for the determination of the equation. The generated quadratic equation of Figure 11 is plotted in Equation 20.

$$GWP_{HP}(HPC) = 4.8912 \cdot HPC^2 - 31.356 \cdot HPC + 3039.8 \tag{20}$$

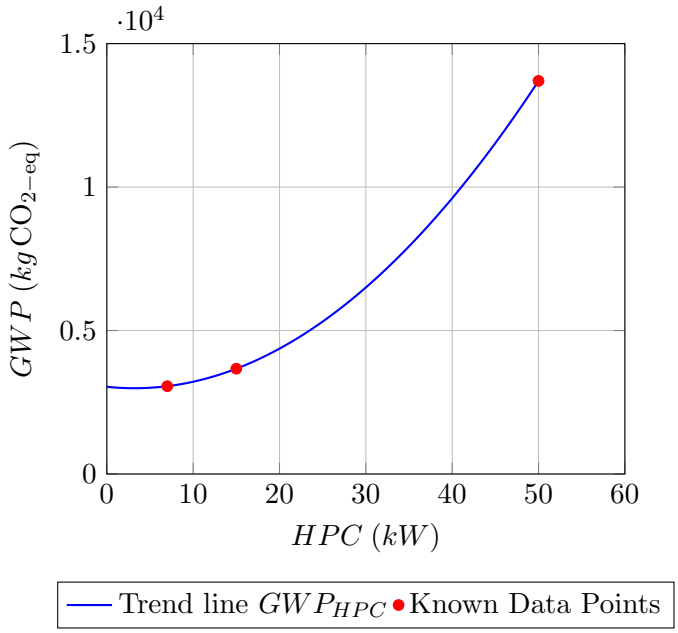

Figure 11: Plot of GWP for various HPCs according to Equation 20 over the known data points [53].

Heat pump refrigerants can contribute significantly (up to 20%) to the Global Warming Potential (GWP) due to leakage during their lifetime and at EOL [50]. This contribution varies with refrigerant type and quantity. For instance, in 2019, most heat pumps used R410A and R134A refrigerants, which have GWPs of 2088 and 1430 CO_{2-eq}, respectively [56]. However, emerging refrigerants R32 and R290, with notably lower GWPs (704 and 0.02 CO_{2-eq}), are increasingly in use [56], [57]. Hence, choosing a refrigerant type can significantly impact a heat pump's GWP.

5.3 Heat storage

The GWP of heat storage is assessed across several scenarios, including the separate DHW storage tank and three variations of sizeable underground storage. The GWP determinations for the DHW storage, VIT storage, and PCM capsules are based on an internal LCA study by L. Sztranyovszky titled 'Comparative life-cycle assessment of energy storage technologies for photovoltaic-heat pump

systems of single-family houses' (see Appendix B). This study, similar to HyTES but on a smaller scale, uses a cradle-to-grave system boundary, excluding the use phase. It applies two system models - cut-off and consequential - with Ecoinvent EF3.0 as the primary Life Cycle Impact Assessment (LCIA) method, supplemented by ReCiPe 2016 (H) and Cumulative energy demand methods for comparison. Version 3.8 of the Ecoinvent database served as the primary data source.

DHW storage tank

The DHW storage tank in the HyTES project is assumed to be the same type of tank used in the LCA on the DHW storage tank done in Appendix B. The used tank has a 2.5mm thick wall of stainless steel (18/8) and a volume of 600l. Furthermore, the tank has a 120mm layer of glass wool insulation. At the EOL, LCA assumes that the steel is recycled as mixed metal scrap, glass wool is landfilled, and the rest is incinerated.

The LCA indicated that an insulated tank of 600l has a GWP of 770 kg $CO_{2-\text{eq}}$ (GWP_{T600l}). To parameterise this, it has to depend on the vessel's volume. The surface area is assumed to scale linearly with the used materials. Furthermore, it is also assumed that the GWP scales linearly with the used materials. However, because the volume of a tank and its surface area do not necessarily linearly scale, a non-linear trend function of this relation is necessary. The calculations use the product range of a prominent hot water tank supplier [37] to calculate this trend, which lists the dimensions of their hot water. The calculations for the surface area assume that the tanks are ideal cylinders. See Table 4 for the data points.

Table 4: Overview of dimensions of DHW tanks from Sirch [37].

Type:	**550**	**800**	**1000**	**1500**	**2000**	**3000**	**4000**	**5000**
Volume, V (l):	536	812	952	1495	1936	3068	3945	5131
Tank diameter, D (mm):	650	790	790	1000	1200	1500	1500	1800
Height, H (mm):	1720	1780	2070	2020	1840	1880	2380	2210
Surface area, A (m^2)	4.18	5.40	6.12	7.92	9.20	12.39	14.75	17.59

This dataset, consisting of eight data points $(V_1, A_1), (V_2, A_2), ..., (V_8, A_8)$, is then used to calculate a polynomial trend line of the surface area. After analysis, it is determined that a 4th-order polynomial provides the best fit for interpolating the data. The desired trend line is given as Equation 21, a 4th-order polynomial to calculate the surface area of a DHW tank as a function of its volume ($A_{DHW}(V)$). Refer to subsection C.2 for the mathematical proof. The trend line is plotted against the known data points of Table 4 in Figure 12 to validate the accuracy, which shows a good match.

$$A_{DHW}(V) = -3.7019 \cdot 10^{-14} \cdot V^4 + 4.5636 \cdot 10^{-10} \cdot V^3 - 2.0559 \cdot 10^{-6} \cdot V^2 + 0.0067483 \cdot V + 1.0958 \quad (21)$$

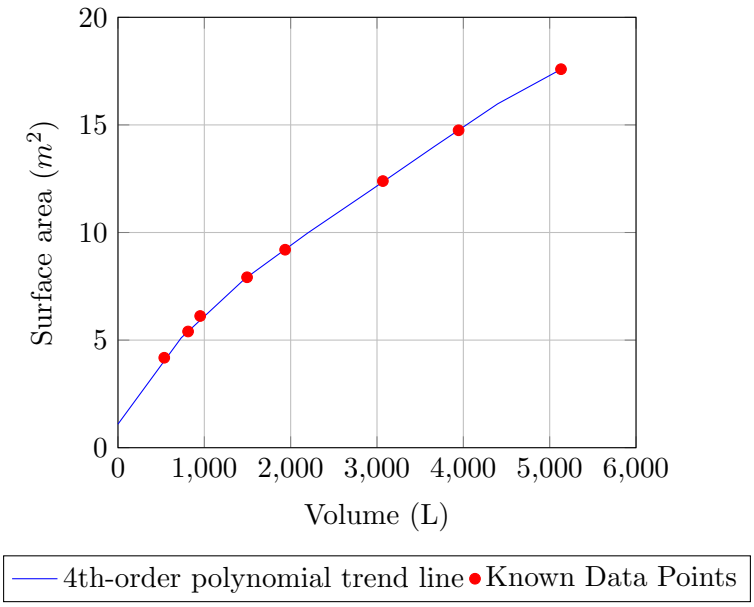

Figure 12: The trend line plotted over the known data points from Sirch [37].

With Equation 21, the relation between the volume of a DHW tank and its surface area is known. To draw up an equation for the GWP of a DHW water tank as a function of the volume ($GWP_{DHW}(V)$), Equation 22 is used. In this equation, the known GWP of the 600l tank is divided by the calculated surface area of that tank. That value is then multiplied by the desired surface, a function of the volume, using Equation 21. This results in the following relation, see Figure 13.

$$GWP_{DHW}(V) = \frac{GWP_{600l}}{A_{DHW}(600)} \cdot A_{DHW}(V) \tag{22}$$

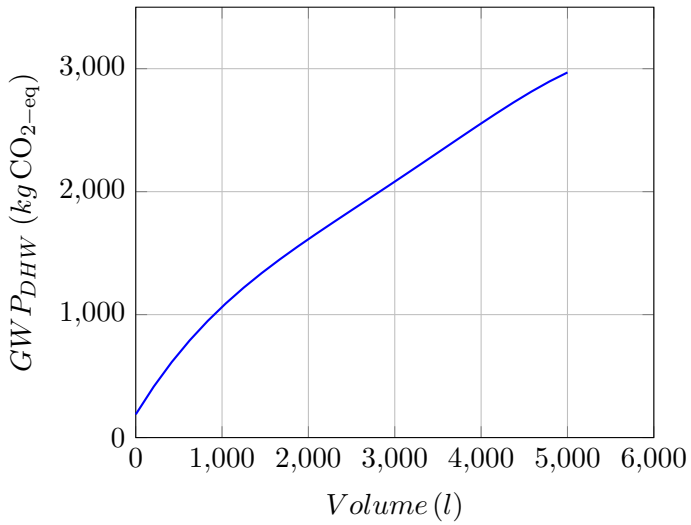

Figure 13: GWP of a DHW tank depending on the volume.

Encapsulated PCM

The HyTES project employs High-density Polyethylene (HDPE) capsules filled with a Sodium Acetate Trihydrate (SAT) based PCM, identical to those used in L. Sztranyovszky's internal LCA. Each capsule has an outer volume of 0.135l and contains SAT, Glycine, Borax (anhydrous), and HDPE. A unique inventory was created for the production process due to the unavailability of reliable SAT production data (refer to Appendix B).

Sztranyovszky's LCA includes the manufacturing process, which involves injection and blow moulding using virgin HDPE granulation, PCM mixing and filling, and logistics. It assumes separate management of plastic and PCM waste post-use, with the latter going to landfills as inert waste (refer to Appendix B for the complete LCA).

The study showed a GWP of 488 kg $CO_{2-\text{eq}}$ per 1000 (0.135 l each) capsules, and it was assumed that GWP linearly scales with capsule volume. The calculations are described in Equation 23, and Figure 14 verifies the assumption, showing that 90% of the GWP is due to the volume of used materials. Hence, deviations will be slight for minor variations in capsule volume.

$$GWP_{Cap}(V_{cap}) = \frac{(\frac{GWP_{1000-capsules}}{1000})}{0.135 \cdot 10^{-3}} \cdot V_{cap} \tag{23}$$

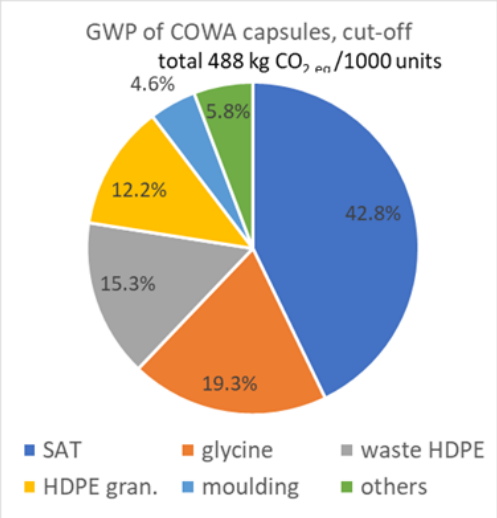

Figure 14: Main contribution for GWP of COWA capsules according to L. Sztranyovszky, Appendix B.

To take the capsules into account for the different storages in the modelling of the system, the about of capsules needs to be known, which depends on the storage volume (V) and packing density (PD). Since these are variables which the model calculates, they are also variables in these equations. Equation 24 describes the GWP of the capsules per volume of storage ($GWP_{1000-capsules}$). Here the $GWP_{Cap}(V_{Cap})$ is multiplied by the number of capsules, which is the total volume multiplied by the PD, both divided by the V_{Cap}.

$$GWP_{Capsules}(V, V_{Cap}, PD) = GWP_{Cap}(V_{cap}) \cdot \frac{V \cdot PD}{V_{cap}} \tag{24}$$

Based on this equation, the V_{Cap} is not a variable in the GWP_{Cap} since calculating the number of capsules divides it away.

Vacuum-Insulated Tank

The first considered underground storage is the VIT. During this project, the Sirch Vacutherm is used [58]. To estimate the GWP of the production of such storage, the two main components are taken into account, the PCM capsules and the vessel containing them. The estimation is made as a function of the storage volume to implement it in the parameterised model of the HyTES project.

Data from the LCA of L. Sztranyovszky is used again to consider the production of the tank. Besides the GWP of the 600 l storage tank, the study also specifies the weight of the steel tank. When the GWP_{600l} is divided by the weight (90kg), a constant of GWP per kg of the storage tank is generated ($GWP_{VIT-weight}$, in $kg\ CO_2\ kg^{-1}_{VIT-tank}$). To use this for the VIT, the GWP per kg of VIT is assumed to be double that of the 600 l tank. The GWP is doubled because the VIT is vacuum insulated, meaning it has a double layer of steel.

$$GWP_{VIT-weight} = 2 \cdot \frac{GWP_{600l}}{W_{600l}} = 2 \cdot \frac{770}{90} = 17.12 \tag{25}$$

Next, the weight of the VIT must be parametrised. The parametrisation is done with data from the 'tank configurator' of Sirch standard tanks, which specifies the weights for many tank volumes [59]. The function of the storage volume is based on this data, using the weights and corresponding volumes to generate a second-order polynomial trend line. This data is plotted in a spread plot, like in Figure 15, on which quadratic regression was applied to create $Weight_{VIT}(V)$.

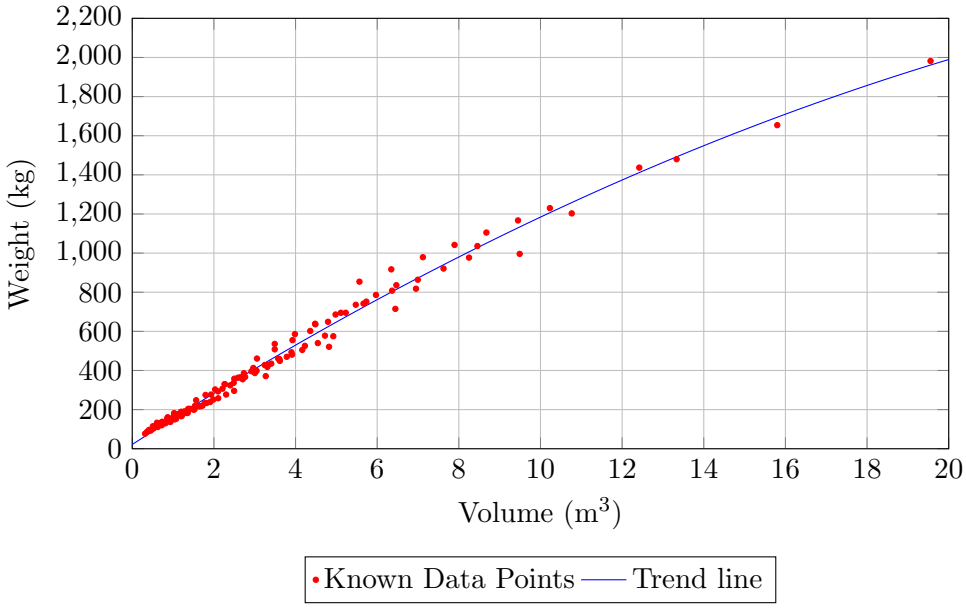

Figure 15: Trendline based on known data points from Sirch [59].

Finally, both Equation 25 and $Weight_{VIT}(V)$ can be combined with the GWp of the capsules to calculate an estimate of the GWP of VIT; see Equation 26. This equation is not an exact way to

consider the GWP of the VIT system, as it only roughly considers the vessel production and not, e.g. the vacuumisation. However, it gives an estimation of the purpose of this study.

$$GWP_{VIT}(V) = GWP_{VIT-weight} \cdot Weight_{VIT}(V) + GWP_{Capsules}(V) \tag{26}$$

Spherical-Shaped Storage tank

The Spherical-Shaped Storage Tank (SSST) that is considered for the HyTES project is the Enersafe storage tank, see Figure 16 from Energy4Me [60]. The tank consists of two layers of Glass-Fibre Reinforced Plastic with a thickness of 7mm each, with a vacuum in between, and a 25cm layer of Polyurethane Foam (PUR).

Figure 16: Spherical-shaped storage enerSAFE from Energy4Me [60].

To determine the GWP of this storage, the GWP of both the tank and its insulation, together with the PCM, is considered. First, the cradle-to-grave GWP of both the GFRP and the PUR is determined. The vessel is assumed to be a perfect sphere with one layer of 14mm GFRP. To estimate the GWP of the GFRP, an Environmental Product Declaration (EPD) for GFRP pipes is used [61]. It is assumed that the production of a spherical tank is similar in GWP to the production of large GFRP pipes. The system description of the production of GFRP pipes involves five stages: raw material preparation and transport, manufacturing, transport to the construction site, installation, and disposal. The disposal stage involves landfill, with 25% of the waste used as an inert filler (possible recycling benefits excluded). The other stages involve assumptions about fuel consumption, transport distances, and installation times. This EPD declared that the GWP per one tonne of GFRP is 2426.04 kg CO_{2-eq} [61]. Based on an average density of GFRP of 2500 kg m^{-3} [62], the GWP per cubic meter is (GWP_{GFRP}) 970.42 kg CO_{2-eq} m^{-3}_{GFRP}.

For the PUR insulation, an EPD is used [63]. The EPD of polyurethane insulation spray foam considers the entire life cycle, from obtaining the raw materials to delivering the finished product to the manufacturer's location. The LCA also encompasses transportation to the construction site, application of the foam, and the disposal of the foam once it is no longer needed (no recycling benefits). The results show a GWP of 541.27 kg CO_{2-eq} m^{-3}_{PUR} of PUR per cubic meter (GWP_{PUR}) m^{-3}_{PUR} [63].

Both the GWP of GFRP and the PUR can be calculated based on the volume of a spherical shell ($V_h(V)$) as a function of the inner volume of the storage (V) and the known Thickness' T'.

Equation 27 gives this function, which is derived in subsection C.3.

$$V_{h-GFRP}(V) = \frac{4}{3} \cdot \pi \cdot (\sqrt[3]{\frac{3 \cdot V}{4 \cdot \pi}} + T)^3 - \frac{4}{3} \cdot \pi \cdot (\sqrt[3]{\frac{3 \cdot V}{4 \cdot \pi}})^3 \tag{27}$$

For the GWP of the GFRP, this function can directly be used, with T=0.014m. However, since the PUR is on the outside of the GFRP, the thickness of the GFRP has to be added to the inner radius. Adding this to the original Equation 27 gives the new function described in Equation 28.

$$V_{h-PUR}(V) = \frac{4}{3} \cdot \pi \cdot ((\sqrt[3]{\frac{3 \cdot V}{4 \cdot \pi}} + 0.014) + T)^3 - \frac{4}{3} \cdot \pi \cdot (\sqrt[3]{\frac{3 \cdot V}{4 \cdot \pi}} + 0.014)^3 \tag{28}$$

To calculate the complete GWP of the Spherical-Shaped Storage Tank, the earlier mentioned GWP_{GFRP} and GWP_{PUR} are multiplied with, respectively, Equation 27 and Equation 28. Both are added together with the $GWP_{capsules}$ of Equation 24, giving the complete function as shown in Equation 29.

$$GWP_{SSST}(V) = GWP_{GFRP} \cdot V_{h-GFRP}(V) + GWP_{PUR} \cdot V_{h-PUR}(V) + GWP_{Capsules}(V) \tag{29}$$

Repurposed Basement Storage

For the Repurposed Basement Storage (RBS), swissporXPS is used as advanced waterproof thermal insulation material to isolate existing basements. SwissporXPS is a product from a former HSLU project GEAS [64]. For calculating the GWP of this type of storage (GWP_{RBS}, the GWP of the XPS (GWP_{XPS}) is combined with the GWP of the encapsulated PCM ($GWP_{Capsules}$).

The GWP can be found using the EPD of swissporXPS [65]. Which calculates the GWP for the manufacturing phase up to the factory gate till the transport and waste treatment phase at the end of the life cycle (Excluding possible recycling reductions). This gives a GWP of 8.85 kg CO_{2-eq} kg_{XPS}. With a specified density of 34.3 kg m^{-3}, the GWP per cubic meter (GWP_{XPS}) is 303.56 kg CO_{2-eq} ${m_{XPS}}^{-3}$.

The surface area has to be considered to calculate the GWP attributed by the XPS since this is where the insulation is. The basement is assumed to be a cuboid with an unknown base plane but an assumed known height (h) of 3 m to calculate the surface area. Based on subsection C.4, the cuboid surface area $A_{cuboid}(V)$ can be calculated using Equation 30. The surface area is multiplied by the insulation thickness (T) to calculate the amount of insulation, resulting in the volume of used insulation ($V_{XPS}(V)$). By adding the $GWP_{Capsules}(V)$ of Equation 24, Equation 31 can be derived.

$$A_{cuboid}(V) = \frac{2 \cdot h^2}{V} + \frac{4 \cdot V}{h} \tag{30}$$

$$GWP_{RBD}(V) = A_{cuboid}(V) \cdot T \cdot GWP_{XPS} + GWP_{Capsules}(V) \tag{31}$$

5.4 Operational lifetime

For the operational lifetime of the complete system, this study assumes that only the used electricity adds an extra GWP to the system. The HyTES system predominantly uses solar electricity but also uses grid electricity. An investigation commissioned by the 'Bundesamtes für Umwelt' determined the Swiss electricity grid's average GWP to be 0.128 kg CO_{2-eq} kWh^{-1} in 2018 (most recent data available from the BFU) [48]. However, Switzerland's electricity is generated from diverse sources, ranging from renewables to fossil fuels, resulting in substantial CO_2 emission fluctuations throughout the day and across different days. A 2018 study demonstrated that the carbon footprint of electricity could temporarily be up to five times higher than the yearly average [66]. The authors of this study created a detailed data set on Switzerland's hourly CO_2 emissions from electricity generation for one year (2015–2016) [67]. This data could provide a more accurate estimation of grid electricity's GWP based on the specific usage pattern, which is out of this project's scope. Therefore, the GWP for the operational lifetime is limited to the average GWP per kWh of Swiss grid electricity.

6 Results

This chapter concentrates solely on the analysis of the VIT tank. Other tank types are excluded due to the high computational demand of the simulation, which cannot be met currently. Furthermore, identifying the optimal HyTES system differs from the project's objective. The goal is to demonstrate the application of the optimisation method and the GWP implementation to the optimisation. Therefore, the chapter starts by illustrating the significance of the chosen optimisation variables and their impact on the KPIs. Subsequently, the normalisation factors are determined for the system incorporating the VIT. Finally, initial optimisation results are presented to glimpse potential outcomes and their interpretations.

6.1 Sensitivity analysis optimisation variables

A sensitivity analysis is carried out to assess the relevance of the optimisation variables selected in subsection 4.4. This analysis explores how the different variables affect the KPIs. The procedure involves varying one variable at a time within its specific range Table 2. The variation values are determined using equal step sizes between the determined ranges (Table 2) in subsection 4.4. Thus, not every variable has the same number of steps, and the relative variation is unequal. The relative variation is shown in Table 5. The actual values used for the sensitivity analysis are shown in Appendix D, Table 12.

While one of the optimisation variables is being adjusted, all the others maintain their base values, which are indicated in the middle column. The base values represent the midpoint of the ranges, providing the best indication of the optimisation variables' influence.

Table 5: Relative variation for each optimisation variable used to check that particular variable's influence.

Optimisation variable:	**Relative variation of variables**						
	1	**2**	**3**	**Base**	**4**	**5**	**6**
HyTES tank height [m]	-60%	-40%	-20%	**0%**	20%	40%	60%
HyTES tank width [m]	-	-80%	-40%	**0%**	40%	80%	100%
PCM packed bed starting position [-]	-50%	-40%	-20%	**0%**	20%	40%	60%
PCM packed bed thickness [-]	-	-70%	-40%	**0%**	40%	80%	100%
Minumum HyTES energy level [-]	-	-25%	-13%	**0%**	13%	25%	-
DHW tank height [m]	-20%	-13%	-5%	**0%**	5%	10%	-
DHW tank width [m]	-50%	-33%	-17%	**0%**	17%	33%	50%
Relative amount of PV panels [-]	-	-80%	-40%	**0%**	40%	80%	100%
PV Azimuth angle [°]	-50%	-33%	-17%	**0%**	17%	33%	50%
PV Tilt angle [°]	-100%	-67%	-33%	**0%**	33%	67%	100%
Electrical power HP [kWelec]	-82%	-55%	-27%	**0%**	27%	55%	82%

Influence on the KPIs

The analysis results are presented in individual graphs for each KPI, showcasing the relative influence of the optimisation variables compared to the outcome of the base values. Each colour denotes the column number from which the specific optimisation variable's value is derived, traceable back to Table 12. Since the relative variation of the variables is unequal, the results in the graphs are normalised to represent the sensitivity of the variables equally. The equalises the importance of the

relative variation of each variable is equal to the range of -100% (Column one) to 100% (column 6) relative variation, with equal step sizes in between.

Influence on LCOH

The results for LCOH are plotted in Figure 17. The results suggest that the dimensions of the HyTES, particularly the tank width, significantly impact the LCOH. The variables related to the DHW tank configurations exert the least influence. For more detailed results, please refer to Appendix D. Table 13 displays the relative values, and Figure 23 provides a zoomed-in version of Figure 17. The detailed results highlight the exact relative difference, showing a clear correlation between the increase in optimisation variable value and LCOH. The only exceptions are the minimum HyTES energy level, which marginally increases LCOH when reduced, and the PV orientation variables, which raise LCOH regardless of direction.

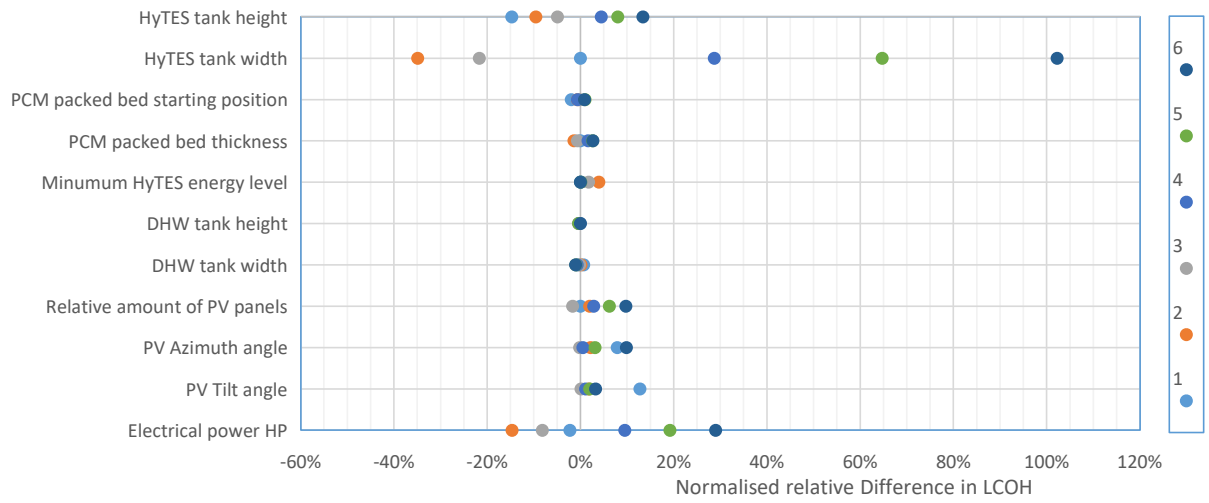

Figure 17: Sensitivity spread LCOH, see Table 13 for the relative values.

Influence on GWP

Figure 18 illustrates the results for GWP. Similar to LCOH, the dimensions of the HyTES tank have the greatest impact on the system's GWP. The influence of the PV system is also large. The DHW tank width has a small but noticeable effect on GWP, whereas the height does not. The starting position of the packed bed and the minimum HyTES energy levels also only exert minimal influence on the GWP of the system.

Detailed information on the GWP influence is available in Appendix D. Table 14 displays the relative values, and Figure 24 offers a more detailed graph with a smaller spread. In Table 14, the trend of increasing the optimisation variable and the relative difference largely remain the same. However, the PV Tilt angle exhibits a counteracting effect as an increase in tilt angle lowers the GWP of the system, given that it reduces the maximum number of PV panels.

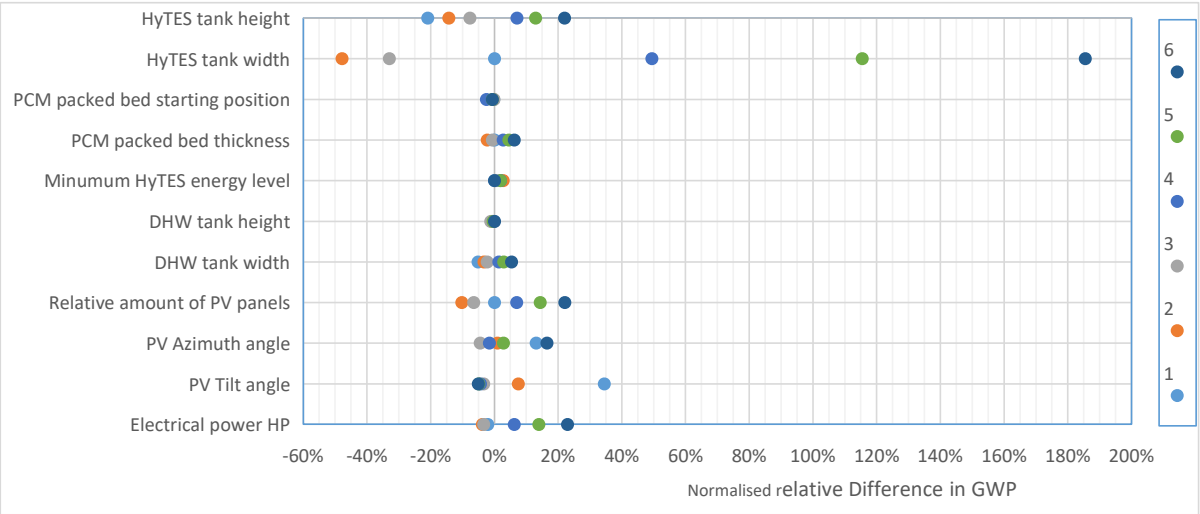

Figure 18: Sensitivity spread GWP, see Table 14 for the relative values.

Influence on SS

Lastly, Figure 19 demonstrates the influence of optimisation variables on SS. SS is primarily affected by the PV-related variables, predominantly the tilt angle and the relative number of PV panels. The dimensions of the HyTES tank continue to be influential, although less so than for the previous KPIs. The dimensions of the DHW tank again have a negligible impact on the system. Interestingly, both an increase and decrease in the heat pump power adversely affect the SS. Detailed results in Appendix D offer a clearer picture of the optimisation variables' influence. Table 15 presents the relative values, and Figure 19 provides a more detailed graph with a smaller spread.

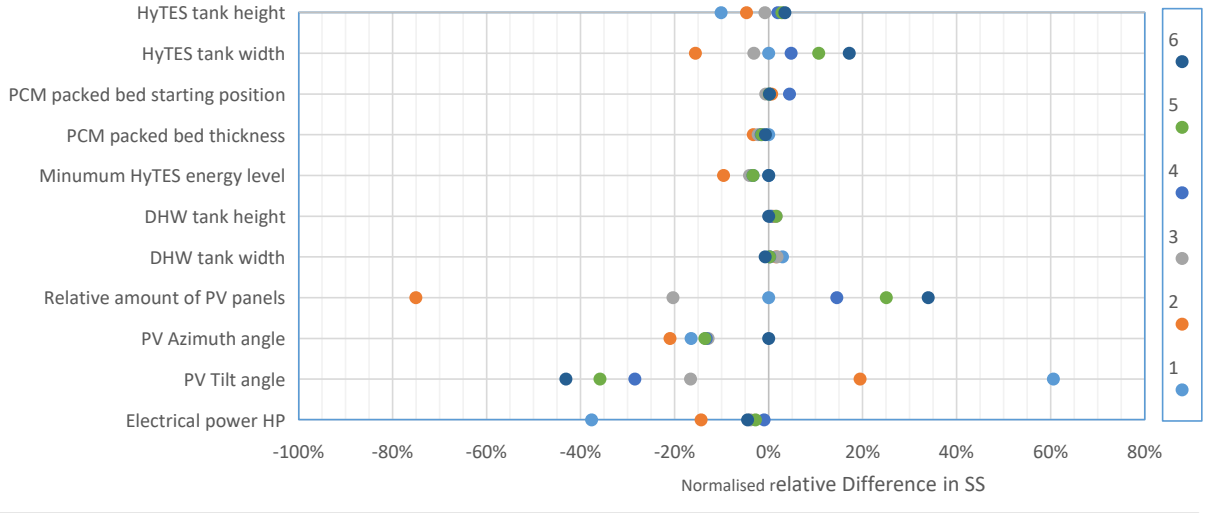

Figure 19: Sensitivity spread SS, see Table 15 for the relative values.

6.2 Normalisation factors determination

This section utilises the methodology described in Equation 4.2 to derive the normalisation factors. As previously noted, this involves executing three optimisations, each targeting a specific KPI, as per Equation 10. The optimisation variables and their respective ranges employed in these runs are detailed in Table 2.

The outcomes of the three optimisations are displayed in Table 6, which also includes the Utopia and Nadir points. The optimal KPI values from the three runs determine the Utopia point coordinates, while the worst possible KPI values determine the Nadir point coordinates. For better comprehension, these points are visually represented in Figure 20.

Table 6: Results of the three optimisation runs and the corresponding Utopia and Nadir point.

KPI	Min LCOH	Min GWP	Max SS	Utopia point	Nadir point
LCOH [CHF kWh^{-1}]	0.181648	0.186661	1.235490	0.181648	1.235490
GWP [CHF kWh^{-1}]	0.005376	0.004681	0.113373	0.004681	0.113373
Self-Sufficiency [-]	0.017106	0.021166	1.000000	1.000000	0.017106

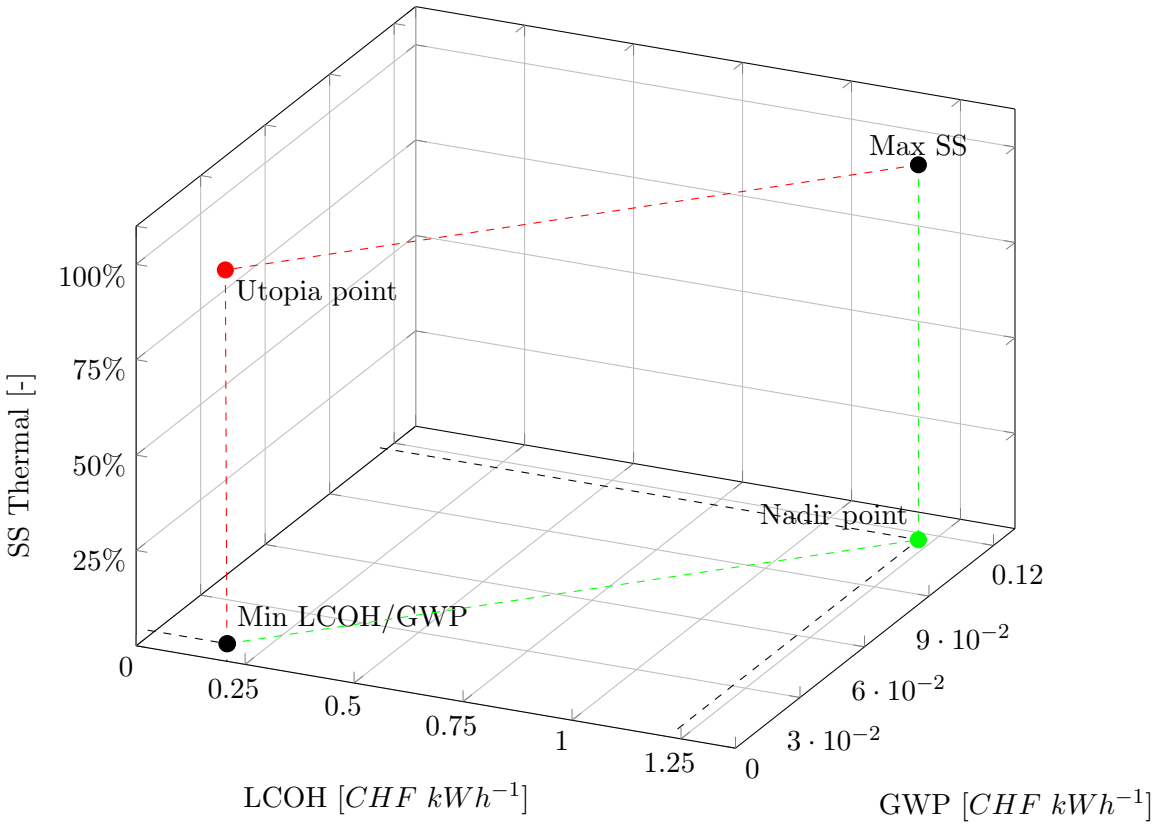

Figure 20: Determination of Normalisation factors 3D.

Both Figure 20 and Table 6 indicate that 'Min LCOH' and 'Min GWP' are pretty close, suggesting that when the system has a low LCOH, the GWP is also low.

The established Utopia and Nadir points are used to complete the coordinates in Equation 11,

facilitating the calculation of the corresponding normalisation factors (refer to Equation 32).

$$\begin{aligned} \theta_{LCOH} &= \frac{1}{N_{LCOH} - U_{LCOH}} \quad \Rightarrow 0.95 = \frac{1}{1.235490 - 0.181648} \\ \theta_{GWP} &= \frac{1}{N_{GWP} - U_{GWP}} \quad \Rightarrow 9.2 = \frac{1}{0.113373 - 0.004681} \end{aligned} \tag{32}$$

6.3 Optimisation of HyTES with VIT

Using the normalisation factors from Equation 32, the final optimisation function is developed in Equation 33. This function then performs multiple optimisations, each with a varying p_{SS}, to illustrate different Self-Sufficiency levels. Any feed-in tariffs and availability are turned off in the model during these optimisations. If left on, these factors would compel the optimiser to maximise the PV system to maximise electricity sell-back. However, they are incorporated post-optimisation as they significantly affect the LCOH.

$$\min_{x \in \Omega} F(x) = \frac{(1 - p_{SS})}{2} \cdot 0.95 \cdot f_{LCOH} + \frac{(1 - p_{SS})}{2} \cdot 9.2 \cdot f_{GWP} + p_{SS} \cdot f_{SS} \tag{33}$$

Three optimisation runs were selected where the Self-Sufficiency values fell within the range, $p_{SS} = 0.25$, $p_{SS} = 0.5$, and $p_{SS} = 0.9$, respectively. Table 7 presents the optimised variables for these selected runs. Runs for $p_{SS} = 0.6$ and $p_{SS} = 0.75$ were also conducted, but their results were similar to those for $p_{SS} = 0.5$ and are thus omitted.

The chosen optimisation variables in Table 7 correspond to SS values of 78%, 84%, and 97%, respectively. These variables reveal specific trends, with the most notable difference being the substantial change in the HyTES tank volume, where the width sees the most increase. As expected from subsection 6.1, this width increase is anticipated. Interestingly, while the tank volume increases with higher SS levels, the thickness of the PCM-packed bed decreases, reducing the proportion of utilised PCM capsules. Lastly, although the PV system orientation is consistent across all systems, the full panel availability is not used for lower SS levels.

Table 7: Output optimisation variables for varying Self-Sufficiency weighting factors.

Optimisation variables	$p_{SS} = 0.25$	$p_{SS} = 0.50$	$p_{SS} = 0.90$
HyTES tank height $[m]$	2.72	3.85	3.86
HyTES tank width $[m]$	1.29	2.05	10.00
PCM packed bed starting position $[-]$	0.57	0.22	0.17
PCM packed bed thickness $[-]$	0.54	0.10	0.12
Minimum HyTES energy level $[-]$	0.11	0.30	0.1
DHW tank height $[m]$	2.00	2.09	2.18
DHW tank width $[m]$	0.5	0.5	0.5
Relative amount of PV panels $[-]$	0.74	1.00	0.99
PV Azimuth angle $[°]$	98	91	99
PV Tilt angle $[°]$	1	0	0
Electrical power HP $[kW_{elec}]$	7	11	11

The results of the KPIs corresponding to the chosen p_{SS} values are exhibited in Table 8 and plotted

in Figure 21. Besides the optimisation results, the 'LCOH with subsidies' (recalculated with available subsidies and feed-in tariffs) and the base case determined in subsection 4.5 are also shown. The results indicate that achieving higher SS levels triggers an exponential increase in the GWP and LCOH. A comparison of the optimisation run with the base case reveals that higher levels of SS can be achieved while being less carbon-intensive than the base case. From an economic standpoint, the system approximates the base case at an SS of 78%, factoring in subsidies and grid sell-back. Slightly lower SS levels should already be cost-competitive compared to the base case while considerably improving the GWP.

Table 8: Results of optimisation for varying Self-Sufficiency weighting factors.

KPI	**Base case**	$p_{SS} = 0.25$	$p_{SS} = 0.50$	$p_{SS} = 0.90$
LCOH $[CHF\ kWh^{-1}]$	0.14	0.27	0.33	0.66
GWP $[CHF\ kWh^{-1}]$	0.038	0.012	0.015	0.091
Self-Sufficiency Thermal $[-]$	0%	78%	84%	97%
LCOH with subsidies $[CHF\ kWh^{-1}]$	-	0.16	0.21	0.55

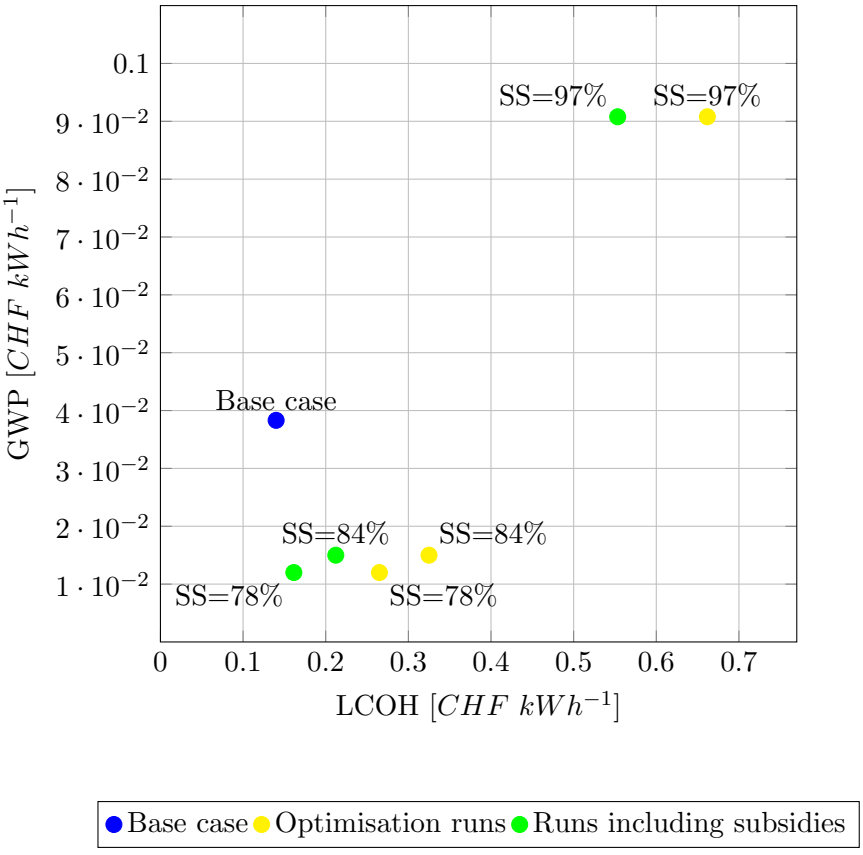

Figure 21: Results of optimisation for varying Self-Sufficiency levels, combined with the base case and LCOH with subsidies.

Contribution to LCOH and GWP of main contributors

Table 9 and Table 10 provide an overview of the main contributors to the LCOH and GWP, respectively, to offer insights into their composition. Both tables display the main contributors'

relative contribution in the LCOH and GWP calculation models. Table 9 includes optimisation runs and the scenarios with subsidies and feed-in tariffs. Since these scenarios do not affect the GWP, Table 10 only shows the optimisation runs.

Table 9: Comparison of relative contribution to the LCOH of the main contributors.

	$SS = 78\%$	$SS = 78\%$, Incl. subs.	$SS = 84\%$	$SS = 84\%$, Incl. subs.	$SS = 97\%$	$SS = 97\%$, Incl. subs.
PV system	25%	18%	22%	16%	11%	8%
Heat Pump	20%	19%	23%	21%	11%	10%
HyTES tank	5%	5%	9%	9%	21%	21%
PCM-capsules	2%	2%	1%	1%	12%	12%
DHW tank	1%	1%	1%	1%	0%	0%
Excavation	1%	1%	1%	1%	3%	3%
Feed-in tariffs	0%	-26%	0%	-23%	0%	-11%
O&M	38%	32%	39%	34%	41%	38%
Grid Electricity	9%	9%	5%	5%	0%	0%
Total	**100%**	**59%**	**100%**	64%	**100%**	83%

LCOH comparison

As displayed in Table 9, Operation and Maintenance (O&M) costs are the most significant contributors to the LCOH across all scenarios, with a consistent impact. These calculations are based on the model's assumption that annual O&M costs equate to 3.5% of the overall system's investment cost, a principle established by T. Yang et al. (2021) [68].

In scenarios with lower SS levels (78%), the second and third most prominent contributors to the LCOH are the PV system and the heat pump. Furthermore, the LCOH contribution of the STES - including the HyTES tank, PCM-capsules and excavation - amounts to only 8% of the LCOH, which is less than the 9% contributed by grid electricity. Similar proportions are observed for SS levels at 84%, except that the heat pump's impact marginally surpasses the PV system's. For nearly fully autonomous systems (SS=97%), the STES costs significantly dominate the LCOH, constituting 36% of it.

A comparison between optimised runs and recalculated ones factoring in subsidies and feed-in tariffs reveals the substantial impact of these extras. In the 78% SS scenario, the cost reduction exceeds 40% compared to the unsubsidised system. As the subsidies only affect the PV system and the heat pump, the relative reduction is more significant when these systems contribute mainly to the LCOH. The impact of feed-in tariffs is also more significant at lower SS levels due to the lower LCOH.

GWP comparison

Table 10 illustrates that the PV system significantly influences the GWP at lower and medium SS levels, followed by grid electricity. Similarly to the LCOH, the STES contribution increases dramatically for nearly fully autonomous systems. Specifically, the GWP contribution for the HyTES tank + PCM-capsules is 89%, primarily attributed to the HyTES tank.

Table 10: Comparison of relative contribution to the GWP of the main contributors.

	$SS = 78\%$	$SS = 84\%$	$SS = 97\%$
PV system	52%	46%	7%
Heat Pump	6%	9%	0%
HyTES tank	8%	21%	78%
PCM-capsules	4%	1%	11%
DHW tank	1%	1%	0%
Grid Electricity	29%	23%	3%
Total	**100%**	**100%**	**100%**

7 Discussion

This chapter presents a comprehensive discussion of the work conducted, potential improvements and future directions, its overall added value, and a reflection on its accuracy.

7.1 Analysis of Sensitivity of Optimisation Variables

This section discusses the results from subsection 6.1, which showed the impact of the different optimisation variables on the LCOH, GWP, and SS, as depicted in Figures 17, 18, and 19, respectively.

Influence of HyTES Tank Dimensions
The dimensions of the HyTES tank, specifically its width, emerged as the most significant variable. The predominant influence of HyTES tank dimensions on KPIs is primarily due to the construction of such a large tank. The tank material is stainless steel, which carries a substantial GWP and investment cost. Furthermore, with a larger volume, more PCM capsules are possible, each with economic and environmental costs. Another added expense escalating with volume is the excavation costs for placing the tank underground.

Besides the costs associated with increased volume, the storage capacity also grows linear with the volume. This capacity significantly influences the system's SS due to the intermittent energy generation by the PV system. As such, an increased storage size ensures less reliance on the grid when solar energy is unavailable. It should be noted, however, that the relative increase in both LCOH and GWP far surpasses the increase in SS. This suggests that merely increasing storage size enhances the SS to a limited extent, necessitating alterations in combination with other variables for optimal results.

Role of Packed Bed
The initial position and thickness of the packed bed exert limited influence on the KPIs. Among the two, the thickness of the packed bed primarily affects the LCOH and GWP the most. This is reasonable, as changes in thickness alter the quantity of PCM capsules used, directly impacting costs and GWP. On the other hand, alterations in thickness indirectly influence LCOH and GWP as changes in SS subsequently affect the used grid electricity. Despite the slightly more considerable influence of thickness on SS, the initial position demonstrates the most substantial positive effect on SS. The effect of the starting position is because it influences the inner workings of the HyTES tank concerning heat transfer between the sensible and latent heat storage. It shows that the packed bed slightly above the middle has the highest SS.

Impact of Minimum HyTES Energy Level
The minimum HyTES energy level has a relative difference of almost 5% in SS. This variable influences the effective storage capacity usage—with higher levels, the system tends to refill the HyTES tank using grid electricity earlier, thereby reducing SS and increasing LCOH and GWP due to the electricity usage.

Effects of DHW Tank Dimensions
The DHW tank dimensions bear similar behaviour to the HyTES tank in terms of impacting the storage volume, with the width exhibiting a quadratic influence on the volume. However, given the considerably smaller scale of the DHW tank, the impact on LCOH and GWP is correspondingly

minor. Due to the DHW tank's small size, its economic and environmental costs are substantially lower, implying that dimensional variations have a lesser impact on the system's overall expenses.

Regarding SS, the DHW tank also has next to no influence. This is unexpected as DHW is typically utilised during solar energy unavailability and needs high power. Given that the DHW tank maintains a higher temperature than the HyTES tank, an inadequate DHW tank size could lead to premature depletion, necessitating the heat pump to provide DHW using grid electricity daily.

Significance of PV System

The PV system is the primary energy source for the entire system, thus rendering all variables affecting it of importance. This principle is particularly shown with the relative quantity of PV panels, a variable that dictates the total number of panels utilised. Since each panel carries economic and environmental costs, increasing their number proportionately increases the LCOH and the GWP. Paradoxically, a higher panel count also decreases the grid electricity consumption (thereby increasing the SS), reducing the LCOH and GWP. This interplay explains why the relative change in LCOH and GWP for the relative PV panel quantity is lower when compared to the substantial variation observed in SS.

The orientation variables, namely the tilt and azimuth angles, influence LCOH and GWP as they impose constraints on the maximum number of PV panels installed within a specified roof area. Different orientation angles impact shading, indirectly determining the feasible number of PV panels. Moreover, the orientation influences the panels' efficiency, especially during winter when solar energy is sparse. Although selecting optimal angles might diminish the overall system efficiency, it could enhance efficiency during periods when solar energy is most crucial. Interestingly, the results indicate a preference for lower tilt angles, which minimises shading and maximises the total number of PV panels. This finding suggests that the model prioritises more panels to achieve elevated SS levels over establishing optimal orientation angles.

Role of Heat Pump

The heat pump's capacity demonstrates an exponential relationship with the associated LCOH and GWP. A reduction in the heat pump's capacity results in a decrease in the LCOH and GWP, although not directly proportional to the degree of increase in capacity. This occurs because, for heat pumps of lower capacities, the associated costs and carbon footprints exhibit a relatively uniform profile once they reach a fundamental level. However, the associated costs and carbon footprints escalate exponentially upon increasing the heat pump's capacity.

The results also indicate that the heat pump significantly influences the SS. However, the heat pump cannot independently augment the SS; it can only reduce it. Consequently, a rise in the heat pump's capacity for enhancing SS proves beneficial only when employed with other variables, most likely the PV system and storage capacity. Given that the heat pump's role involves the conversion of electricity into heat, increasing its capacity in the absence of additional solar energy will not augment the SS; it will only lead to an increase in both LCOH and SS. A similar situation arises if the storage capacity is not concurrently expanded. However, increasing the storage and heat pump capacity facilitates improved utilisation of available solar energy, as it allows rapidly converting accessible solar energy into heat when needed.

For a comprehensive overview of the sensitivity of the KPIs to each optimisation variable, see Figure 22, within Appendix D.

7.2 Initial optimisation results of VIT

This chapter discusses the outcomes of three system optimisations for achieving SS levels of 78%, 84%, and 97%, as outlined in section subsection 6.3. At a SS level of 78%, the system does not require using all available PV panels, while it maximises the surface area by minimising the panel tilt angle. The corresponding system configuration comprises a small heat pump, HyTES tank, and DHW tank, as detailed in Table 8.

Upon comparison of 78% and 84% SS systems, it becomes apparent that the latter already needs maximum PV panel utilisation to generate more energy independently. Consequently, this necessitates an increase in the heat pump capacity and the size of the HyTES tank, indicating a greater reliance on solar energy for achieving higher SS levels. The augmented heat pump capacity allows for better utilisation of solar energy peaks and increased storage in a larger HyTES tank.

In contrast, when comparing the 84% SS system with a 97% SS system, the latter cannot increase the PV generation further. This results in a considerable expansion of its seasonal storage capacity, nearly to its maximum limit. Despite this, the heat pump power remains the same, reinforcing the findings in subsection 6.1 that an increase in heat pump power without a corresponding increase in PV capacity has negligible effects on the SS. Enhancing PV capacity could achieve higher SS levels without needing ample HyTES storage and its associated costs.

Meanwhile, the system maintains a low quantity of PCM in storage, despite significant increases in storage capacity. In the 97% SS system, the PCM-capsules account for 12% of the total LCOH share (Table 9) and 11% of the GWP (Table 10). This implies a considerable impact of PCM capsules on LCOH and GWP, even with their limited use. This also explains the system's reduction of PCM capsules in high SS systems.

According to the LCA in Appendix B, possible methods to lower the GWP of the PCM-capsules include manufacturing the capsules' content in Europe (which reduces GWP by 13%) or recycling the HDPE of the capsule at the end of its lifespan. However, this could potentially increase the cost of the capsules.

The size of the DHW tank shows slight variation across different SS levels, echoing the results in subsection 6.1 that the DHW tank has a minimal impact on the SS. Nevertheless, increasing DHW tank sizes are linked to a rise in GWP, which is most likely why the DHW tank is kept small.

Subsequently, the optimisation outcomes (Figure 21) reveal that the system has lower GWP at 78% and 84% SS levels compared to the base case. However, this figure significantly rises with increased SS levels. This suggests that specific renewable technology components still contribute substantially to the GWP. Table 10 show that the PV system and the VIT tank are primarily responsible for the system's GWP.

The GWP of PV panels is mainly associated with production, which consumes considerable electricity and thus contributes to GWP, particularly in fossil-fuel-dominant regions like China. With its lower electricity GWP, manufacturing PV systems locally in Switzerland could mitigate this issue. As for the VIT tank, its high GWP can be attributed to the extensive use of stainless steel required for its double tank configuration. Other tank options within the HyTES system would significantly lower associated GWP.

On the contrary, the LCOH of the HyTES system remains higher than the base case at all investigated SS levels, despite subsidies for the PV system and heat pump and Feed-in tariffs. The PV system and heat pump are significant contributors to the LCOH, implying that reducing their production

costs could enhance the HyTES system's economic feasibility. Additionally, a rise in the base case's LCOH, specifically the cost of fuel oil, could improve the cost competitiveness of the HyTES system.

Improving the system's quality to extend its lifespan could lower the LCOH and GWP by allowing for longer investment payback times.

Best initial configuration
The most favorable system resulting from the preliminary optimisation runs is the one achieving a SS level of 78%, as per the predefined objectives. Notably, this system lies within the desired self-sufficiency range of 70-100%. Additionally, it exhibits the lowest LCOH compared to other optimized systems. By incorporating feed-in tariffs and subsidies, this system becomes nearly cost-competitive with traditional oil boilers. Furthermore, the environmental impact of this optimized system is commendable, with its GWP being three times lower than the baseline case.

7.3 Improvements and future work

Throughout the study, several areas for improvement have been identified that can enhance the accuracy and robustness of the findings.

GWP of VIT
One area where accuracy can be improved is data acquisition for calculating the GWP of VITs. It is recommended to acquire better data by obtaining information about the type(s) of steel used in the storage tanks. This would allow for a more precise estimation of the GWP per kilogram of the tank. Additionally, having an overview of tank weights corresponding to different volumes would provide valuable insights for accurately establishing the relationship between storage capacity and associated weight. Such data would enhance the reliability of the environmental impact assessment by enabling a more informed estimation of the GWP for various storage tanks.

Operation and Maintenance costs assumption
Another area needing improvement is the investigation of assumptions made regarding the O&M costs by the authors of the original simulation model. Based on an article, the model assumes an annual O&M cost of 3.5% of the initial investment cost. However, given the significant contribution of O&M costs to the LCOH, conducting a thorough analysis of these costs is recommended. Such an analysis would provide a more accurate estimation of the O&M costs, ensuring the reliability of the economic assessment.

Electricity GWP
Furthermore, to enhance the accuracy of the environmental impact assessment, it is proposed to consider the time-dependent GWP of electricity as mentioned in subsection 5.4. Currently, this study assumes a general GWP for the electricity consumed throughout the year. However, variations in energy sources and generation methods result in the GWP of electricity varying based on the time and season. Therefore, it is advisable to incorporate time-dependent GWP values for electricity consumption, considering the specific GWP associated with electricity usage at different times, for example, given by D. Vuarnoz et al. (2018) [67]. This approach would result in a more precise assessment of the system's environmental impact.

It also has to be noted it is likely that the GWP of Swiss electricity will decrease the following year, and at some point, also might be zero. This trend is currently not taken into account. It would be

interesting to look at how this decrease could be considered to increase the accuracy of electricity GWP. Besides that, a scenario in which a carbon-free Swiss electricity grid would be considered could also be interesting to investigate as this is a possible future scenario to take into account.

PV technologies
In addition, the model could be further improved by considering other PV technologies. Currently, the model relies on a pre-selected PV system for the data, but as shown in section 5, different PV technologies can have varying impacts. Another technology may be better suited for this specific system. Exploring alternative PV technologies would provide a more comprehensive analysis.

Necessity of GWP in optimisation function
The normalisation results (subsection 6.2) and sensitivity analysis (subsection 6.1) suggest a parallel trend between LCOH and GWP. To examine the importance of incorporating GWP in the optimisation objective, the optimisation could also be run by excluding the GWP. By comparing the results, the relevance of including GWP in the optimisation function could be better determined.

Mesh size and time steps
An aspect that also remained unexplored in the present thesis is the mesh size and the increments in time steps. As described in subsection 2.2, the optimisation process involves a grid-based approach, wherein the optimiser navigates a mesh grid of potential variables to identify an optimal value. Subsequently, based on the outcomes, the optimiser hones in on the mesh, reducing the step size.

The level of detail that the optimiser can archive significantly influences computation time. Therefore, in the optimisation undertaken in this study, the mesh size was estimated relative to the size of the specific optimisation variable. The intent was to keep the optimiser from honing in on the mesh too much to ensure the computational time remained within feasible limits for generating the requisite results for this report.

Besides the mesh size, consideration must also be given to the time steps. These indicate that the time between the system model is recalculated throughout its simulation year. In this case, the time step adhered to the standard the model's authors predetermined and was not subjected to additional modifications.

More precise analysis and determination of both the mesh size and time steps could increase the precision of the optimisations. This could reduce computation time if the current choice of values needs to be more significant. Therefore, it is recommended to investigate the mesh size and time steps.

The HyTES system
The complete HyTES system, as represented in Figure 2, is a viable solution for addressing the problems mentioned in section 1. However, there is still room for improvement in this system. Presently, the only sustainable energy source is the PV system, as solar collectors were excluded due to the limited flexibility in the OPSAIS project. However, implementing a combination of PV panels and solar thermal collectors could be an improvement. The thermal collectors could primarily supply the DHW throughout the year, benefiting from their ability to produce higher temperatures. This would allow the heat pump to operate more efficiently, as it performs better when supplying lower temperatures. By incorporating thermal collectors to supply the main portion of the DHW, the heat pump's capacity could be reduced. Implementing this would require a solar collector model that supplies the heat via an additional heat exchanger in the outgoing line of the heat pump before

the three-way valve. This setup would enable the collectors to supply the DHW tank and utilise the HyTES tank as a heat sink when the DHW tank is full.

It would be beneficial to assess the impact of incorporating this additional heat supply in the model and analyse the system's behaviour. This improvement could provide valuable insights into the system's performance.

Future work
Addressing these areas of improvement in future work would significantly enhance the accuracy and reliability of the study's findings. By acquiring better data, investigating assumptions, considering time-dependent factors, and exploring alternative PV technologies, a more comprehensive and precise evaluation of the environmental impact and cost-effectiveness of the HyTES system can be achieved. Additionally, future work should involve running optimisations for the different tank types possible for the HyTES system. This would include determining normalisation factors for the two other tank types and conducting multiple optimisations with varying weighting factors. While this study provides the optimisation method and offers initial results, concluding the HyTES project necessitates finding the optimal HyTES system configuration.

7.4 Added value of presented work

The presented study focuses on optimising the HyTES system, offering a comprehensive strategy to improve its efficiency and performance. This optimisation strategy is a significant contribution, as it has the potential to enhance the practical applicability of HyTES systems.

In addition to optimising the system's functionality, the research also addresses the environmental impact by considering GWP in the optimisation process. Integrating environmental concerns alongside performance improvements adds a unique and valuable dimension to the HyTES project.

To gain a deeper understanding of the factors influencing the LCOH and GWP, the research provides an overview of their main contributors. This understanding is essential in identifying the lever arms contributing to these performance indicators and can guide future efforts in reducing LCOH and GWP for the HyTES system.

Furthermore, the research compares the performance of the HyTES system at different levels of self-sufficiency. This comparison offers insights into the trade-offs between self-sufficiency, cost, and environmental impact. Such insights can aid decision-making processes in determining the optimal level of self-sufficiency for the HyTES system.

Overall, this study significantly contributes to understanding and optimising HyTES systems. By providing valuable insights and tools, it guides future research and development efforts in this system.

7.5 Accuracy of work

The accuracy of the research conducted in this project is of utmost importance to establish the results' reliability and validity. Several vital aspects contribute to ensuring the accuracy of the work.

Firstly, the project demonstrates a high methodological rigour by aligning with established scientific principles and employing well-accepted modelling and simulation techniques. Therefore, the research builds upon a foundation that has been widely used.

The accuracy of the results heavily relies on the quality and reliability of the data utilised in the analysis. While much data used in the modelling was already determined prior to this thesis, the collected data during this thesis are carefully chosen from reputable sources such as scientific literature and industry standards. This careful selection of data sources enhances the accuracy of the analysis. Also, for the data used in the modelling, as described earlier, the previous authors extensively validated the model to prove its accuracy. By executing the sensitivity analysis of the optimisation variables, even better insight was archived. this analysis gave a good insight into the influence the various variables had and which trend they followed. This also increases the level of confidence in the modelling results.

However, it is crucial to acknowledge that any modelling or simulation work inherently involves assumptions and limitations. Recognising this, the work explicitly states the assumptions and limitations, ensuring transparency regarding the scope and boundaries of the analysis.

8 Conclusion and recommendations

This chapter finalises this thesis, with a conclusion on the presented work and recommendations.

8.1 Conclusion

The primary objective of this thesis was to develop a method for calculating the carbon footprint of the HyTES system, formulate an optimisation-objective function, and identify the optimisation variables and their appropriate ranges. This is all to develop the optimisation strategy, which can be used in future work to find the optimal HyTES system configuration.

The approach to calculating the carbon footprint focused on implementing a carbon footprint model for the main components of the HyTES system. The thesis provided equations to calculate the GWP of the heat pump and PV system based on the literature. Furthermore, the thesis examined the GWP of different heat storage options, including DHW storage tanks, vacuum-insulated tanks, spherical-shaped storage tanks, and repurposed basement storage. Equations were derived to estimate the GWP of each storage option based on their respective volumes and material properties. Finally, the thesis considered carbon emissions associated with electricity usage. The gathered information and equations were implemented into the simulation model to analyse the HyTES system's carbon footprint.

The methodology continued with a multi-objective optimisation function for the optimisation algorithm, considering three key performance indicators; minimal system costs, self-sufficiency, and carbon footprint.

The optimisation function implemented flexible self-sufficiency ranges and weighting factors, enhancing the function's adaptability to specific project requirements. The Utopia and Nadir points were identified to normalise the objective functions. A vital feature of the methodology is variable self-sufficiency within the optimisation, providing multiple potential solutions to the clients instead of a single outcome.

The methodology expands into examining various optimisation variables such as tank types and dimensions, PCM capsules packed bed size, minimum HyTES energy level, DHW tank size, number of PV panels, and PV orientation, recognising the unique role of each of these variables in enhancing the system's overall efficiency.

To further elaborate on the optimisation, one specific case was selected in which the HyTES system uses a vacuum-insulated tank as Seasonal thermal energy storage.

For this case, the selected optimisation variables were verified using sensitivity analysis to assess the influence of various optimisation variables on selected KPIs. The sensitivity analysis revealed that the dimensions of the HyTES tank and PV system variables were the most influential. In contrast, those relating to the DHW tank had the most negligible effect.

Following the sensitivity analysis, initial optimisation runs were done to give insight into how the results of the optimisation strategy and how they are interpreted. Three optimisation scenarios were selected with differing levels of SS (78%, 84%, 97%). The primary trend identified was the significant increase in the HyTES tank volume as SS increased. The optimisation results also revealed the substantial impact of subsidies and feed-in tariffs on LCOH, reducing it by over 40% in the 78% SS scenario.

A comparison of the main contributors to LCOH and GWP across different scenarios indicated that

Operation and Maintenance costs and the PV system were the most significant contributors to LCOH. Simultaneously, the PV system and grid electricity significantly influenced GWP. However, the STES contribution to LCOH and GWP increased dramatically at nearly full autonomy (SS=97%).

The most optimal system of the initial optimisation runs achieved an SS of 78%, falling within the desired range. It boasts the lowest LCOH among the optimised systems and, with incentives, is almost cost-competitive with oil boilers. Moreover, its GWP is three times lower than the base case.

The results were instrumental in understanding how HyTES system optimisation can contribute to energy sustainability. Moreover, the economic viability of such systems is significantly influenced by the availability of subsidies and grid sell-back schemes, demonstrating the critical role of policy in advancing sustainable energy solutions.

In summary, the primary objective of this thesis was successfully achieved, with an effective method developed to calculate the HyTES system's carbon footprint, an optimisation-objective function formulated, and the identification and delineation of optimisation variables and their ranges. By presenting the initial optimisation results, the effectiveness was confirmed.

8.2 Recommendations

Following the areas of improvement identified in section 7, the following recommendations are made.

Model
Several vital areas warrant further investigation and improvement to enhance the accuracy and reliability of the model. Firstly, conducting a sensitivity analysis by comparing the optimisation results with and without the GWP in the objective function would provide valuable insights into the significance of incorporating GWP. Additionally, a thorough examination of the mesh size and time steps used in optimisation is recommended to improve computation efficiency and precision. Secondly, for a more accurate estimation of the GWP of VIT type, acquiring better data on the type(s) of steel used in storage tanks and tank weights corresponding to different volumes is essential. This data would enable a more informed estimation of the GWP per kilogram of the tank and its relationship with storage capacity. Thirdly, conducting a detailed analysis of O&M costs, rather than relying on a general assumption, would lead to a more reliable economic assessment. Finally, to enhance the environmental impact assessment, considering time-dependent GWP values for electricity consumption and accounting for potential future trends in the GWP of Swiss electricity would yield a more precise evaluation of the system's environmental impact. The model's accuracy and applicability would be significantly improved by addressing these areas, making it a valuable tool for sustainable decision-making in the energy sector.

technology
To further enhance the technological capabilities, it is recommended to consider alternative PV technologies beyond the currently pre-selected PV system. Different PV technologies can have varying impacts, and exploring these alternatives would lead to a more comprehensive analysis, allowing the identification of the most suitable PV technology for this specific system.

Additionally, while the complete HyTES system offers a viable solution, combining PV panels and solar thermal collectors could improve its sustainability. Using thermal collectors to supply DHW throughout the year primarily, the heat pump's efficiency could be enhanced, as it performs better when delivering lower temperatures. This change would require a solar collector model that

efficiently supplies heat to the DHW tank while using the HyTES tank as a heat sink when the DHW tank reaches capacity.

To assess the impact of this improvement, the model should be extended to include the additional heat supply from the solar thermal collectors and analyze the system's behaviour accordingly. Such an enhancement would provide valuable insights into the system's overall performance, contributing to its continual improvement and optimisation.

References

[1] A. Kemmler and T. Trachsel, "Analyse des schweizerischen Energieverbrauchs 2000–2021," Bundesamt für Energie, Bern, Tech. Rep., 10 2022. [Online]. Available: https://pubdb.bfe.admin.ch/de/publication/download/11144

[2] Bundesamt für Statistik (BFS), "Bau- und Wohnungswesen 2014," Bundesamt für Statistik (BFS), Neuchatel, Tech. Rep., 2016. [Online]. Available: https://www.bfs.admin.ch/bfs/de/home/statistiken/kataloge-datenbanken/publikationen.assetdetail.350354.html

[3] Bundesamt für Energie BFE, "Wärmestrategie 2050," Bundesamt für Energie, Bern, Tech. Rep., 1 2023. [Online]. Available: https://www.admin.ch/gov/de/start/dokumentation/medienmitteilungen.msg-id-92576.html

[4] Swiss Federal Office of Energy, "What is the Energy Strategy 2050?" 2020. [Online]. Available: https://www.bfe.admin.ch/bfe/en/home/policy/energy-strategy-2050/what-is-the-energy-strategy-2050.html

[5] C. Hewicker, O. Werner, M. Ebert, T. Dr. Mennel, and N. R. Dr. Verhaegh, "Energiespeicher in der Schweiz: Bedarf, Wirtschaftlichkeit und Rahmenbedingungen im Kontext der Energiestrategie 2050," Bundesamt für Energie, Bern, Tech. Rep., 2013. [Online]. Available: https://www.news.admin.ch/NSBSubscriber/message/attachments/33125.pdf

[6] European Technology Platform on Renewable Heating and Cooling, "RHC Platform: Strategic Research Priorities for Geothermal Electricity." European Technology Platform on Renewable Heating and Cooling, Brussel, Tech. Rep., 2012.

[7] Jenni Energietechnik, "Solarüberbauung Allmend, Huttwil," *Jenni Energietechnik*, 11 2016. [Online]. Available: https://jenni.ch/files/jenni/inhalte/pdf/ueber_uns/Dokumentation_Bauprojekt_Huttwil.pdf

[8] R. Hendry, W. Villasmil, and J. Worlitschek, "OPTSAIS – Exergetic and Economic Optimization of Seasonal Thermal Energy Storage Systems," 2019. [Online]. Available: https://www.researchgate.net/publication/344364908_OPTSAIS_-_Exergetic_and_Economic_Optimization_of_Seasonal_Thermal_Energy_Storage_Systems

[9] "HyTES: Optimierung hybrider saisonaler Wärmespeichersysteme mithilfe von Phasenwechselmaterialien — Lucerne University of Applied Sciences and Arts." [Online]. Available: https://www.hslu.ch/en/lucerne-university-of-applied-sciences-and-arts/research/projects/detail/?pid=5718

[10] Schweizerischer Ingenieur- und Architektenverein, ""SIA 385/2 (2015): Anlagen für Trinkwarmwasser in Gebäuden - Warmwasserbedarf, Gesamtanforderungen und Auslegung."," Schweizerischer Ingenieur- und Architektenverein, Zurich, Tech. Rep., 2014.

[11] R. Stropnik, R. Koželj, E. Zavrl, and U. Stritih, "Improved thermal energy storage for nearly zero energy buildings with PCM integration," *Solar Energy*, vol. 190, pp. 420–426, 2019. [Online]. Available: https://www.sciencedirect.com/science/article/pii/S0038092X19308229

[12] W. Delgado, M. Troxler, R. Hendry, P. Roos, W. Villasmil, and J. Worlitschek, "Interim Report HyTES - Optimization of hybrid seasonal thermal storage systems using phase change materials," Swiss Federal Office of Energy SFOE, Tech. Rep., 2022.

[13] C. Audet and J. E. Dennis, "Mesh Adaptive Direct Search Algorithms for Constrained Optimization," *https://doi-org.ezproxy2.utwente.nl/10.1137/040603371*, vol. 17, no. 1, pp. 188–217, 7 2006. [Online]. Available: https://epubs-siam-org.ezproxy2.utwente.nl/doi/10.1137/040603371

[14] N. Nallusamy, S. Sampath, and R. Velraj, "Experimental investigation on a combined sensible and latent heat storage system integrated with constant/varying (solar) heat sources," *Renewable Energy*, vol. 32, no. 7, pp. 1206–1227, 2007. [Online]. Available: https://www.sciencedirect.com/science/article/pii/S0960148106001121

[15] S. Padmaraju, M. Viginesh, and N. Nallusamy, "Comparitive study of sensible and latent heat storage systems integrated with solar water heating unit," *Renewable Energy and Power Quality Journal*, vol. 1, 3 2008.

[16] A. Frazzica, M. Manzan, A. Sapienza, A. Freni, G. Toniato, and G. Restuccia, "Experimental testing of a hybrid sensible-latent heat storage system for domestic hot water applications," *Applied Energy*, vol. 183, pp. 1157–1167, 2016. [Online]. Available: https://www.sciencedirect.com/science/article/pii/S0306261916313782

[17] G. Zanganeh, M. Commerford, A. Haselbacher, A. Pedretti, and A. Steinfeld, "Stabilization of the outflow temperature of a packed-bed thermal energy storage by combining rocks with phase change materials," *Applied Thermal Engineering*, vol. 70, no. 1, pp. 316–320, 2014. [Online]. Available: https://www.sciencedirect.com/science/article/pii/S1359431114003780

[18] L. Geissbühler, M. Kolman, G. Zanganeh, A. Haselbacher, and A. Steinfeld, "Analysis of industrial-scale high-temperature combined sensible/latent thermal energy storage," *Applied Thermal Engineering*, vol. 101, pp. 657–668, 2016. [Online]. Available: https://www.sciencedirect.com/science/article/pii/S135943111501412X

[19] C. Suresh and R. P. Saini, "An experimental study on the performance evaluation of a combined sensible-latent heat thermal energy storage," *International Journal of Energy Research*, vol. 45, no. 4, pp. 5730–5746, 2021. [Online]. Available: https://onlinelibrary.wiley.com/doi/abs/10.1002/er.6196

[20] N. Delalić, R. Blažević, M. Alispahić, and M. Torlak, "A Small-Scale Solar System with Combined Sensible- and Latent-Heat Thermal Energy Storage," *Lecture Notes in Networks and Systems*, vol. 60, pp. 582–588, 2019. [Online]. Available: https://link.springer.com/chapter/10.1007/978-3-030-02577-9_57

[21] D. Lafri, D. Semmar, A. Hamid, and M. Ouzzane, "Experimental investigation on combined sensible and latent heat storage in two different configurations of tank filled with PCM," *Applied Thermal Engineering*, vol. 149, pp. 625–632, 2 2019.

[22] G. Englmair, S. Furbo, M. Dannemand, and J. Fan, "Experimental investigation of a tank-in-tank heat storage unit utilizing stable supercooling of sodium acetate trihydrate," *Applied Thermal Engineering*, vol. 167, p. 114709, 2 2020.

[23] A. Frazzica, V. Palomba, and A. Freni, "Development and Experimental Characterization of an Innovative Tank-in-Tank Hybrid Sensible–Latent Thermal Energy Storage System," *Energies*, vol. 16, no. 4, 2023. [Online]. Available: https://www.mdpi.com/1996-1073/16/4/1875

[24] C. Zauner, F. Hengstberger, B. Mörzinger, R. Hofmann, and H. Walter, "Experimental characterization and simulation of a hybrid sensible-latent heat storage," *Applied Energy*, vol. 189, pp. 506–519, 3 2017.

[25] N. Ahmed, K. E. Elfeky, L. Lu, and Q. W. Wang, "Thermal performance analysis of thermocline combined sensible-latent heat storage system using cascaded-layered PCM designs for medium temperature applications," *Renewable Energy*, vol. 152, pp. 684–697, 6 2020.

[26] ——, "Thermal and economic evaluation of thermocline combined sensible-latent heat thermal energy storage system for medium temperature applications," *Energy Conversion and Management*, vol. 189, pp. 14–23, 6 2019.

[27] O. G. Pop and M. C. Balan, "A numerical analysis on the performance of DHW storage tanks with immersed PCM cylinders," *Applied Thermal Engineering*, vol. 197, p. 117386, 10 2021.

[28] A. Frazzica, M. Manzan, V. Palomba, V. Brancato, A. Freni, A. Pezzi, and B. M. Vaglieco, "Experimental Validation and Numerical Simulation of a Hybrid Sensible-Latent Thermal Energy Storage for Hot Water Provision on Ships," *Energies*, vol. 15, no. 7, 2022. [Online]. Available: https://www.mdpi.com/1996-1073/15/7/2596

[29] S. Shah, L. Aye, and B. Rismanchi, "Multi-objective optimisation of a seasonal solar thermal energy storage system for space heating in cold climate," *Applied Energy*, vol. 268, 2020.

[30] K. Siraganyan, A. T. D. Perera, J.-L. Scartezzini, and D. Mauree, "Eco-Sim: A Parametric Tool to Evaluate the Environmental and Economic Feasibility of Decentralized Energy Systems," *Energies*, vol. 12, no. 5, 2019. [Online]. Available: https://www.mdpi.com/1996-1073/12/5/776

[31] V. Tulus, D. Boer, L. F. Cabeza, L. Jiménez, and G. Guillén-Gosálbez, "Enhanced thermal energy supply via central solar heating plants with seasonal storage: A multi-objective optimization approach," *Applied Energy*, vol. 181, pp. 549–561, 11 2016.

[32] M. Ehrgott, "Multicriteria optimization: Second edition," *Multicriteria Optimization: Second Edition*, pp. 1–323, 2005.

[33] F. PELELLA, G. ZSEMBINSZKI, L. VISCITO, A. William MAURO, and L. F. CABEZA, "Thermo-economic optimization of a multi-source (air/sun/ground) residential heat pump with a water/PCM thermal storage," *Applied Energy*, vol. 331, p. 120398, 2 2023.

[34] "Understanding Global Warming Potentials — US EPA." [Online]. Available: https://www.epa.gov/ghgemissions/understanding-global-warming-potentials

[35] R. T. Marler and J. S. Arora, "The weighted sum method for multi-objective optimization: New insights," *Structural and Multidisciplinary Optimization*, vol. 41, no. 6, pp. 853–862, 6 2010. [Online]. Available: https://link-springer-com.ezproxy2.utwente.nl/article/10.1007/s00158-009-0460-7

[36] O. Grodzevich and O. Romanko, "Normalization and other topics in multi-objective optimization," *Proceedings of the Fields-MITACS Industrial Problems Workshop*, 8 2006.

[37] Sirch Tankbau-Tankservice Speicherbau GmbH, "Serienspeicher Plus X: Pufferspeicher, Speichertechnik, Wärmespeicher, Brauchwasserspeicher, Schichtspeicher." [Online]. Available: https://pufferspeicher-sirch.de/speicher/serienspeicher-plus-x/

[38] Suntech, "IEC-STP-Ultra-Smini-NO2.02-rev2021." [Online]. Available: https://www.suntech-power.com/wp-content/uploads/download/product-specification/EN_Ultra_S_mini_STP380S_B60_Wnh.pdf

[39] A. Diehl, "Determining Module Inter-Row Spacing." [Online]. Available: https://www.greentechrenewables.com/article/determining-module-inter-row-spacing

[40] timeanddate, "Bern, Bern, Switzerland — Sunrise, Sunset, and Daylength, December 2023." [Online]. Available: https://www.timeanddate.com/sun/switzerland/bern?month=12&year=2023

[41] Galletti, "Water chillers and heat pumps using air as thermal source." [Online]. Available: https://www.galletti.com/en/chillers_and_heat_pumps_564/dissipation-with-air

[42] M. J. S. Zuberi, K. Narula, S. Klinke, J. Chambers, K. N. Streicher, and M. K. Patel, "Potential and costs of decentralized heat pumps and thermal networks in Swiss residential areas," *International Journal of Energy Research*, vol. 45, no. 10, pp. 15 245–15 264, 8 2021. [Online]. Available: https://doi.org/10.1002/er.6801

[43] FOEN, "Switzerland's Greenhouse Gas Inventory 1990–2016," FOEN, Bern, Tech. Rep., 2018. [Online]. Available: https://www.infras.ch/media/filer_public/e0/a9/e0a95eca-7e83-4123-89cc-6bf4f70a6f37/che-2018-nir.pdf

[44] J. Peng, L. Lu, and H. Yang, "Review on life cycle assessment of energy payback and greenhouse gas emission of solar photovoltaic systems," *Renewable and Sustainable Energy Reviews*, vol. 19, pp. 255–274, 3 2013.

[45] R. Frischknecht, P. Stolz, L. Krebs, M. de Wild-Scholten, Sinha P., V. Fthenakis, H. C. Kim, M. Raugei, and M. Stucki, "Life Cycle Inventories and Life Cycle Assessment of Photovoltaic Systems," *International Energy Agency (IEA) PVPS Task 12*, vol. Report T12-19:2020, 2020.

[46] V. Fthenakis and H. Kim, "Photovoltaics: Life-cycle analyses," *Solar Energy*, vol. 85, no. 8, pp. 1609–1628, 2011.

[47] F. Cucchiella and I. Dadamo, "Estimation of the energetic and environmental impacts of a roof-mounted building-integrated photovoltaic systems," *Renewable and Sustainable Energy Reviews*, vol. 16, no. 7, pp. 5245–5259, 2012.

[48] L. Krebs and R. Frischknecht, "Umweltbilanz Strommixe Schweiz 2018," Treeze, Uster, Tech. Rep., 2021.

[49] M. Smith, A. Bevacqua, S. Tembe, and P. Lal, "Life cycle analysis (LCA) of residential ground source heat pump systems: A comparative analysis of energy efficiency in New Jersey," *Sustainable Energy Technologies and Assessments*, vol. 47, p. 101364, 10 2021.

[50] E. P. Johnson, "Air-source heat pump carbon footprints: HFC impacts and comparison to other heat sources," *Energy Policy*, vol. 39, no. 3, pp. 1369–1381, 3 2011.

[51] B. Greening and A. Azapagic, "Domestic heat pumps: Life cycle environmental impacts and potential implications for the UK," *Energy*, vol. 39, no. 1, pp. 205–217, 3 2012.

[52] L. Gang, "Comprehensive investigations of life cycle climate performance of packaged air source heat pumps for residential application," *Renewable and Sustainable Energy Reviews*, vol. 43, pp. 702–710, 3 2015.

[53] T. Kägi, L. Waldburger, C. Kern, G. Roberts, M. Zschokke, F. Conte, L. Weber, and Carbotech AG, "Life cycle inventories of heating systems: Heat from natural gas, biomethane, district heating, electric heating, heat pumps, PVT, wood, cogeneration," Federal Office for the Environment (FOEN), Zurick, Tech. Rep., 2021.

[54] Viessmand Werke GmbH & Co. KG, "Aktualisierte Umwelterklarung 2019," Viessmann, Tech. Rep., 2019.

[55] R. Frischknecht, N. Jungbluth, H.-J. Althaus, G. Doka, R. Dones, T. Heck, S. Hellweg, R. Hischier, T. Nemecek, G. Rebitzer, M. Spielmann, and G. Wernet, "ecoinvent report No. 1: Overview and Methodology ," Ecoinvent: Swiss Centre for Life Cycle Inventories, Dübendorf, Tech. Rep., 2007.

[56] BSRIA, "BSRIA's view on refrigerant trends in AC and Heat Pump segments." [Online]. Available: https://www.bsria.com/uk/news/article/bsrias_view_on_refrigerant_trends_in_ac_and_heat_pump_segments/

[57] V. Masson-Delmotte, P. Zhai, A. Pirani, S.L. Connors, S. B. C. Péan, N. Caud, Y. Chen, L. Goldfarb, M.I. Gomis, M. Huang, K. Leitzell, E. Lonnoy, J.B.R. Matthews, T.K. Maycock, T. Waterfield, O. Yelekçi, R. Yu, and B. Zhou (eds.), "Climate Change 2021: The Physical Science Basis. Contribution of Working Group I to the Sixth Assessment Report of the Intergovernmental Panel on Climate Change," Cambridge University Press, Cambridge, Tech. Rep., 2021.

[58] SirchSirch Tankbau-Tankservice Speicherbau GmbH, "Sirch Vacutherm." [Online]. Available: https://pufferspeicher-sirch.de/speicher/vakuum-pufferspeicher/

[59] "Anfragen-Konfigurator: Pufferspeicher, Speichertechnik, Wärmespeicher, Brauchwasserspeicher, Schichtspeicher." [Online]. Available: https://pufferspeicher-sirch.de/speicher/anfragen-konfigurator/

[60] Energy4Me, "Speicherlösung - energy4me Warmwasserspeicher enerSAFE." [Online]. Available: https://www.energy4me.ch/speicherloesung/

[61] Metsims, "ENVIRONMENTAL PRODUCT DECLARATION In accordance with ISO 14025 and EN 15804:2012+A2:2019 for Glassfiber Reinforced Plastic (GRP) Pipes from Subor Boru San. ve Tic. A.Ş." EPD International AB, Kağıthane-Istanbul, Tech. Rep., 2021. [Online]. Available: https://api.environdec.com/api/v1/EPDLibrary/Files/10897adf-b617-448e-1ef0-08db090ef553/Data

[62] I. S. Abbood, S. A. Odaa, K. F. Hasan, and M. A. Jasim, "Properties evaluation of fiber reinforced polymers and their constituent materials used in structures – A review," *Materials Today: Proceedings*, vol. 43, pp. 1003–1008, 1 2021.

[63] IBU - Institut Bauen und Umwelt e.V., "ENVIRONMENTAL PRODUCT DECLARATION: Polyurethane thermal insulation spray foam," IBU - Institut Bauen und Umwelt e.V., Berlin, Tech. Rep., 2014.

[64] CC Thermal Energy Storage, "Wärmegedämmtes Abdichtungssystem für saisonale Warmwasserspeicher im Hochbau." [Online]. Available: https://www.hslu.ch/en/lucerne-university-of-applied-sciences-and-arts/research/projects/detail/?pid=3894

[65] R. Frischknecht, "UMWELTPRODUKTDEKLARATION NACH NORM SN EN 15804+A1:2013: swissporXPS, Wärmedämmplatten aus extrudiertem Polystyrol," treeze GmbH fair life cycle thinking, Uster, Tech. Rep., 2017.

[66] D. Vuarnoz and T. Jusselme, "Temporal variations in the primary energy use and greenhouse gas emissions of electricity provided by the Swiss grid," *Energy*, vol. 161, pp. 573–582, 10 2018.

[67] ——, "Dataset concerning the hourly conversion factors for the cumulative energy demand and its non-renewable part, and hourly GHG emission factors of the Swiss mix during a one year period (2015–2016)," *Data in Brief*, vol. 21, pp. 1026–1028, 12 2018.

[68] T. Yang, W. Liu, G. J. Kramer, and Q. Sun, "Seasonal thermal energy storage: A techno-economic literature review," *Renewable and Sustainable Energy Reviews*, vol. 139, p. 110732, 2021. [Online]. Available: https://www.sciencedirect.com/science/article/pii/S1364032121000290

[69] C. Hill, A. Norton, and J. Dibdiakova, "A comparison of the environmental impacts of different categories of insulation materials," *Energy and Buildings*, vol. 162, pp. 12–20, 3 2018.

[70] "Air Source Heat Pump — Alternative Heating — Viessmann UK." [Online]. Available: https://www.viessmann.co.uk/en/products/heat-pump/air-source-heat-pumps.html

[71] L. Geissbühler, M. Kolman, G. Zanganeh, A. Haselbacher, and A. Steinfeld, "Analysis of industrial-scale high-temperature combined sensible/latent thermal energy storage," *Applied Thermal Engineering*, vol. 101, pp. 657–668, 2016. [Online]. Available: https://www.sciencedirect.com/science/article/pii/S135943111501412X

[72] "CO2 levy." [Online]. Available: https://www.bafu.admin.ch/bafu/en/home/topics/climate/info-specialists/reduction-measures/co2-levy.html

[73] Nationale Dienstleistungszentrale nDLZ Ernst Basler + Partner, "Das Gebäudeprogramm im Jahr 2015; Jahresbericht," Konferenz Kantonaler Energiedirektoren EnDK, Bern, Tech. Rep., 2015. [Online]. Available: https://www.dasgebaeudeprogramm.ch/media/filer_public/b3/16/b3163204-b86a-4d6b-b1e3-fa6292f66b11/jahresbericht_2015.pdf

[74] C. Audet and W. Hare, *Derivative-Free and Blackbox Optimization*, 1st ed. Cham: Springer International Publishing, 2017.

[75] C. Arpagaus, B. Vetsch, and S. Bertsch, "Domestic Hot Water Heat Pumps: Task 1 Market Overview Country Report Switzerland," Interstaatliche Hochschule für Technik Buchs, NTB Institut für Energiesysteme IES, Buchs, Tech. Rep., 2016.

[76] C. Rathgeber, E. Lävemann, and A. Hauer, "Economic top-down evaluation of the costs of energy storages-A simple economic truth in two equations," *Journal of Energy Storage*, vol. 2, pp. 43–46, 2015. [Online]. Available: https://www.researchgate.net/publication/279188024_Economic_top-down_evaluation_of_the_costs_of_energy_storages_-_A_simple_economic_truth_in_two_equations

[77] A. T. Perera, V. M. Nik, D. Mauree, and J. L. Scartezzini, "Electrical hubs: An effective way to integrate non-dispatchable renewable energy sources with minimum impact to the grid," *Applied Energy*, vol. 190, pp. 232–248, 3 2017.

[78] D. Erdemir, A. Ozbekler, and N. Altuntop, "Experimental investigation on the effect of the ratio of tank volume to total capsulized paraffin volume on hot water output for a mantled hot water tank," *Solar Energy*, vol. 239, pp. 294–306, 6 2022.

[79] C. Suresh and R. P. Saini, "Experimental study on combined sensible-latent heat storage system for different volume fractions of PCM," *Solar Energy*, vol. 212, pp. 282–296, 12 2020.

[80] R. Schuetz Philipp
}and Scoccia, G. Damian, W. Remo, S. David, E. Peru, A. Beñat, S. Alessandro, A. Marcello, and W. Jörg, "Fast Simulation Platform for Retrofitting Measures in Residential Heating," in *Cold Climate HVAC 2018*, H. Johansson Dennis
}and Bagge and W. Åsa, Eds. Cham: Springer International Publishing, 2019, pp. 713–723.

[81] P. Garcia and J. Pouvreau, "High temperature combined sensible-latent thermal energy storage," *AIP Conference Proceedings*, vol. 2126, no. 1, p. 200020, 7 2019. [Online]. Available: https://aip-scitation-org.ezproxy2.utwente.nl/doi/abs/10.1063/1.5117735

[82] M. Gutschner and S. Nowak, "Potenzialabschätzung zum solarthermischen Beitrag zur Wärmeversorgung im schweizerischen Wohngebäudepark," Bundesamt für Energie, Bern, Tech. Rep., 2012. [Online]. Available: https://www.swissolar.ch/fileadmin/user_upload/Swissolar/Unsere_Dossiers/SolarthermischesPotenzialSchweizerWohngebaeudepark_20120116_BFE.pdf

[83] Valentin Software, "PV*SOL." [Online]. Available: https://valentin-software.com/produkte/pvsol/

[84] C. Suresh and R. P. Saini, "Review on solar thermal energy storage technologies and their geometrical configurations," *International Journal of Energy Research*, vol. 44, no. 6, pp. 4163–4195, 5 2020. [Online]. Available: https://onlinelibrary-wiley-com.ezproxy2.utwente.nl/doi/full/10.1002/er.5143https://onlinelibrary-wiley-com.ezproxy2.utwente.nl/doi/abs/10.1002/er.5143https://onlinelibrary-wiley-com.ezproxy2.utwente.nl/doi/10.1002/er.5143

[85] R. Marler and J. Arora, "Survey of Multi-Objective Optimization Methods for Engineering," *Structural and Multidisciplinary Optimization*, vol. 26, pp. 369–395, 4 2004.

[86] T. Heck, "Teil X: Warmepumpen data v2.0," *Ecoinvent centre*, 2007.

[87] Bundesamt für Energie BFE, "Wärmestrategie 2050," Bundesamt für Energie, Bern, Tech. Rep., 1 2023. [Online]. Available: https://www.admin.ch/gov/de/start/dokumentation/medienmitteilungen.msg-id-92576.html

Appendix

A Appendix 1: Literature review matrix of paper that are about hybrid latent-Sensible heat storage

Table 11: Literature review matrix of paper that are about hybrid latent-Sensible heat storage

Authors, year, Journal	**Goal of research**	**Type**	**Main findings**
N. Nallusamy et. al., 2007, Renewable Energy [14]	Predict thermal behavior of system for DHW	Encapsulated PCMs in water tank - General Domestic Heating	Hybrid TES enhances performance and is effective for intermittent heat needs
S.A.Vijay Padmaraju et. al., 2008 [15]	Experiment with PCMs for solar energy storage	Encapsulated PCMs in water tank - General Domestic Heating	PCM-based storage is more effective than traditional sensible heat storage
G. Zanganeh et. al. 2014, Applied Thermal Engineering [17]	Develop hybrid TES for CSP stabilization	Double packed bed with stacked PCMs and sensible storage - CSP	Encapsulated PCM in packed-bed storage maintains temperature stability
L. Geissbühler et. al. 2016, Applied Thermal Engineering [18]	Compare exergy efficiency of industrial TES	Double packed bed with stacked PCMs and sensible storage - Industrial heat H. temp.	Integrated storage systems decrease material expenses while meeting energy efficiency targets
A. Frazzica et. al., 2016, Applied Energy [16]	Compare two different PCMs for small-scale heat storage	Encapsulated PCMs in water tank - DHW	PCM-based hot water systems improve delivery capability by 10%
C. Zauner et. al., 2017, Applied Energy [24]	Study hybrid TES with inverted shell-and-tube configuration	Shell-and-tube heat exchanger - Heating Networks	Increasing PCM volume and tube diameter reduces material expenses per kWh
N. Delalic et. al., 2019, Advance Technologies, System, and Applications [20]	Investigate solar thermal heat storage with hybrid TES	Tank-in-tank with inner PCM - General Domestic Heating	PCM stabilizes temperatures and increase heat absorption
N. Ahmed et. al., 2019, Energy conversion and Management [26]	Develop hybrid TES for medium temp. applications	Encapsulated PCM impregnated between solid rods - General Heat Storage M. Temp.	Hybrid TES is the most viable option with optimized performance and comparatively low cost

Continued on next page

Table 11: Literature review matrix of paper that are about hybrid latent-Sensible heat storage (Continued)

P. Garcia et. al., 2019	Develop hybrid TES for CSP with high efficiency cycles	Encapsulated PCMs in molten salt - CSP	AlSi is a superior PCM material for high temperatures
D. Lafri et. al., 2019, Applied Thermal Engineering [21]	Optimize charging/discharging of latent heat storage	Tank-in-tank with a comparison of PCM placement - General Heat Storage	Proper arrangement of PCM layers is crucial for cascading PCM with vertical rod storage configurations
C. Suresh et. al., 2020, Energy Research [84]	Evaluate thermal energy storage methods	Various systems described - General Heat Storage	Higher volume fractions of PCM result in greater energy storage and transfer
N. Ahmed et. al., 2020, Renewable Energy [25]	Design hybrid TES for medium temp. applications	Cascading encapsulated PCM impregnated between solid rods - General Heat storage	Discontinuous discharge method with intervals of 2-24 hours increases discharge time and utilization
C. Suresh et. al., 2020, Solar Energy [79]	Design hybrid TES to combat thermocline degradation	Double packed bed with stacked PCMs and sensible storage	Combined sensible-latent heat storage system performs better than conventional sensible heat storage
G. Englmaira et. al., 2020, Applied Thermal Engineering [22]	Develop economically attractive compact TES	Tank-in-tank with inner PCM - General Domestic Heating	Adding PCM capsules above concrete spheres increases discharge time and reduces temperature drop
C. Suresh et. al., 2021, Int. J. of Energy Research [19]	Suggest hybrid TES to address limitations of SHS and LHS	Double packed bed with stacked PCMs and sensible storage	PCM reduces storage tank volume by 25% and reduces fuel consumption from gas fuel boilers
O.G. Pop et. al., 2021, Applied Thermal Engineering [27]	Evaluate DHW storage tanks with and without PCMs	PCM encapsulated in vertical rods in water tank - DHW	Novel system increases storage density up to 35% compared to only sensible storage
A. Frazzica et. al., 2022, Energies [28]	Develop hybrid TES for DHW for ships	PCM encapsulated in vertical rods in water tank - DHW	Maximum of 13 large PCM capsules increases DHW by 20%, after which the capsules take up too much space

Continued on next page

Table 11: Literature review matrix of paper that are about hybrid latent-Sensible heat storage (Continued)

D. Erdemir et. al., 2022, Solar Energy [78]	Determine effect of paraffin amount on hot water output	Large encapsulated PCMs in water tank - General Heat Storage	New configuration increases energy storage and DHW provision by up to 16% with an optimal charging temperature of 62-68°C.
A. Frazzica et. al., 2023, Energies [23]	Develop hybrid TES for DHW provision in residential buildings	Tank-in-tank with inner PCM and outer water tank - DHW	A new configuration can increase energy storage capacity and corresponding DHW provision by up to 16%.

B Appendix 2: Comparative life-cycle assessment of energy storage technologies for photovoltaic-heat pump systems of single-family houses

Author: Sztranyovszky Lóránt

TES – Thermal energy storage
SFH – Single family house
PCM – Phase change material
SPF – Seasonal performance factor
LCIA – Life cycle impact assessment
SD – Standard deviation
SAT – Sodium acetate trihydrate
GWP – Global warming potential
EoL – End of life
CH – Switzerland
RER – Europe
RoW – Rest of the world
GLO – Global
CN – China

Goal and scope definition

The goal of this study is to quantitatively compare the potential environmental impact of different energy storage technologies including a novel TES based on encapsulated phase-change material. Scope: Energy storage systems on a typical scale for an SFH. Namely,

- A 600l hot-water tank filled with an encapsulated phase-change material (COWA capsules)
- This is compared to a sensible TES with identical capacity. Assuming that the energy storage density of the latent TES is exactly a factor of 2 higher, this translates to Two identical hot-water tanks, without COWA capsules
- This is further compared to a Li-ion battery. The equivalent battery capacity is calculated with an SPF of 2.8 (heat pump) as a conversion factor, with additional adjustment for degradation and a shorter lifetime. Li-ion battery pack (NMC111) with a nominal capacity of 13.5 kWh

A cradle-to-grave system boundary is used with the assumption that different storage technologies of equivalent capacity have an identical effect on the energy system of the SFH. Therefore, an analysis of the use phase can be omitted as no difference between the compared alternatives is expected. The analysis was performed using the two system models cut off by classification and consequential. The EF3.0 was the primary LCIA method used, although, some of the results have been additionally computed with the ReCiPe 2016 (H) and the Cumulative energy demand methods. The impact category of main interest was climate change. Some further impact categories were computed additionally but not discussed in detail. The primary data source is version 3.8 of the Ecoinvent database.

Inventory analysis

Information about provider processes is included for each entry - note that these are typically market activities. All provider processes not specifically analyzed can be found in the Ecoinvent database. There is also an inherent uncertainty attached to every exchange modelled as a lognormal probability distribution with the square of the geometric standard deviation SDgeo^2 indicated for each entry ('amount' corresponds to the arithmetic mean).

Sodium acetate

This material serves as the base of the PCM, but its production process is not modelled in the database. Due to the lack of reliable information about the industrial production process of SAT, the inventory is largely based on estimates. The SAT is assumed to be produced by reacting acetic acid with sodium hydroxide according to the following reaction:

$$CH_3COOH + NaOH + 2H_2O \longrightarrow CH_3COONa \cdot 3H_2O$$

The required amount of input materials can be estimated by stochiometric calculation, assuming a yield of 95%. Although the above reaction is exothermic, the production process likely still requires additional energy input in form of heat and electricity.. The input materials are assumed to be marketed in 50% solution, and it is assumed that the water remaining after the reaction must be evaporated. This allows a rough estimate of the heat demand with rather high uncertainty. The electricity demand, however, cannot be reasonably estimated. The inventories of other chemicals typically include electricity in the range of 0.05-0.45 kWh, but these values are often "standard assumptions" i.e., not process-specific. The additional inputs considered include water for cooling, the construction of the chemical factory and the required transportation. The production location is China with the corresponding transportation distance of 1 200 km by a mix of freight train and lorry, plus 14 000 km by container ship. The complete inventories of SAT production are:

	amount	SD_{geo}^2	provider (remark)
reference product:			
sodium acetate, trihydrate	1 kg		(incl. shipment)
inputs:			
water, unspecified natural origin	0.024 m^3	1.8	GLO
sodium hydroxide	0.310 kg	1.35	GLO market
acetic acid	0.465 kg	1.35	GLO market
water, deionized	0.774 kg	1.35	RoW market
transport, container ship	14 tkm	2.2	GLO market
transport, freight train	0.8 tkm	2.2	GLO market
transport, lorry >32t, euro5	0.4 tkm	2.2	GLO market
electricity, medium voltage	0.15 kWh	4.0	CN market group
heat, district or industrial, natural gas	2 MJ	2.3	RoW, industrial furnace >100 kW
chemical factory, organics	4E-10	4.0	GLO market
emission/waste flows:			
heat, waste	2 MJ	2.0	emission to air
sodium hydroxide	0.015 kg	3.0	emission to water (rough estimates from literature, little relevance to the final result)
ethyl acetate	0.004 kg	3.0	
BOD (Biological Oxygen Demand)	0.006 kg	2.0	
COD (Chemical Oxygen Demand)	0.006 kg	2.0	
TOC (Total Organic Carbon)	0.002 kg	2.0	
wastewater, average	0.001 m^3	2.0	RoW market

Hot water tank

The inventory is modelled for a tank made of stainless steel with wall thickness of 2.5mm, insulated by a 120mm layer of glass wool. Based on a similar product in the Ecoinvent database, a small amount of PVC is also included as well as some softwood for packaging. The input "metal working" includes an estimate of the energy demand as well as infrastructure use and material waste during production. The EoL treatment of steel, glass wool and PVC are accounted for as output waste flows. It is assumed that steel is disposed of in mixed metal scrap while glass wool is landfilled, and PVC is incinerated.

	amount	SD_{geo}^2	provider (remark)
reference product:			
hot water tank, 600l, without heat exchanger	1 unit		
inputs:			
steel, chromium steel 18/8, hot rolled	90 kg	1.25	GLO market
glass wool mat	20 kg	1.25	GLO market
sawnwood, softwood	0.0222 m3	1.40	RER market
polyvinylchloride	2 kg	1.25	GLO market
alkyd paint, white	1 kg	1.25	RER market
metal working, average for chromium steel product manufacturing	90 kg	1.25	GLO market
tap water	600 kg	1.05	CH
emission/waste flows:			
water	0.09 m^3	1.50	emission to air
ferrous metal, in mixed metal scrap	90 kg	1.25	CH market
waste mineral wool	20 kg	1.25	CH market
waste polyvinylchloride	2 kg	1.25	CH market
wastewater, from residence	600 kg	1.05	CH market

Production of COWA capsules

The COWA capsules are made of HDPE and are filled with an SAT-based PCM. The included process steps are the production of capsules and covers from (virgin) HDPE granulate by injection- and blow moulding, mixing and filling of the PCM, and logistics. These steps are not considered separately but rather as one unit process with the inventory reflecting the in- and outputs of the listed process steps. The production location is Germany. Sodium acetate is provided by the production process described above. It is assumed that the plastic and PCM waste are handled separately at the EoL, the latter being landfilled as inert waste.

	amount	SD_{geo}^2	provider (remark)
reference product:			
COWA capsule	1000 units		
inputs:			
sodium acetate, trihydrate	119.46 kg	1.07	CN production (incl. shipment)
glycine	19.42 kg	1.07	GLO market
borax, anhydrous	2.84 kg	1.07	GLO market
polyethylene, high density, granulate	24.76 kg	1.07	GLO market
injection moulding	24.145 kg	1.07	RER processing (capsule)
blow moulding	0.765 kg	1.07	RER processing (cover)
transport, lorry >32t, euro5	45 tkm	2	RER market
transport, lorry 16-32t, euro5	30 tkm	2	RER market
electricity, medium voltage	22 kWh	1.78	DE market
storage building, chemicals	2E-8	4	GLO market
emissions/waste flows:			
waste polyethylene	25 kg	1.07	CH market (incineration)
inert waste	141 kg	1.07	CH inert material landfill
waste, unspecified	1 kg	3	final waste flow

TES with COWA capsules

An additional process was created to combine the hot water tank and COWA capsules. The number of capsules was calculated based on a packing density of 0.61 and an external capsule volume of 0.135l.

	amount	SD_{geo}^2	(remark)
reference product:			
latent TES, 600l, with COWA capsules	1 unit		
inputs:			
COWA capsule	2711 units	1.07	
hot water tank, 600l, without heat exchanger	1 unit	1.00	

Li-ion battery

Production and EoL treatment processes of some types of Li-ion batteries are included in the Ecoinvent database. The product 'Battery, Li-ion, NMC111, rechargeable, prismatic' has been selected as a base of comparison for the TES with COWA capsules. This process, as well as the waste treatment, is based on kg battery mass rather than kWh battery capacity. A conversion was necessary using a battery energy density of 0.143 kWh/kg given in the reference of the Ecoinvent process's documentation. A simple process has been created to represent a battery of desired capacity and link the production and EoL treatment process.

	amount	SD_{geo}^2	provider (remark)
reference product:			
battery pack, Li-ion NMC111, 13.5 kWh	1 unit		
inputs:			
battery, Li-ion, NMC111, rechargeable, prismatic	94.4 kg	1.07	GLO market
emissions/waste flows:			
used Li-ion battery	94.4 kg	1.07	GLO market

Impact Assessment

The product systems have been analyzed separately using different system models and LCIA methods. The impact category of primary interest is climate change/GWP with a time horizon of 100 years. A summary of the results can be seen below.

system model: cut-off by classification LCIA method: EF3.0 impact category: climate change

Product	LCIA result
Sodium acetate, trihydrate	1.75 kg $CO_{2\,eq}$ / kg
COWA capsule	488 kg $CO_{2\,eq}$ / 1000 units
hot water tank, 600l, without heat exchanger	789 kg $CO_{2\,eq}$ / unit
latent TES, 600l, with COWA capsules	2 112 kg $CO_{2\,eq}$ / unit
battery pack, Li-ion NMC111, 13.5 kWh	1 742 kg $CO_{2\,eq}$ / unit

If one additionally assumes that the battery has approximately 25% shorter lifetime than the latent TES system (e.g., 7,500 vs. 10,000 cycles), the difference can be accounted for by comparing 1 unit of latent TES with 1.33 units of the battery pack.

Main Contributions

The GWP impact of COWA capsules can be split up as shown below on the left. The largest contribution is sodium acetate, which can be further split up, as shown on the right.

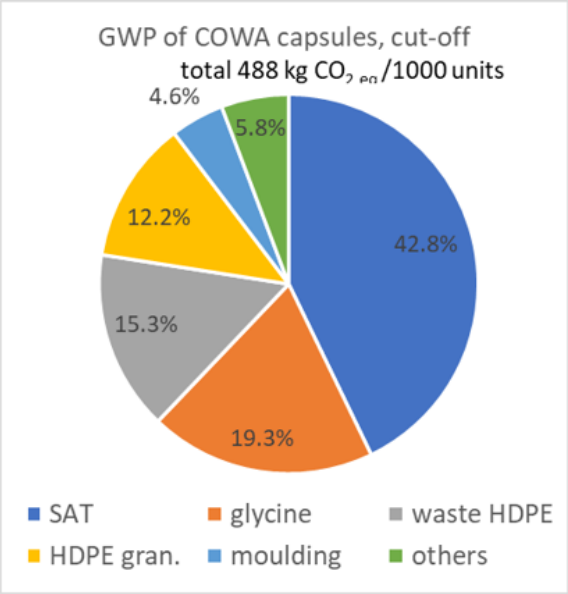

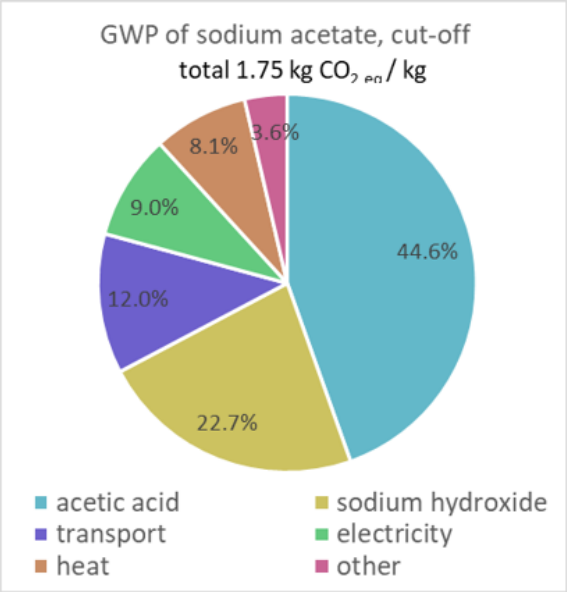

Alternative methods

The analyzes were repeated in the consequential system model, with the following results:

system model: consequential	LCIA method: EF3.0	impact category: climate change
Product	LCIA result	
Sodium acetate, trihydrate	1.78	kg $CO_{2\,eq}$ / kg
COWA capsule	460	kg $CO_{2\,eq}$ / 1000 units
hot water tank, 600l, without heat exchanger	770	kg $CO_{2\,eq}$ / unit
latent TES, 600l, with COWA capsules	2 017	kg $CO_{2\,eq}$ / unit
battery pack, Li-ion NMC111, 13.5 kWh	1 740	kg $CO_{2\,eq}$ / unit

Finally, the results were also calculated with the LCIA method 'ReCiPe 2016 Midpoint (hierarchist)'.

system model: cut-off	LCIA method: ReCiPe 2016 (H)	impact category: climate change
Product	LCIA result	
Sodium acetate, trihydrate	1.74	kg $CO_{2\,eq}$ / kg
COWA capsule	485	kg $CO_{2\,eq}$ / 1000 units
hot water tank, 600l, without heat exchanger	786	kg $CO_{2\,eq}$ / unit
latent TES, 600l, with COWA capsules	2 001	kg $CO_{2\,eq}$ / unit
battery pack, Li-ion NMC111, 13.5 kWh	1730	kg $CO_{2\,eq}$ / unit

It appears that the different methods deliver similar results.

Comparison of technologies

Three storage technologies of equivalent capacities are compared, based on the assumption that they interact with the heating system identically (i.e., the same autarky is achieved). The cut-off system model and the EF3.0 LCIA method are used for the comparison*. The comparison was done for several impact categories. The results are depicted in the plots below:

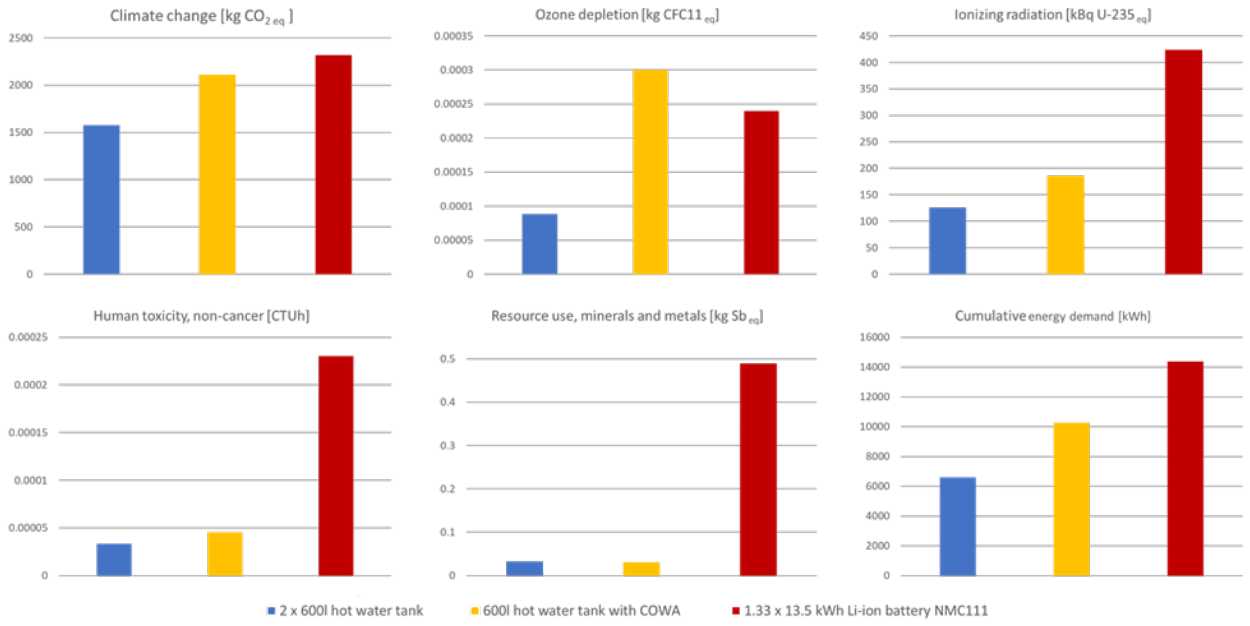

Interpretation

It appears that the environmental impact associated with the production of COWA capsules is quite significant and that sensible storage systems of equivalent capacity are preferable from an environmental perspective. Note that such sensible TES would have a higher space requirement which is not always available. However, if one attempts to compare storage systems of different capacities, it is imperative to understand the (potential) environmental impact mitigated by increasing the autarky of an SFH. Such an analysis is out of the scope of this project. Battery storage systems seem to underperform both latent and sensible thermal storage technologies for most impact categories. Note that the presented results must not be interpreted as precise predictions of the environmental impact triggered by the storage systems. For a better understanding of the implications, there are further points to consider.

Sensitivity

Considering the impact of COWA capsules, the following alternative assumptions lead to a significant change in the result (relative to the GWP of COWA capsules):

Sodium acetate is produced as anhydrate	approx.**+9%**
SAT and all its inputs are produced in Europe	approx. **-13%**
HDPE is recycled at EoL	approx.**-15/-20%** depending on system model

For the outcome of the comparison, the following parameters play a decisive role:

- Hot water tank material (especially type of steel) and wall thickness
- Battery type and charge/discharge characteristics during operation
- Recycling scenarios

Uncertainty

At the time of this study, all commercially available LCA software is either unable to execute an uncertainty analysis, or this feature is impaired by errors. For this reason, a limited calculation was performed only including uncertainties of climate change impact attached to flows contributing at least 3% to the overall impact. The calculated uncertainty is therefore necessarily an underestimate. The probability distribution representing the uncertainties of the results was computed with the Monte Carlo method (106 samples), using MatLab (R2022A). The results can be seen on the following graph, with the whiskers representing the limits of the 95% confidence interval. This analysis was only done for results obtained by the cut-off system model, the LCIA method EF3.0 and the impact category climate change.

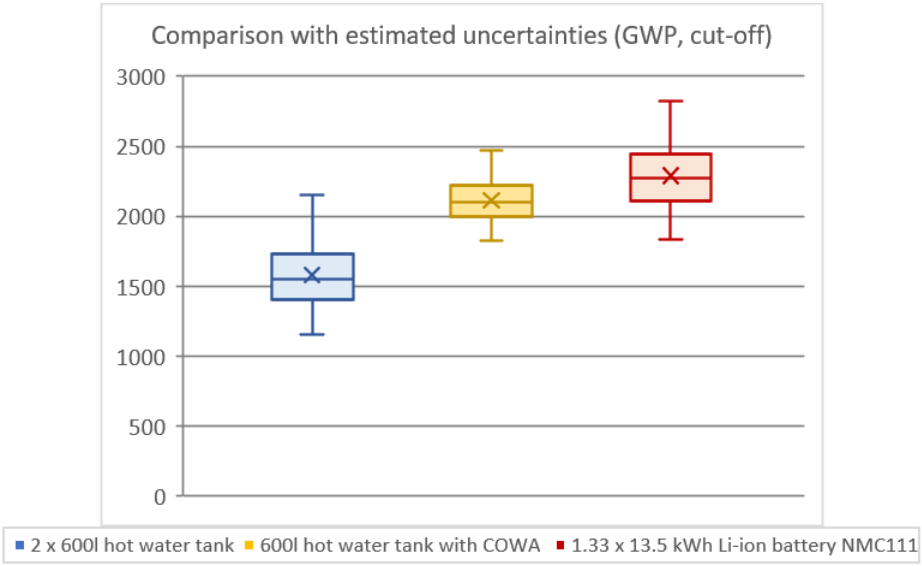

The above plot shows that the uncertainties are quite considerable and that there is some overlap between the confidence intervals of the three technologies. The arrays of samples were compared piecewise to determine the performance of the three technologies relative to each other, taking uncertainties into account. The GWP of latent TES was higher than that of the sensible TES for 99.8% of the samples. However, it was lower than that of the battery storage for only 71.5% of the samples, to which the following interpretation is proposed: Based on the available data, it is not possible to determine the 'better' technology (regarding GWP) with a reasonable level of confidence.

C Appendix 3: Calculations of Global Warming Potential

C.1 Heat pump

1. Starting with the general form of a 2nd-order polynomial equation:

$$GWP(HPC) = a * HPC^2 + b * HPC + c \tag{34}$$

2. The system of three equations in three variables (a, b, c), using data from Table 3:

$$\begin{aligned} GWP_1 &= a * HPC_1^2 + b * HPC_1 + c \Rightarrow 3,060 = a * 7^2 + b * 7 + c \\ GWP_2 &= a * HPC_2^2 + b * HPC_2 + c \Rightarrow 3,670 = a * 15^2 + b * 15 + c \\ GWP_3 &= a * HPC_3^2 + b * HPC_3 + c \Rightarrow 13,700 = a * 50^2 + b * 50 + c \end{aligned} \tag{35}$$

3. The matrix form of the system of equations from Equation 35:

$$\begin{bmatrix} HPC_1^2 & HPC_1 & 1 \\ HPC_2^2 & HPC_2 & 1 \\ HPC_3^2 & HPC_3 & 1 \end{bmatrix} \begin{bmatrix} a \\ b \\ c \end{bmatrix} = \begin{bmatrix} GWP_1 \\ GWP_2 \\ GWP_3 \end{bmatrix} \Rightarrow \begin{bmatrix} 7^2 & 7 & 1 \\ 15^2 & 15 & 1 \\ 50^2 & 50 & 1 \end{bmatrix} \begin{bmatrix} a \\ b \\ c \end{bmatrix} = \begin{bmatrix} 3,060 \\ 3,670 \\ 13,700 \end{bmatrix} \tag{36}$$

4. Next, Equation 36 can be used for solving the unknowns, generating the specific quadratic equation that fits the three data points:

$$GWP_{HP}(HPC) = 4.8912 \cdot HPC^2 - 31.356 \cdot HPC + 3039.8 \tag{37}$$

C.2 DHW storage tank

To determine the unknown constants (a_0, a_1, a_3, a_4) of Equation 38, a system of equations is filled with all data points from Table 4, resulting in eight equations (refer to Equation 39). These equations are solved using their matrix form in Equation 40), which leads to the solution of the unknown constants presented in Equation 41. when to constants are inserted in Equation 38 the resulting Equation 21 represents the trend line.

$$A_{DHW}(V) = a_0 + a_1 \cdot V + a_2 \cdot V^2 + a_3 \cdot V^3 + a_4 \cdot V^4 \tag{38}$$

$$\begin{aligned} A_1 &= a_0 + a_1V_1 + a_2V_1^2 + a_3V_1^3 + a_4V_1^4 \Rightarrow 4.18 = a_0 + 536a_1 + 536^2a_2 + 536^3a_3 + 536^4a_4 \\ A_2 &= a_0 + a_1V_2 + a_2V_2^2 + a_3V_2^3 + a_4V_2^4 \Rightarrow 5.40 = a_0 + 812a_1 + 812^2a_2 + 812^3a_3 + 812^4a_4 \\ A_3 &= a_0 + a_1V_3 + a_2V_3^2 + a_3V_3^3 + a_4V_3^4 \Rightarrow 6.12 = a_0 + 952a_1 + 952^2a_2 + 952^3a_3 + 952^4a_4 \\ A_4 &= a_0 + a_1V_4 + a_2V_4^2 + a_3V_4^3 + a_4V_4^4 \Rightarrow 7.92 = a_0 + 1495a_1 + 1495^2a_2 + 1495^3a_3 + 1495^4a_4 \\ A_5 &= a_0 + a_1V_5 + a_2V_5^2 + a_3V_5^3 + a_4V_5^4 \Rightarrow 9.20 = a_0 + 1936a_1 + 1936^2a_2 + 1936^3a_3 + 1936^4a_4 \\ A_6 &= a_0 + a_1V_6 + a_2V_6^2 + a_3V_6^3 + a_4V_6^4 \Rightarrow 12.39 = a_0 + 3068a_1 + 3068^2a_2 + 3068^3a_3 + 3068^4a_4 \\ A_7 &= a_0 + a_1V_7 + a_2V_7^2 + a_3V_7^3 + a_4V_7^4 \Rightarrow 14.75 = a_0 + 3945a_1 + 3945^2a_2 + 3945^3a_3 + 3945^4a_4 \\ A_8 &= a_0 + a_1V_8 + a_2V_8^2 + a_3V_8^3 + a_4V_8^4 \Rightarrow 17.59 = a_0 + 5131a_1 + 5131^2a_2 + 5131^3a_3 + 5131^4a_4 \end{aligned} \tag{39}$$

$$\begin{bmatrix} 1 & V_1 & V_1^2 & V_1^3 & V_1^4 \\ 1 & V_2 & V_2^2 & V_2^3 & V_2^4 \\ 1 & V_3 & V_3^2 & V_3^3 & V_3^4 \\ 1 & V_4 & V_4^2 & V_4^3 & V_4^4 \\ 1 & V_5 & V_5^2 & V_5^3 & V_5^4 \\ 1 & V_6 & V_6^2 & V_6^3 & V_6^4 \\ 1 & V_7 & V_7^2 & V_7^3 & V_7^4 \\ 1 & V_8 & V_8^2 & V_8^3 & V_8^4 \end{bmatrix} \begin{bmatrix} a_0 \\ a_1 \\ a_2 \\ a_3 \\ a_4 \end{bmatrix} = \begin{bmatrix} A_1 \\ A_2 \\ A_3 \\ A_4 \\ A_5 \\ A_6 \\ A_7 \\ A_8 \end{bmatrix} \Rightarrow \begin{bmatrix} 1 & 536 & 536^2 & 536^3 & 536^4 \\ 1 & 812 & 812^2 & 812^3 & 812^4 \\ 1 & 952 & 952^2 & 952^3 & 952^4 \\ 1 & 1495 & 1495^2 & 1495^3 & 1495^4 \\ 1 & 1936 & 1936^2 & 1936^3 & 1936^4 \\ 1 & 3068 & 3068^2 & 3068^3 & 3068^4 \\ 1 & 3945 & 3945^2 & 3945^3 & 3945^4 \\ 1 & 5131 & 5131^2 & 5131^3 & 5131^4 \end{bmatrix} \begin{bmatrix} a_0 \\ a_1 \\ a_2 \\ a_3 \\ a_4 \end{bmatrix} = \begin{bmatrix} 4.18 \\ 5.40 \\ 6.12 \\ 7.92 \\ 9.20 \\ 12.39 \\ 14.75 \\ 17.59 \end{bmatrix} \tag{40}$$

$$\begin{bmatrix} a_0 \\ a_1 \\ a_2 \\ a_3 \\ a_4 \end{bmatrix} = \begin{bmatrix} 1.09576 \\ 0.00674831 \\ -2.05591 \cdot 10^{-6} \\ 4.56355 \cdot 10^{-10} \\ -3.70187 \cdot 10^{-14} \end{bmatrix} \tag{41}$$

C.3 Spherical-Shaped Storage Tank

To calculate the GWP of the Spherical-Shaped Storage Tank as a function of the volume of the storage, it is started with the volume of a solid sphere with a radius r, given by Equation 42. Let the inner radius be r_i and the outer radius be r_o. The difference between them is the Thickness of the respective material in meters (T), the difference between the outer and inner radii can be written as Equation 43. The next step is to calculate the outer volume in terms of the inner radius, using the formula for the volume of a solid sphere. This can be used to express the outer volume V_o in terms of the inner radius r_i in Equation 44. Then, the hollow volume is calculated in terms of the inner radius. The hollow volume is the difference between the outer and inner volumes: $V_h = V_o - V$. Substitute the expressions for V_o and V_i in terms of the inner radius and Equation 45 is generated. The final step is to adjust the equation as a function of the inner volume instead of the inner radius. This is done by using the formula for the volume of a sphere, Equation 42. Which is solved for r in Equation 46. Substituting this expression for r into the original formula for the volume of the hollow sphere (Equation 45), Equation 27 is generated. This function describes the volume of the spherical shell ($V_h(V_i)$), as a function of the storage volume (V).

$$V = \frac{4}{3} \cdot \pi \cdot r^3 \tag{42}$$

$$r_o = r_i + T \tag{43}$$

$$V_o = \frac{4}{3} \cdot \pi \cdot (r_i + T)^3 \tag{44}$$

$$V_h = V_o - V_i \Rightarrow V_h = \frac{4}{3} \cdot \pi \cdot (r_i + T)^3 - \frac{4}{3} \cdot \pi \cdot r_i^3 \tag{45}$$

$$r = \sqrt[3]{\frac{3 \cdot V}{4 \cdot \pi}} \tag{46}$$

$$V_{h-GFRP}(V) = \frac{4}{3} \cdot \pi \cdot (\sqrt[3]{\frac{3 \cdot V}{4 \cdot \pi}} + T)^3 - \frac{4}{3} \cdot \pi \cdot (\sqrt[3]{\frac{3 \cdot V}{4 \cdot \pi}})^3 \tag{47}$$

C.4 Repurposed-Basement Storage

The surface area A_{cuboid} of a cuboid can be expressed as Equation 48, and the volume (V_{RBS}) as Equation 49, where l is the length and w is the width of the base plane. One of the variables is eliminated to express the surface area as a function of the volume. Solving for l or w in the other terms gives Equation 50. Substituting these values in Equation 48, and Equation 51 comes out. Therefore, by simplifying, the surface area of a cuboid as a function of its volume, where the height is known as 3m, is given by Equation 30. To calculate the Volume of the used insulation, Equation 30 is multiplied by the insulation thickness (T_{XPS}) as in Equation 49. This can be used to calculate the GWP of the used XPS by multiplying it with GWP_{XPS}. This is combined with the GWP of the PCM capsules (Equation 24, to give the complete function of the GWP of the RBS, see Equation 31.

$$A = 2 \cdot l \cdot w + 2 \cdot l \cdot h + 2 \cdot w \cdot h \tag{48}$$

$$V = l \cdot w \cdot h \tag{49}$$

$$\begin{aligned} l &= \frac{V}{wh} \\ w &= \frac{V}{lh} \end{aligned} \tag{50}$$

$$A = 2\left(\frac{V}{h}\right) + 2h\left(\frac{V}{l \cdot h}\right) + 2\left(\frac{V}{l \cdot h}\right) h \tag{51}$$

$$A_{cuboid}(V) = \frac{2 \cdot 3^2}{V} + \frac{4 \cdot V}{3} \tag{52}$$

$$V_{XPS}(V) = A_{cuboid}(V) \cdot T_{XPS} \tag{53}$$

$$GWP_{RBD}(V) = V_{XPS}(V) \cdot GWP_{XPS} + GWP_{Capsules}(V) \tag{54}$$

D Appendix 4: Influence of variables

Table 12: Variation values for each optimisation variable used to check that particular variable's influence, the middle column indicates the base values of the variables.

Optimisation variable	**Variation values**						
Column no.:	**1**	**2**	**3**	**Base**	**4**	**5**	**6**
HyTES tank height $[m]$	1	1.5	2	**2.5**	3	3.5	4
HyTES tank width $[m]$	-	1	3	**5**	7	9	10
PCM packed bed starting position $[-]$	0.2	0.3	0.4	**0.5**	0.6	0.7	0.8
PCM packed bed thickness $[-]$	-	0.15	0.3	**0.5**	0.7	0.9	1
Minimum HyTES energy level $[-]$	-	0.4	0.3	**0.2**	0.1	0	-
DHW tank height $[m]$	1.6	1.75	1.9	**2**	2.1	2.2	-
DHW tank width $[m]$	0.5	0.8	1	**1.2**	1.4	1.6	1.8
Relative amount of PV panels $[-]$	-	0.1	0.3	**0.5**	0.7	0.9	1
PV Azimuth angle $[°]$	90	120	150	**180**	210	240	270
PV Tilt angle $[°]$	0	7.5	15	**22.5**	30	37.5	45
Electrical power HP $[kW_{elec}]$	2	5	8	**11**	14	17	20

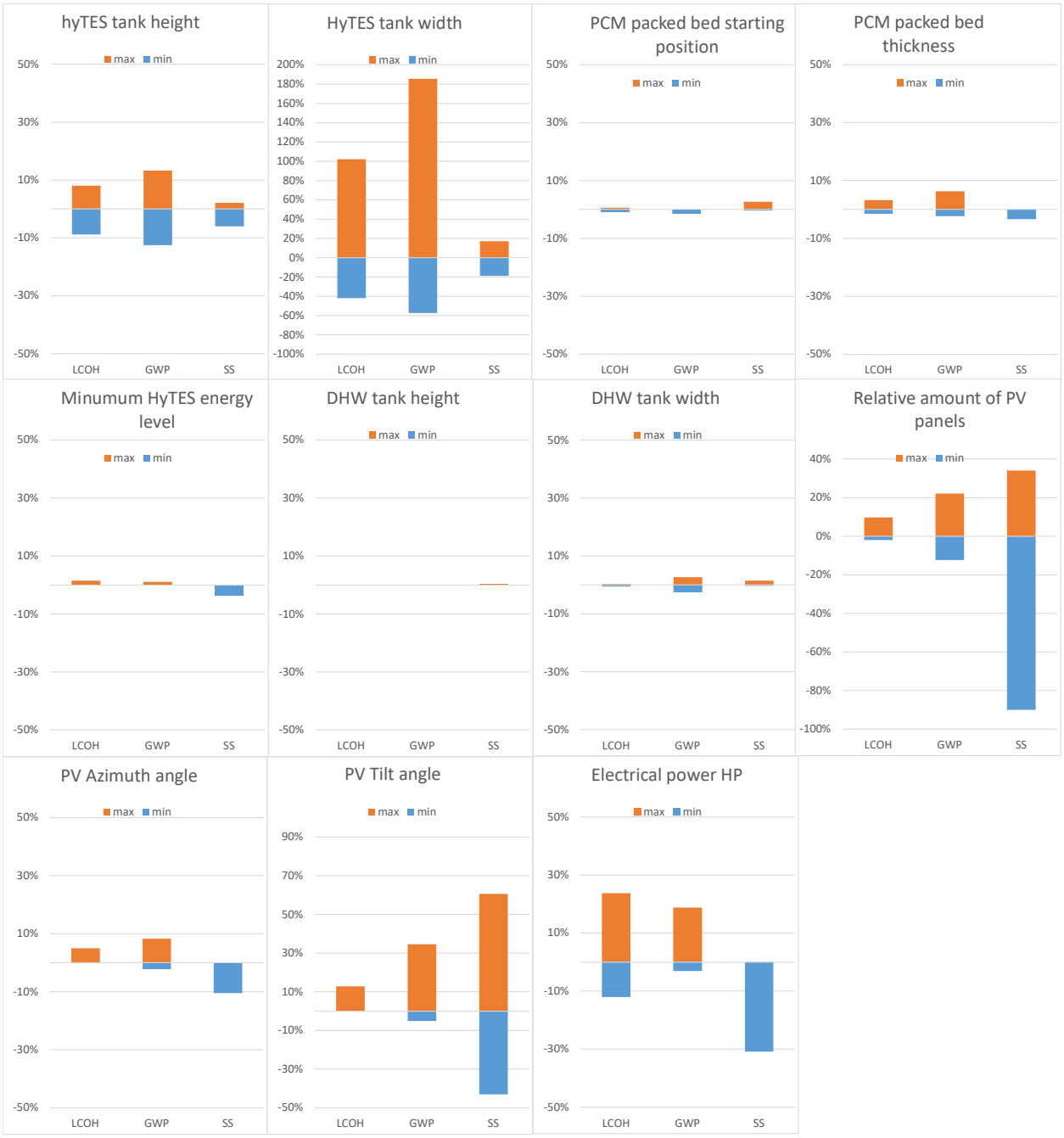

Figure 22: Influence spread of the different optimisation variables.

Sensitivity LCOH

Table 13: Normalised relative difference in LCOH per optimisation variable, compared to the results of the base value.

Optimisation variable:	**Relative Difference in LCOH**						
Column no.:	**1**	**2**	**3**	**Base**	**4**	**5**	**6**
HyTES tank height	-15%	-10%	-5%	**0%**	4%	8%	13%
HyTES tank width	-	-35%	-22%	**0%**	29%	65%	102%
PCM packed bed starting position	-2%	-1%	0%	**0%**	-1%	1%	1%
PCM packed bed thickness	-	-1%	-1%	**0%**	2%	3%	3%
Minimum HyTES energy level	-	4%	2%	**0%**	0%	0%	-
DHW tank height	0%	0%	0%	**0%**	0%	0%	-
DHW tank width	1%	0%	0%	**0%**	-1%	-1%	-1%
Relative amount of PV panels	-	2%	-2%	**0%**	3%	6%	10%
PV Azimuth angle	8%	2%	0%	**0%**	1%	3%	10%
PV Tilt angle	13%	2%	0%	**0%**	1%	2%	3%
Electrical power HP	-2%	-15%	-8%	**0%**	10%	19%	29%

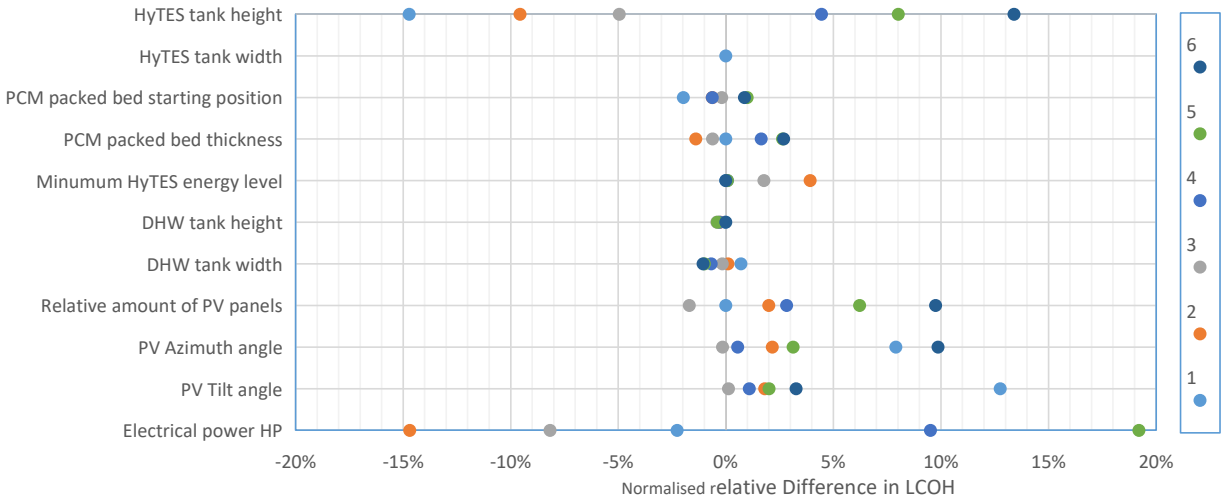

Figure 23: Sensitivity spread LCOH zoomed in

Sensitivity GWP

Table 14: Normalised relative difference in GWP per optimisation variable, compared to the results of the base value.

Optimisation variable:	**Relative Difference in GWP**						
Column no.:	**1**	**2**	**3**	**Base**	**4**	**5**	**6**
HyTES tank height	-21%	-14%	-8%	**0%**	7%	13%	22%
HyTES tank width	-	-48%	-33%	**0%**	49%	115%	186%
PCM packed bed starting position	0%	0%	0%	**0%**	-3%	-1%	-1%
PCM packed bed thickness	-	-2%	-1%	**0%**	3%	5%	6%
Minimum HyTES energy level	-	3%	1%	**0%**	2%	2%	-
DHW tank height	-1%	-1%	-1%	**0%**	0%	0%	-
DHW tank width	-5%	-3%	-2%	**0%**	1%	3%	5%
Relative amount of PV panels	-	-10%	-6%	**0%**	7%	14%	22%
PV Azimuth angle	13%	1%	-4%	**0%**	-2%	3%	17%
PV Tilt angle	34%	8%	-3%	**0%**	-4%	-5%	-5%
Electrical power HP	-2%	-4%	-3%	**0%**	6%	14%	23%

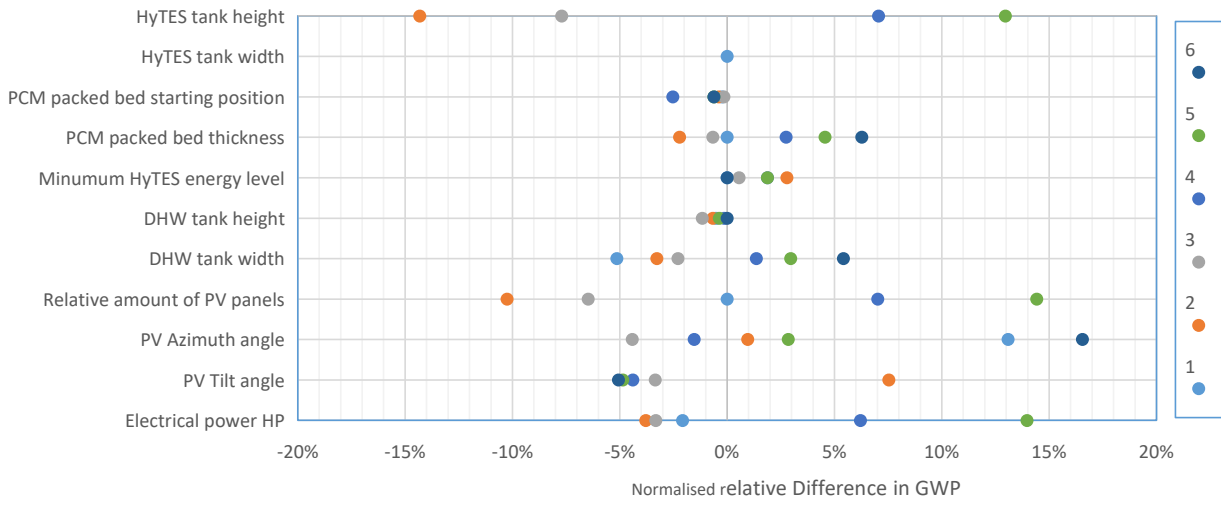

Figure 24: Sensitivity spread GWP zoomed in

Sensitivity SS

Table 15: Normalised relative difference in SS per optimisation variable, compared to the results of the base value.

Optimisation variable:	**Relative Difference in SS**						
Column no.:	**1**	**2**	**3**	**Base**	**4**	**5**	**6**
HyTES tank height	-10%	-5%	-1%	**0%**	2%	3%	3%
HyTES tank width	-	-16%	-3%	**0%**	5%	11%	17%
PCM packed bed starting position	0%	1%	-1%	**0%**	4%	0%	0%
PCM packed bed thickness	-	-3%	-2%	**0%**	-2%	-1%	-1%
Minimum HyTES energy level	-	-10%	-4%	**0%**	-3%	-3%	-
DHW tank height	0%	1%	2%	**0%**	1%	2%	-
DHW tank width	3%	2%	2%	**0%**	0%	0%	-1%
Relative amount of PV panels	-	-75%	-20%	**0%**	15%	25%	34%
PV Azimuth angle	-17%	-21%	-13%	**0%**	-13%	-14%	0%
PV Tilt angle	61%	19%	-17%	**0%**	-28%	-36%	-43%
Electrical power HP	-38%	-14%	-4%	**0%**	-1%	-3%	-4%

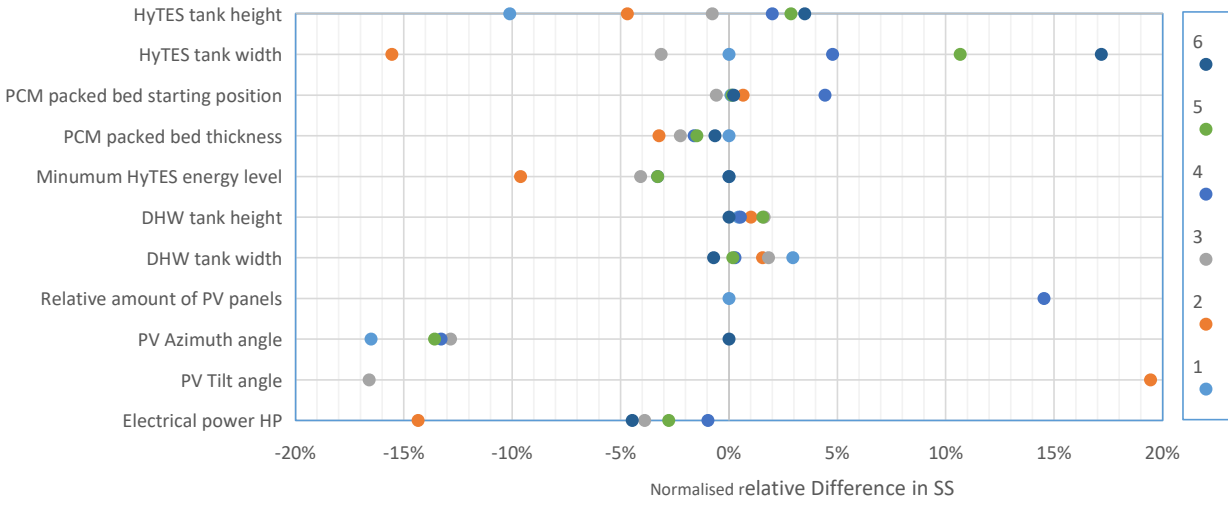

Figure 25: Sensitivity spread SS zoomed in